

Micro and Nano-Tomography of Biological Tissues

Marco Stampanoni and Kevin Mader

Swiss Light Source, Paul Scherrer Institut
Institute for Biomedical Engineering, University and ETH Zürich

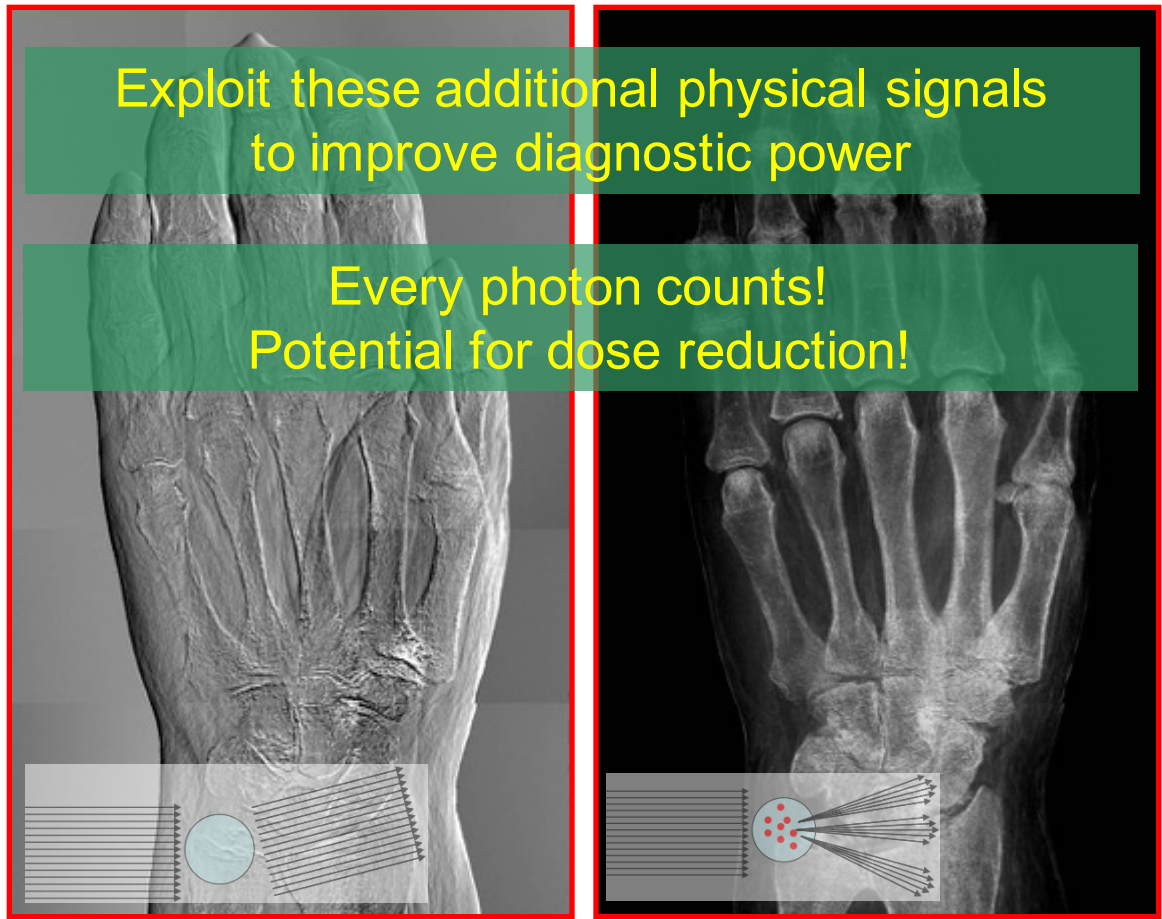
ETH-227-0965-00 L



Vision: new radiological capabilities



 Absorption image
Conventional radiography
(since 1895...)



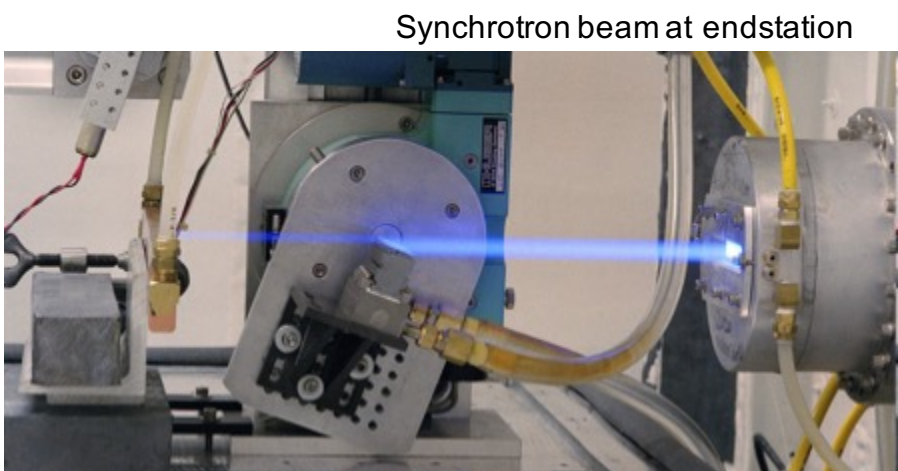
"Differential Phase image"

"Scatter image"

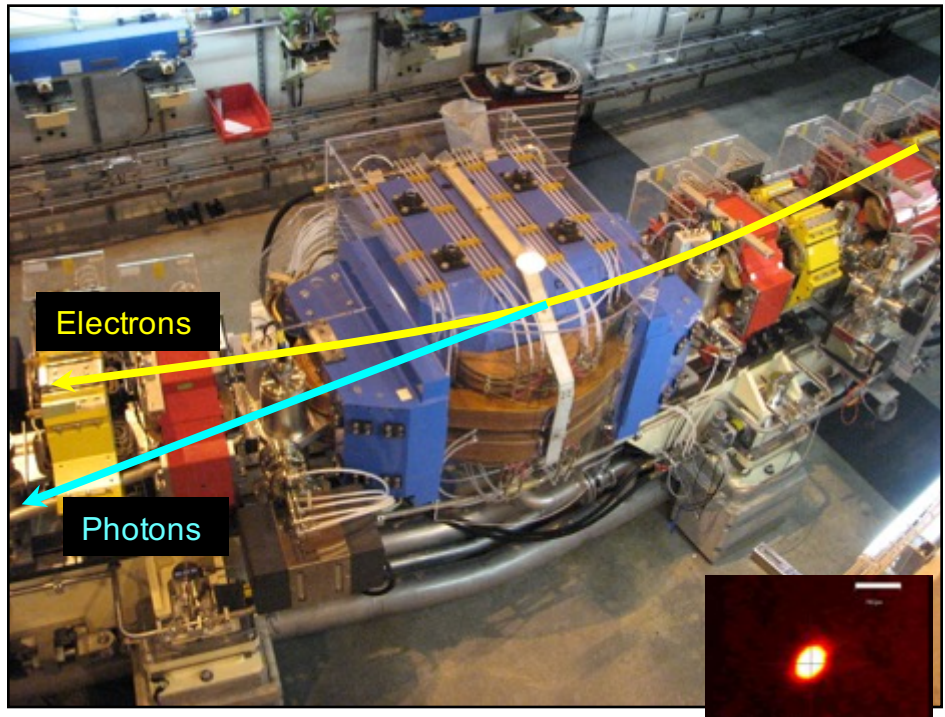
$$\text{Index of refraction: } n = 1 - \frac{\delta}{\lambda} + i\frac{\beta}{\lambda}$$

Phase Absorption

A remind...



Synchrotron beam at endstation



Experiment



30-200 m !!

Source

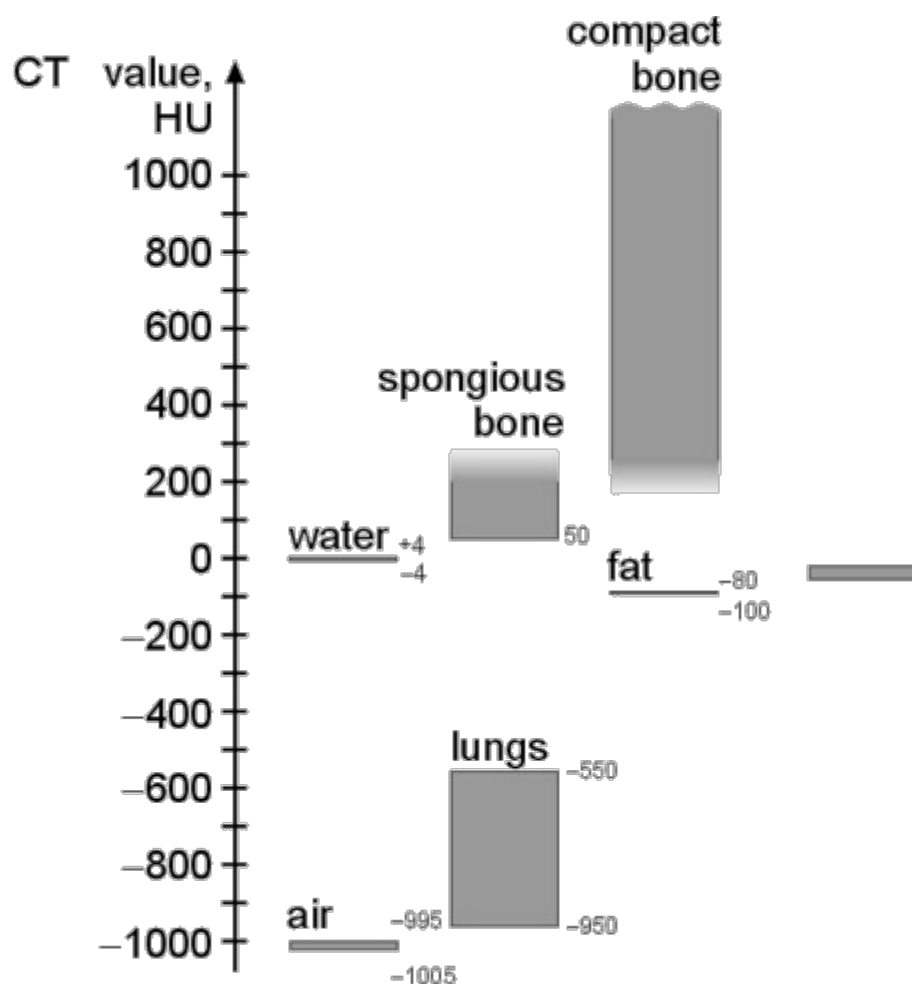
(10-50 microns)

- Very small source size
- Strong collimated beam
- Large distance between source and experiment

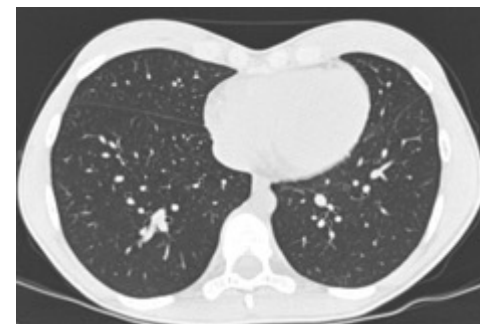
→ We can observe interference phenomena with X-rays and exploit them for imaging!

→ Phase contrast

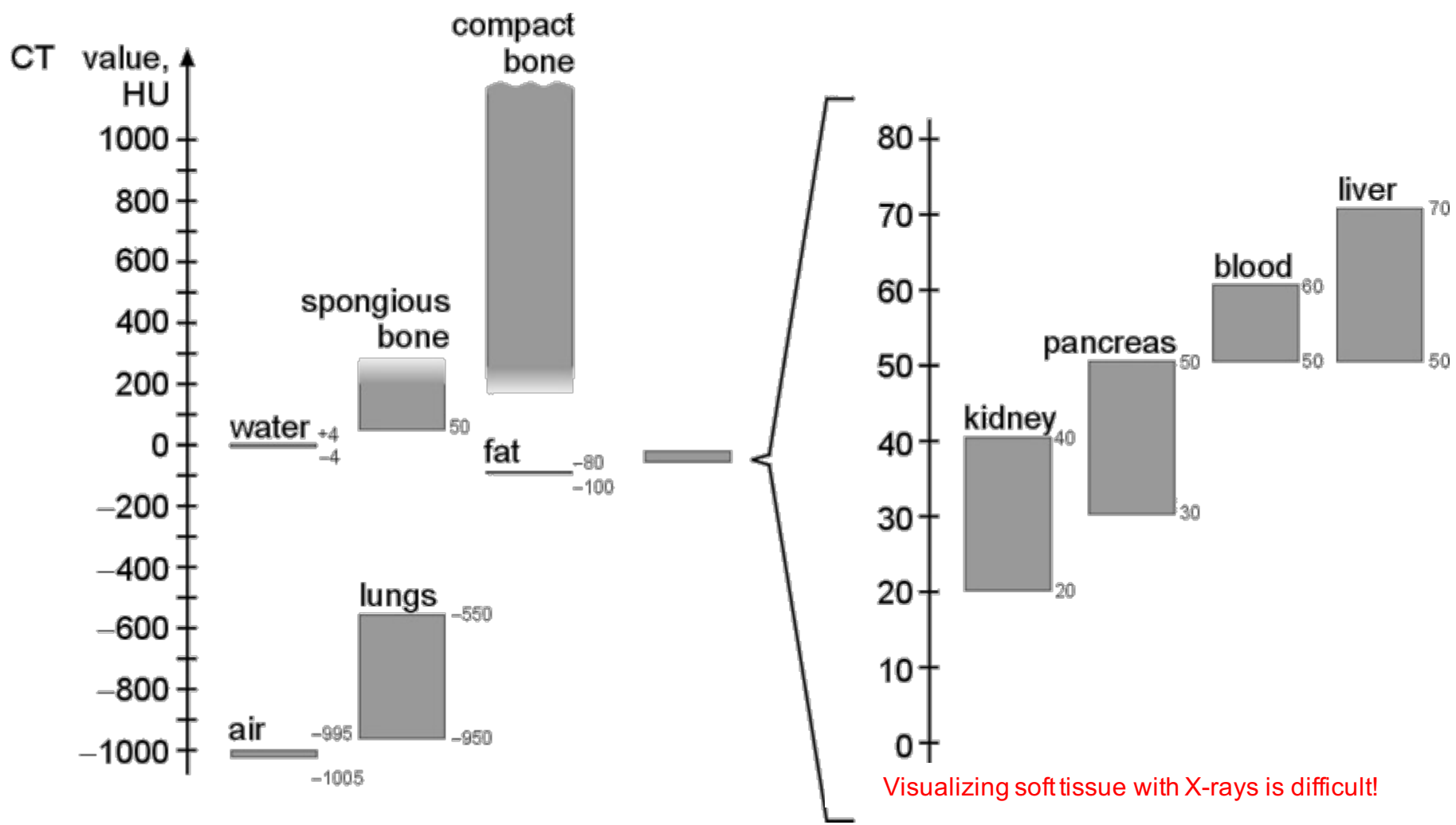
Why phase contrast imaging?



$$CT \text{ value} = \frac{(\mu_{Tissue} - \mu_{water})}{\mu_{water}} \cdot 1000 \text{ HU}$$

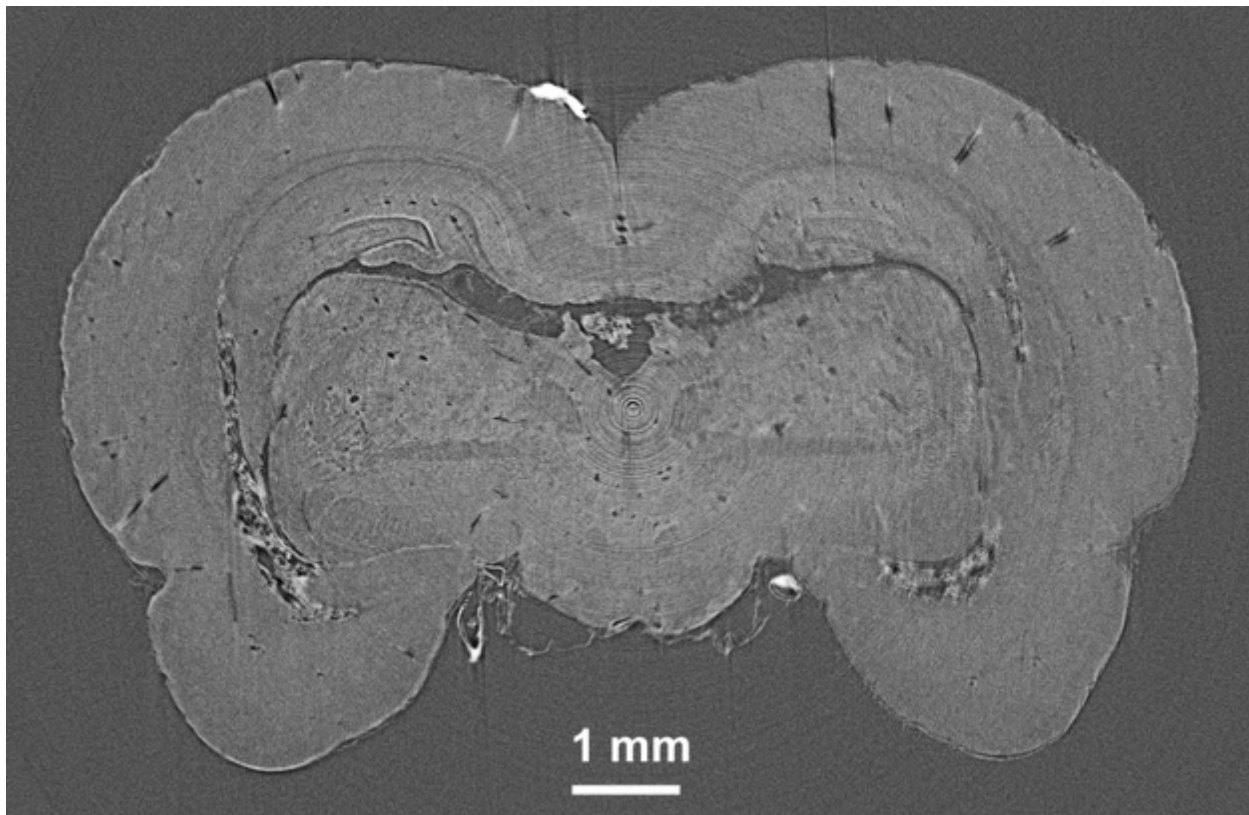


Why phase contrast imaging?



Why phase contrast imaging?

- Absorption-based radiography and tomography yield little contrast for light materials and materials with similar atomic numbers.

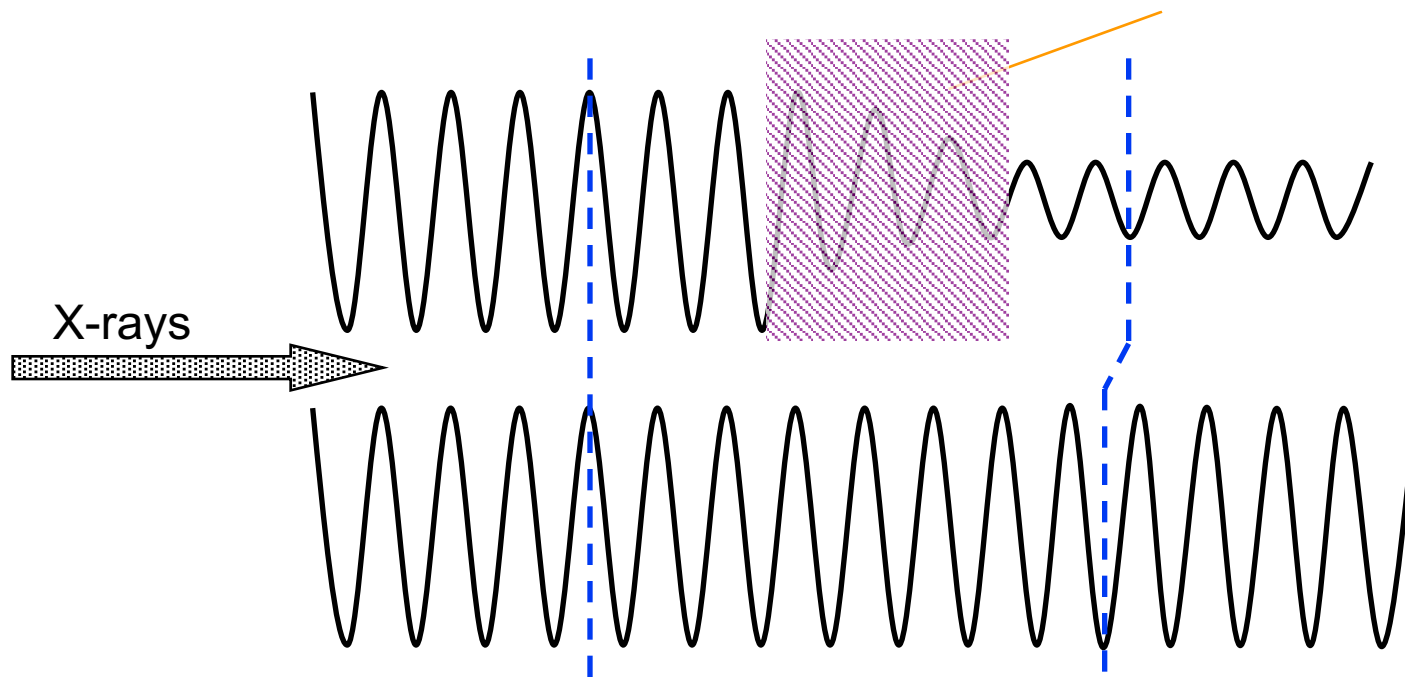


$$\text{AbsorptionCT} \propto Z^4 E^{-3}$$

Sample: rat brain fixed, embedded in paraffin

Phase contrast

Index of refraction: $\nu = 1 - \delta + i\beta$



Example:

- 20 keV x-rays
- Organic sample (polymer, biological, medical...)
- 50 μm thickness

\rightarrow only 0.2 % absorption }
 \rightarrow but π phase shift!! }

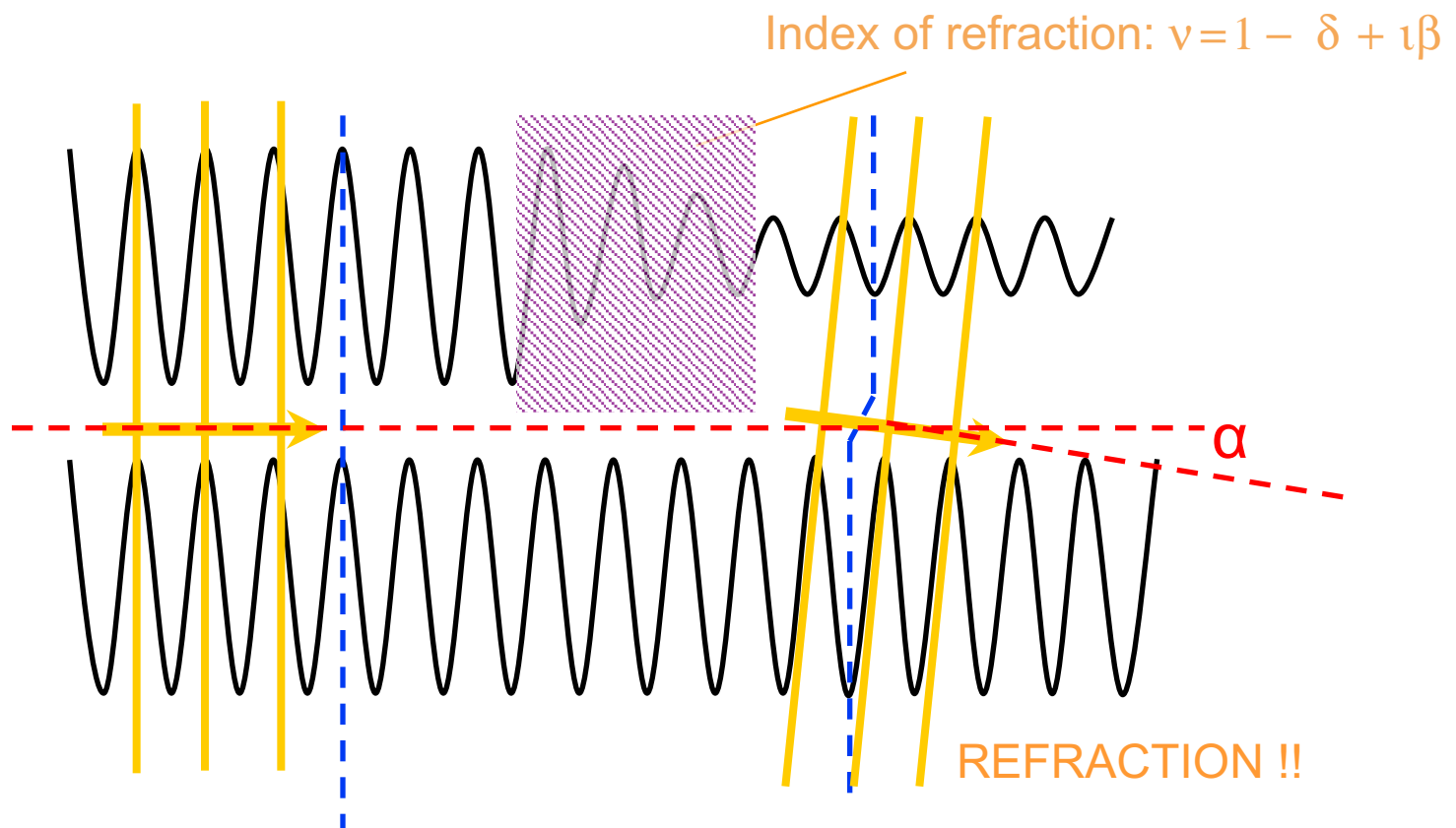
- Higher contrast !!
- Lower dose

$$\begin{aligned} A' &= A \exp(ik[1+i\beta-\delta]D) \\ &= A \exp(-k\beta D) \exp(ik[1-\delta]D) \end{aligned}$$

Detectors just measure intensities and therefore “conventional” imaging relies on absorption!!

$$|A'|^2 = |A|^2 \exp(-2k\beta D) = |A|^2 \exp(-\mu D)$$

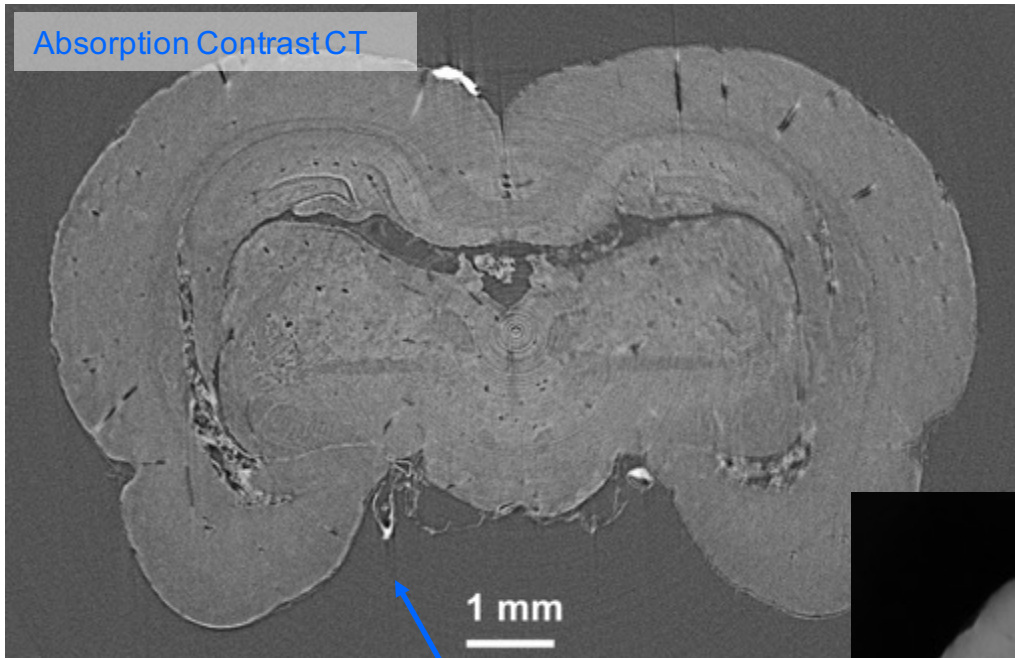
Phase contrast



X-rays

$$\alpha = \frac{\lambda}{2\pi} \frac{\partial \Phi}{\partial x} = \frac{\partial}{\partial x} \int \delta(x, y, z) dz$$

Improve contrast from soft tissue

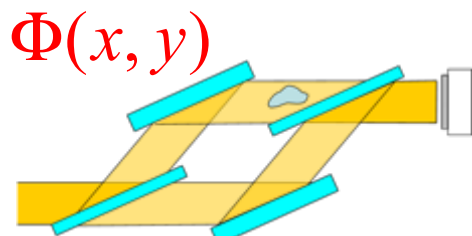


$$\nu = 1 - \delta + \beta$$

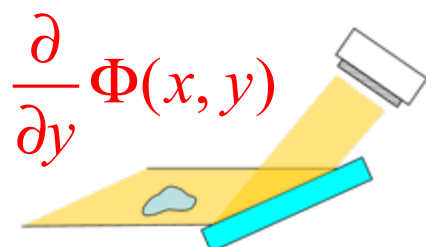
Same dose!!



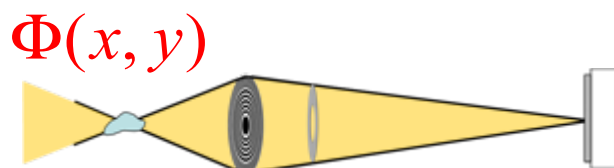
X-ray phase contrast techniques



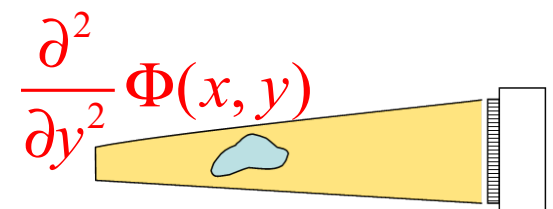
$\Phi(x, y)$
Crystal interferometry
Bonse et al. APL 6, 155 (1965)



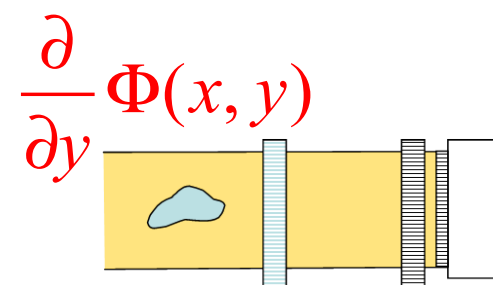
$\frac{\partial}{\partial y} \Phi(x, y)$
Analyser-based (DEI)
Chapman et al., PMB, 42, 2015 (1997)
Davis et al., JOSAA 13, 1193 (1996)



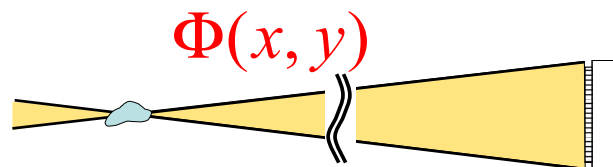
$\Phi(x, y)$
Zernike Phase Contrast
Weiss et al., UM 84, 185 (2000)
Stampanoni et al., PRB 81, 140105R (2010)



$\frac{\partial^2}{\partial y^2} \Phi(x, y)$
Free Space Propagation (TIE)
Snigirev et al., RSI 66, 5486 (1995)
Cloetens et al., APL 75, 2912 (1999)
Groso et al., OptExp 14, 8103 (2006)



$\frac{\partial}{\partial y} \Phi(x, y)$
Grating interferometry (DPC)
Weitkamp et al., OptExp 13, 6296 (2005)
Pfeiffer et al., Nature Phys 2, 258 (2006)



$\Phi(x, y)$
Coherent Diffraction Imaging (CDI)
Miao et al., Nature 400 (1999)
Thibault et al., Science, 321, 379 (2008).

PHILosophical
TRANSACTIONS
OF
THE ROYAL
SOCIETY A

rsta.royalsocietypublishing.org

Review

CrossMark

On the evolution and relative
merits of hard X-ray
phase-contrast imaging
methods

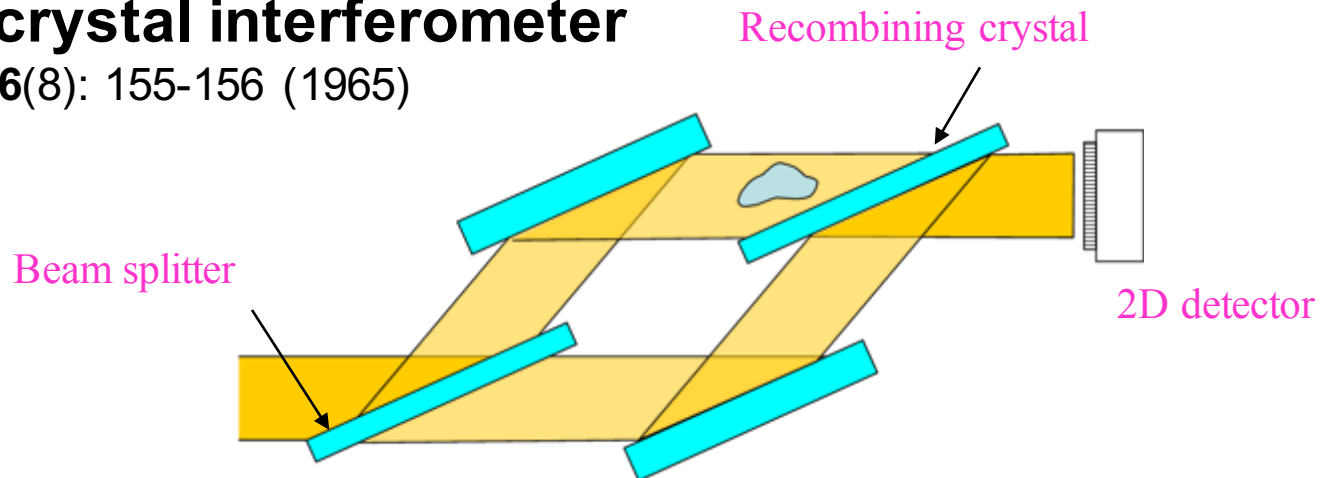
S. W. Wilkins¹, Ya. I. Nesterets, T. E. Gureyev,
S. C. Mayo, A. Pogany² and A. W. Stevenson

CSIRO Materials Science and Engineering, PB33, Clayton South,
Victoria 3169, Australia

Crystal Interferometer

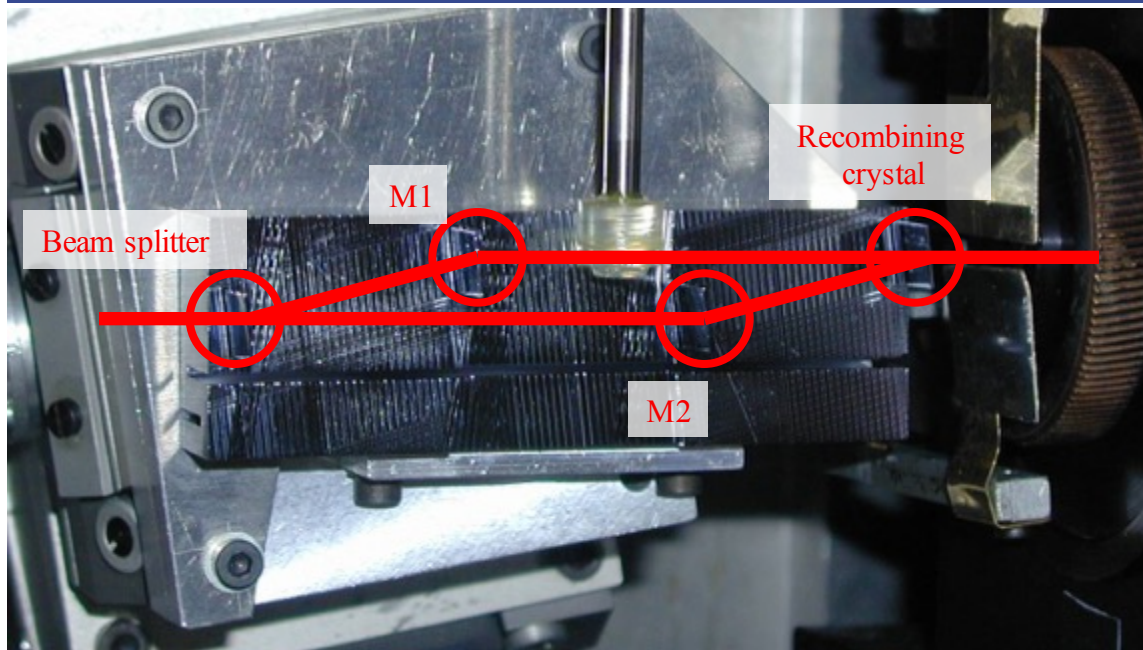
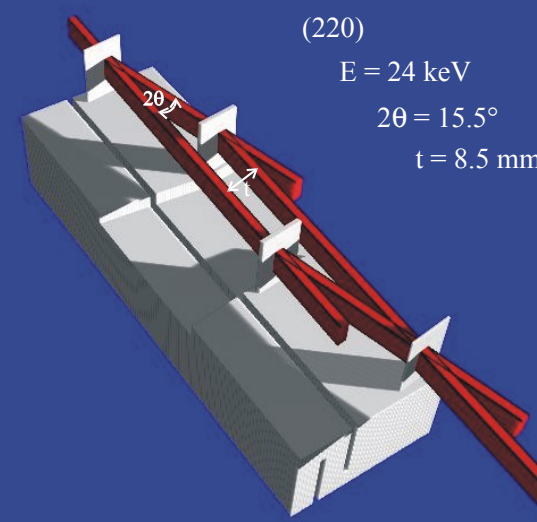
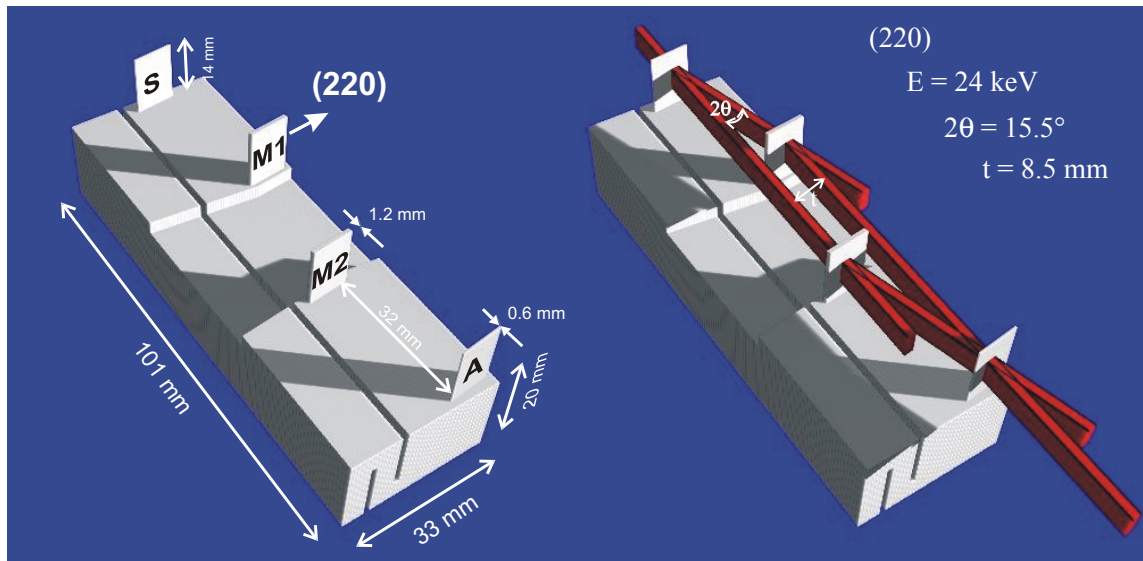
- **Bonse-Hart crystal interferometer**

Bonse et al. APL 6(8): 155-156 (1965)



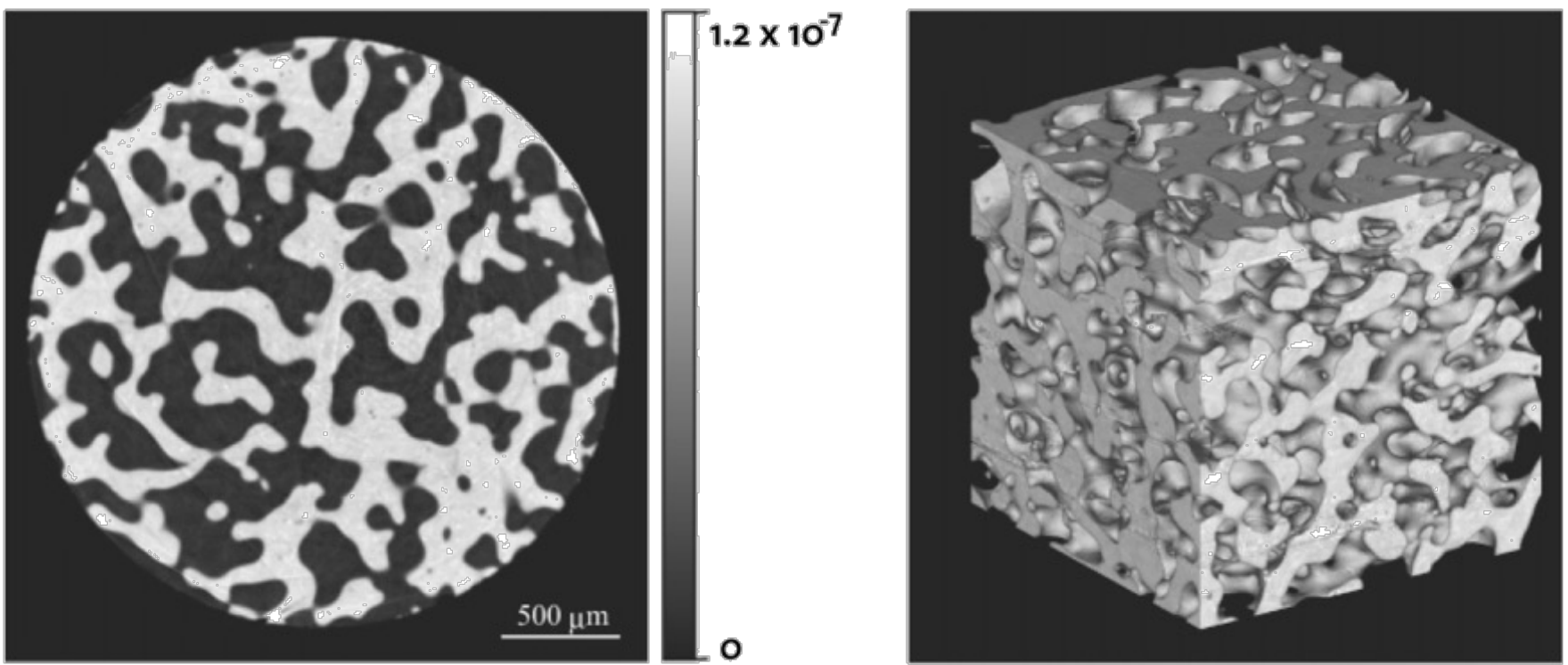
- A Bragg reflection (and transmission) used as beam splitter !
 - The signal recorded measures directly the phase
 - The system is extremely sensitive to small phase variations
 - Limited field of view (by crystal acceptance)
 - Extremely sensitive to mechanical and thermal drift
 - Acts as a monochromator, tight bandwidth!
- + -

Hard X-ray crystal interferometry



Images courtesy F. Beckmann, GKSS

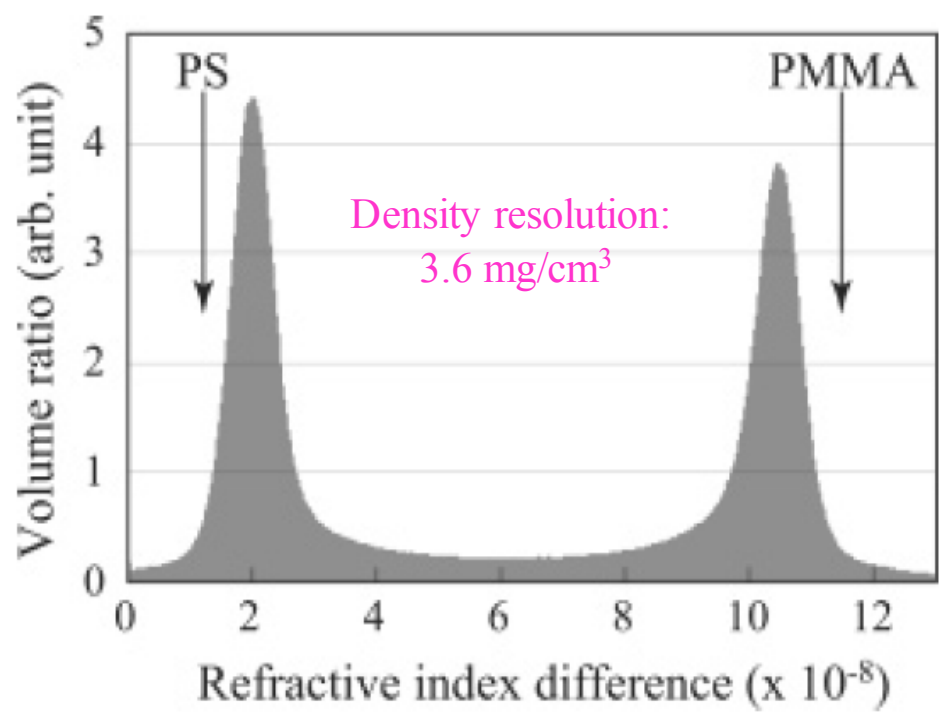
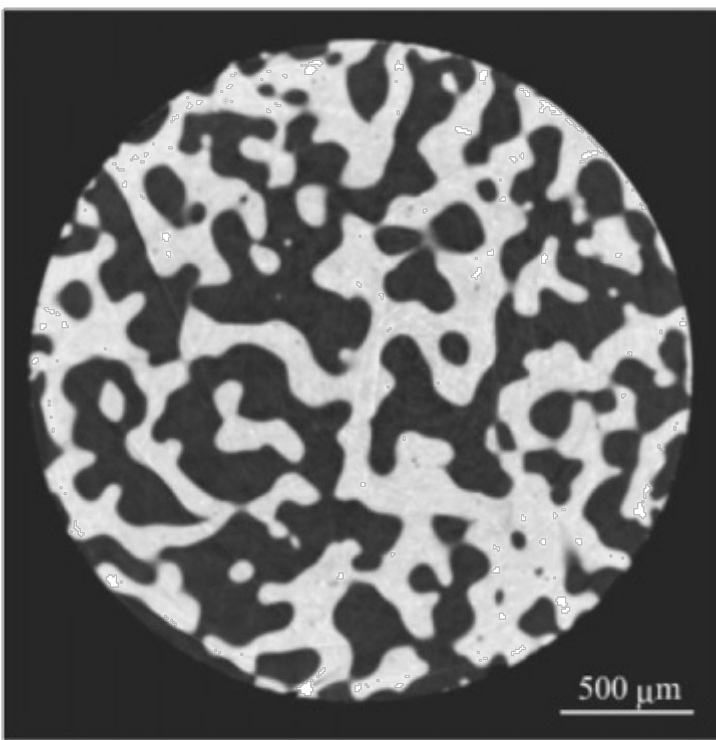
Polystyrene / PMMA plastic composite



Reconstructed image of polystyrene (PS)/poly (methyl methacrylate) (PMMA) blend by X-ray phase tomography: phase tomogram (left) and volume rendering view (right) of reconstructed three-dimensional data, where PS region has been made transparent. Spatial resolution: 10 microns.

A. Momose et al., Macromolecules, Vol. 38, No. 16, 2005

Polystyrene / PMMA plastic composite

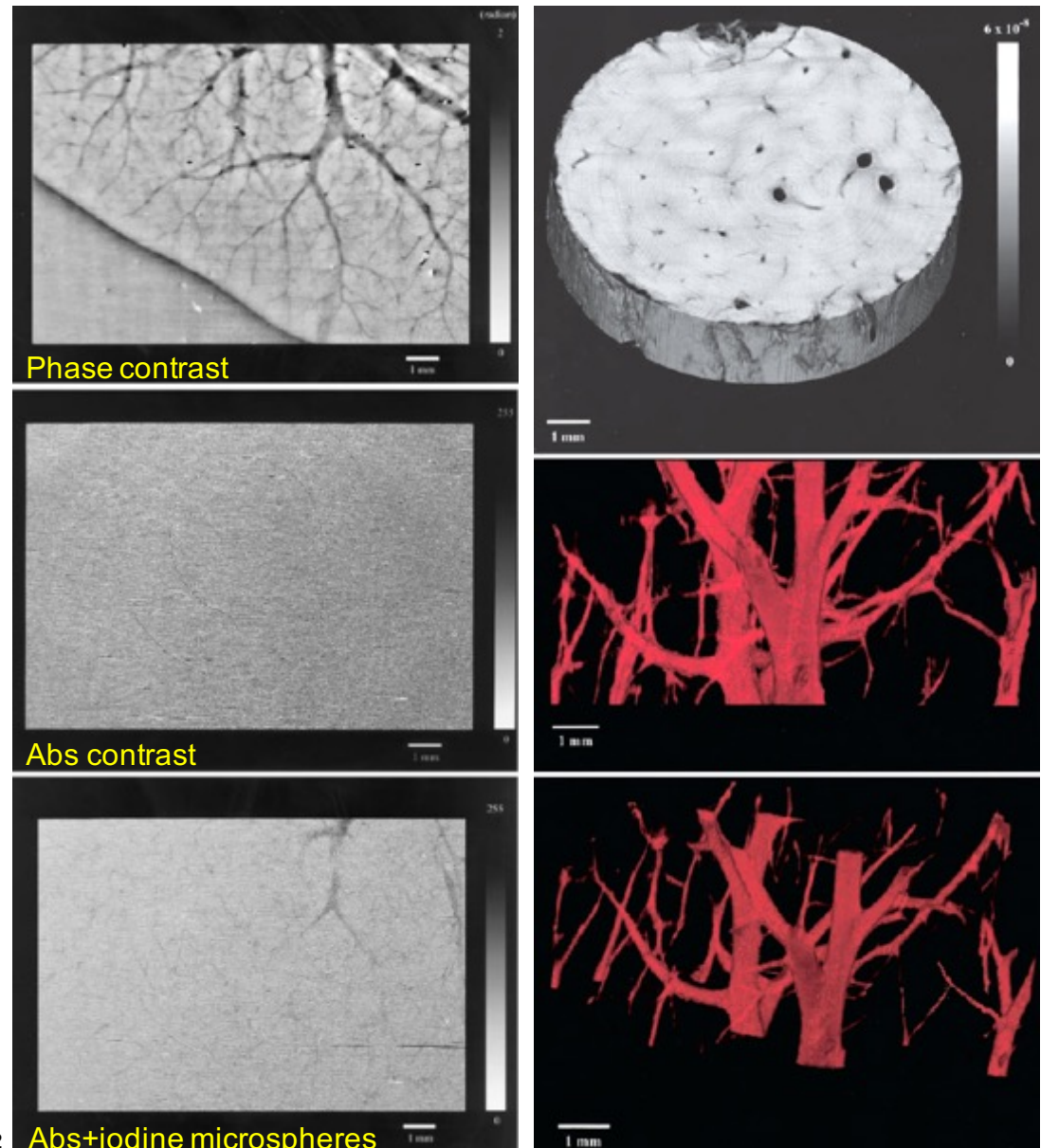


Reconstructed image of polystyrene (PS)/poly (methyl methacrylate) (PMMA) blend by X-ray phase tomography: phase tomogram (left) and volume rendering view (right) of reconstructed three-dimensional data, where PS region has been made transparent. Spatial resolution: 10 microns.

A. Momose et al., Macromolecules, Vol. 38, No. 16, 2005

Vessel Imaging

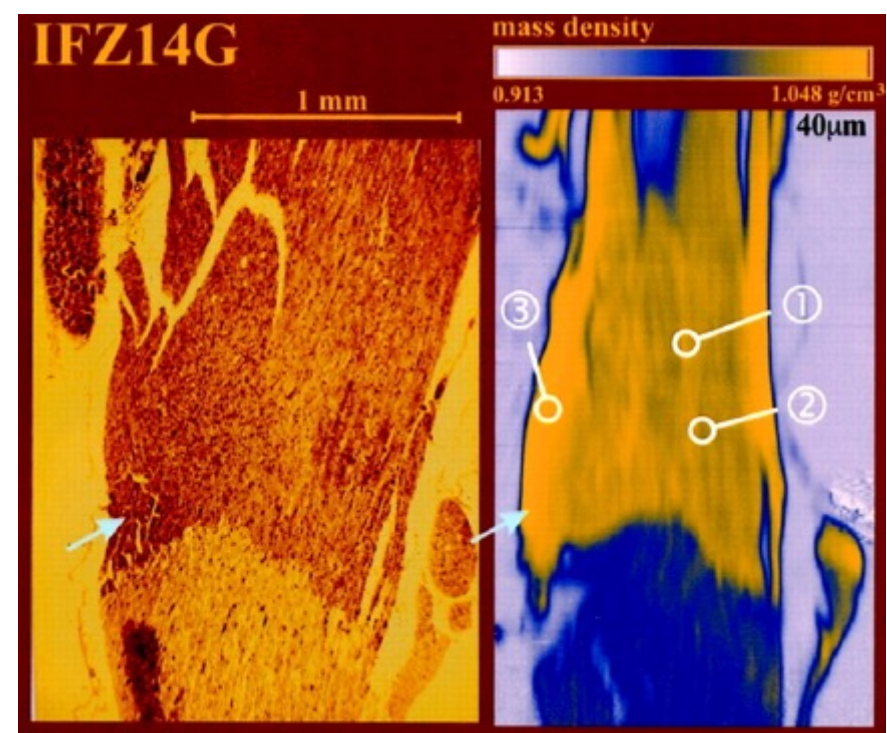
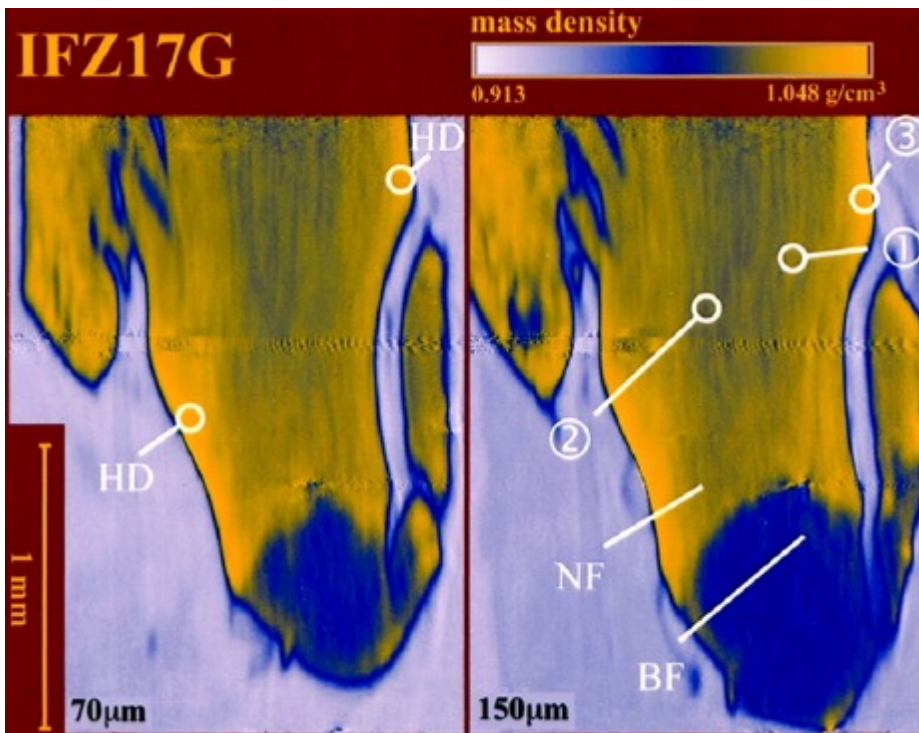
- Phase map (top) and absorption-contrast x-ray image (center) of a rat liver filled with physiological saline, and absorption contrast x-ray image with iodine-loaded acrylic microspheres (bottom). Vessels of liver are shown as gray in phase map, and minimal diameter is 30 microns.
- The absorption-contrast x-ray image with physiological saline does not reveal vessel at all, and that with iodine-loaded acrylic microspheres only depicted the large portal veins of 100 microns in diameter. The edge of the liver is not shown in B and C because the excised liver is set in a cell filled with physiological saline.
- Phase-contrast x-ray CT image (top) and 3D image of vessel (lateral view [center] and 20° anterior oblique view [bottom]) of a rabbit liver. Hepatic vessels are demonstrated as rounded structures with gray in phase-contrast x-ray CT image. The 3D image depicts vessel trees, and minimal vessel diameter is 30 microns.



T. Takeda., Circulation, April 9, 2002

Rat trigeminal nerve

Nerve fibers (diameter 25 μm), noticeable density change 1 mg/cm^3



Yellow corresponds to nerve and blue to brain tissue. Light violet is the paraffin used as embedding material. Note the nerve fibers (NF) following the nerve axis. Some of the nerve fibers cross the brain/nerve boundary (BF).

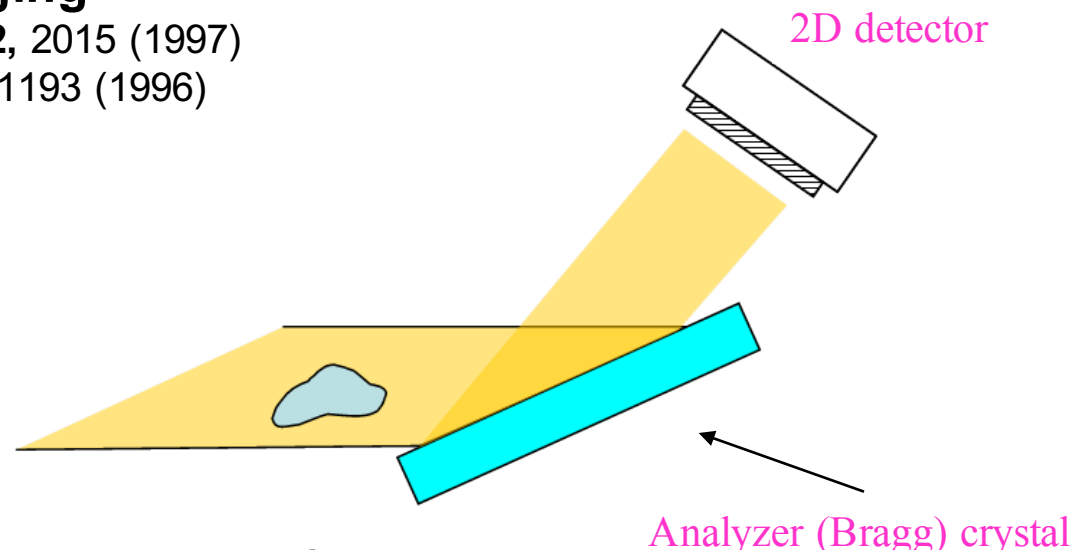
Beckmann et al., Biophys J, January 1999, p. 98-102, Vol. 76, No. 1

Diffraction enhanced (analyser) method

- **Diffraction enhanced imaging**

Chapman et al., *Phys. Med. Biol.* **42**, 2015 (1997)

Davis et al., *J. Opt. Soc. Am. A* **13**, 1193 (1996)

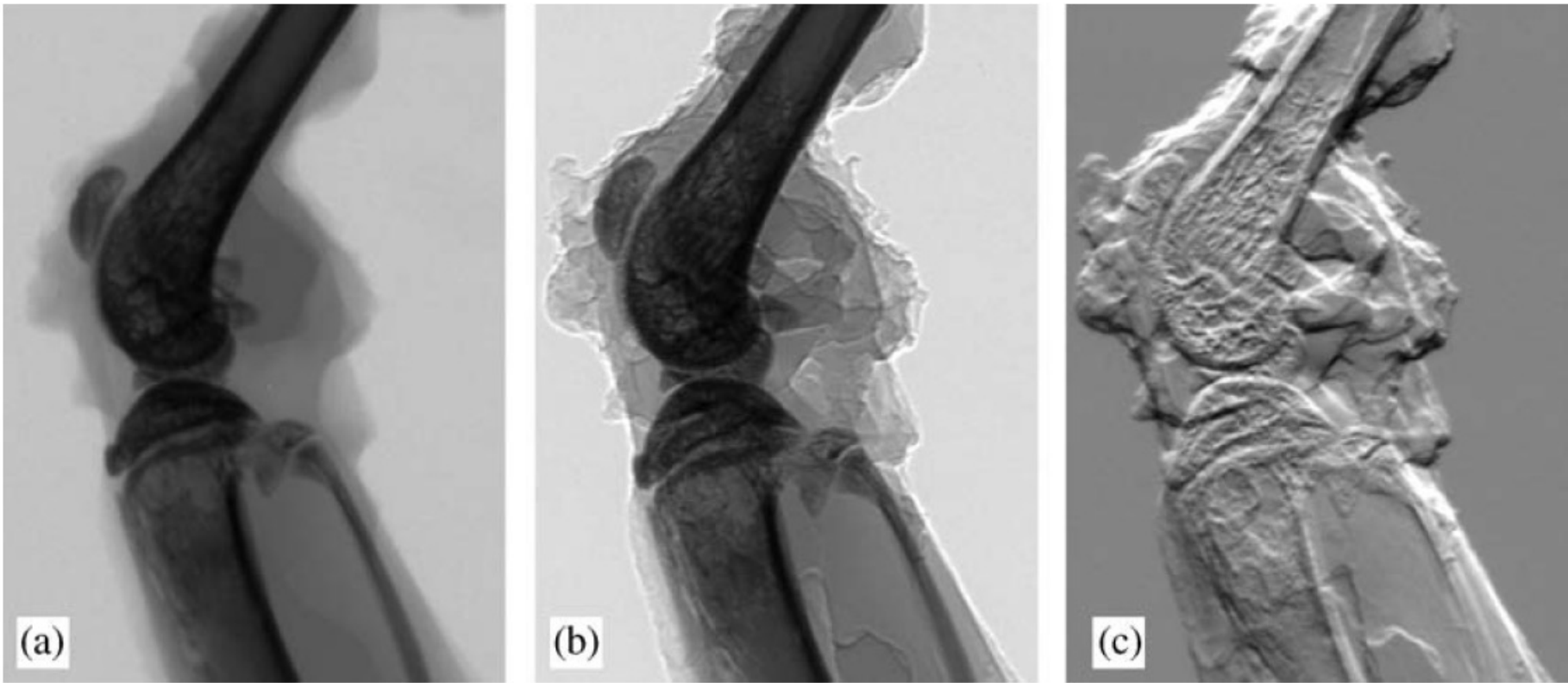


- The Bragg crystal selects the momentum !
- Local beam deflection are measured, the first spatial derivative of the phase $\partial\Phi / \partial y$ is detected
- Large field of view
- Need synchrotron radiation
(monochromaticity and collimated beam!)

+

-

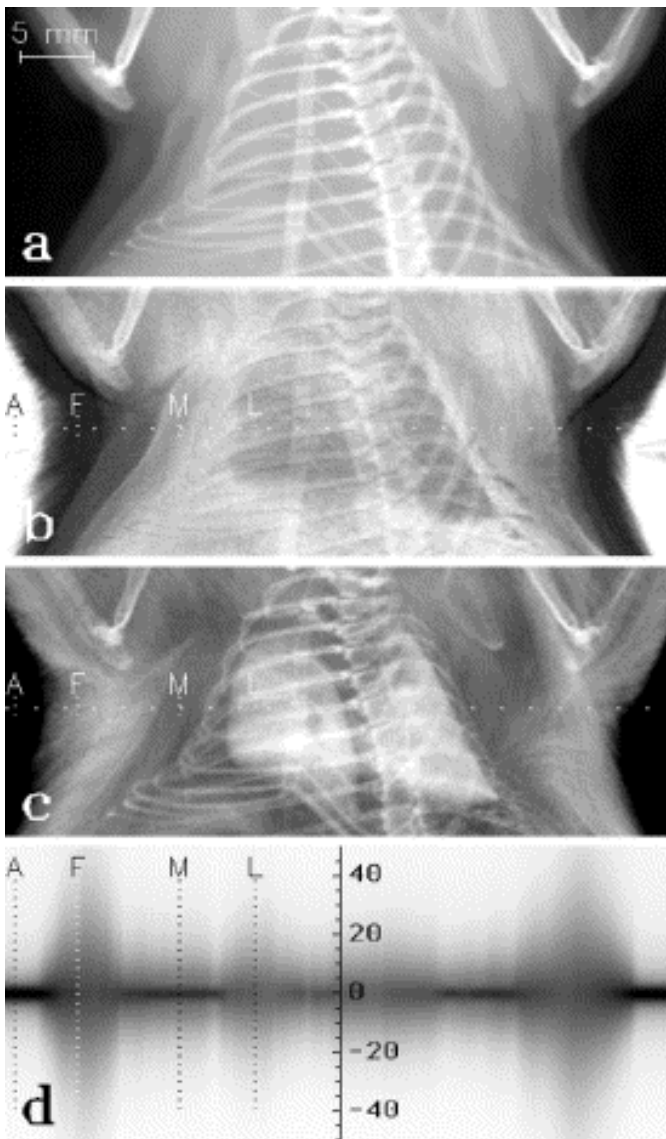
Bone AND soft tissue imaging



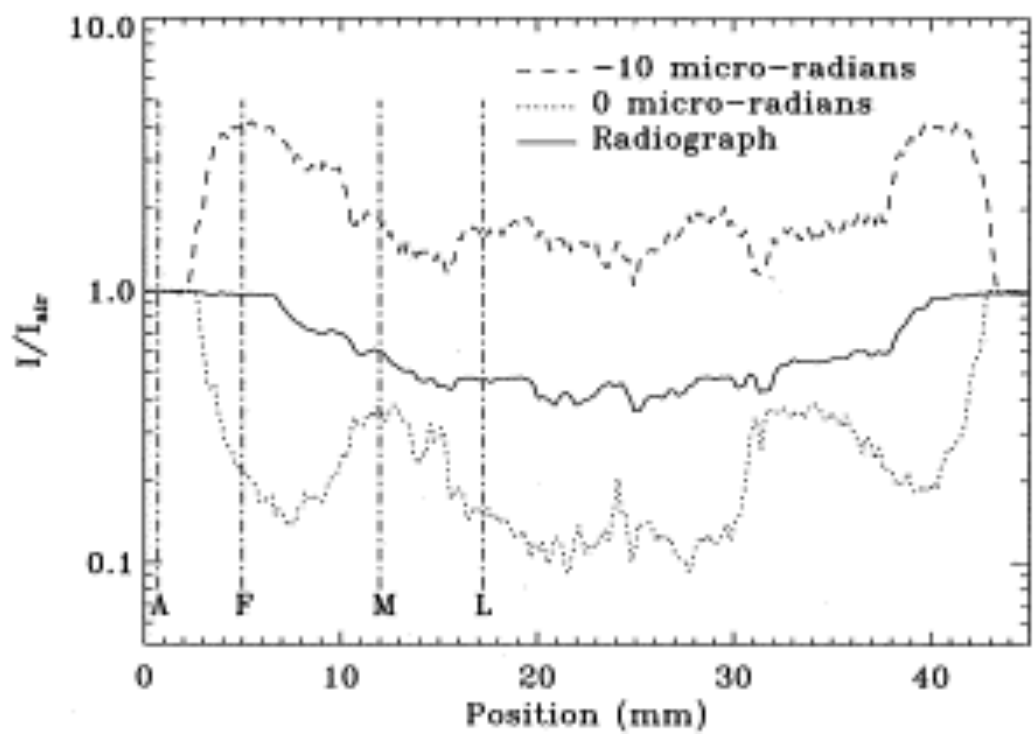
(a) Transmission image; (b) and (c) are the apparent absorption and the refraction images, respectively. It is readily seen that the apparent absorption (b) is similar to the conventional transmission image (a), but gives a considerably clearer view of the soft tissues. The trabecular structure of the bones is also enhanced in the DE images. These improvements are due to extinction, i.e. the rejection of ultra-small angle scattering. The refraction effects are singled out in image (c), which represents a quantitative map of the deviation angle. This image, which does not rely on absorption, looks quite different from the others and conveys complementary information. For instance, it allows the visualization of bones and soft tissue with similar brightness and contrast, so that the trabecular structure of the bones and the details of the soft tissue are visualized on the same grayscale.

R.H. Menk et al. NIMA 548 (2005) 213–220

Lung imaging

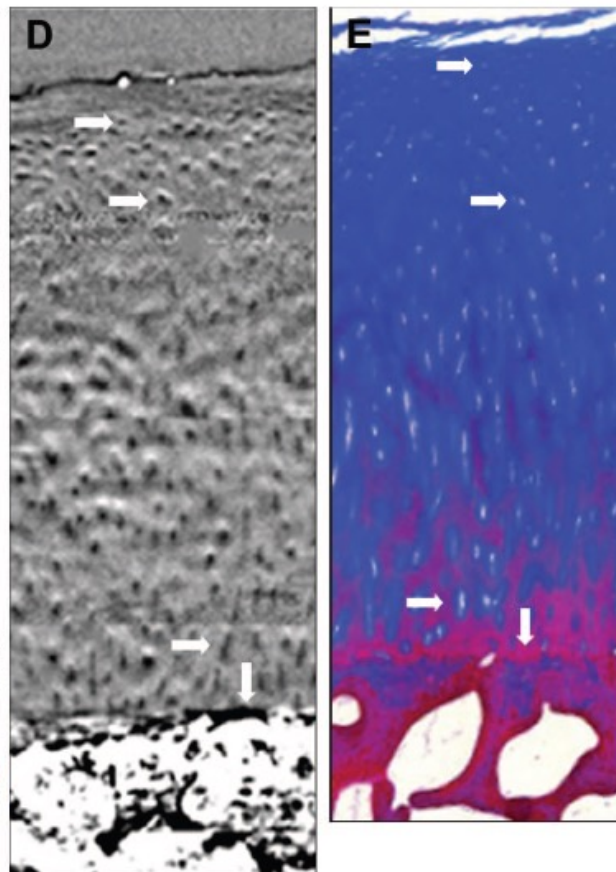
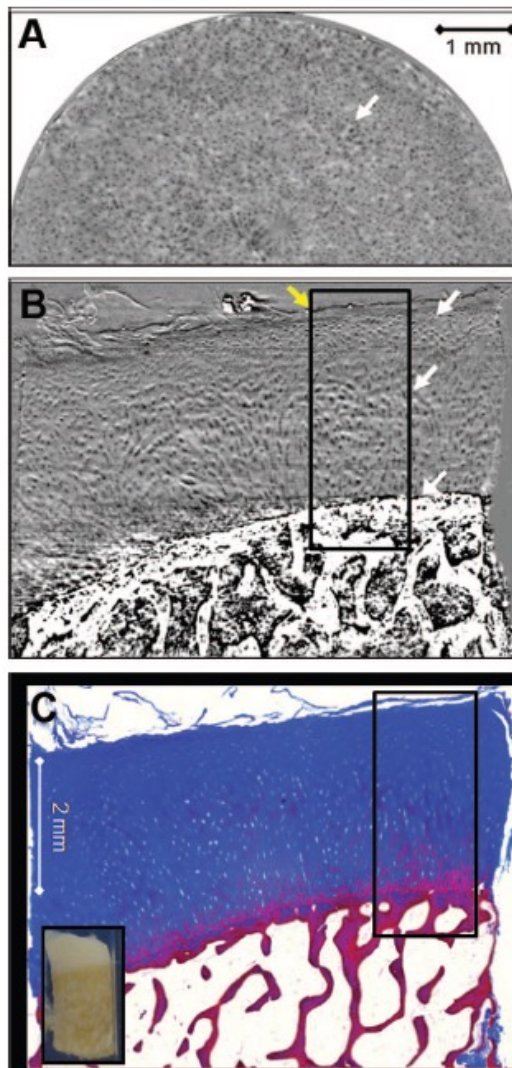
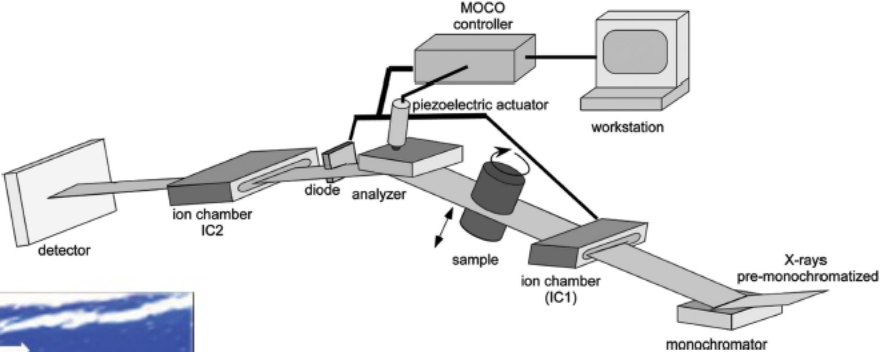


- (a) Normal radiograph of a mouse at 18 keV. Darker color represents greater X-ray intensity.
- (b) DEI images with the analyzer at -10 murad
- (c) DEI images with the analyzer at 0 murad.
- (d) Rocking-curve scan through the middle of the lung, indicated by the horizontal dashed lines on the left; Vertical axis corresponds to changing analyzer angle from -50 to 50 murad



Zhong et al., NIMA, 450 (2-3), (2000), pp. 556-567

Visualization of cartilage



CT of a normal cartilage sample (50% slope position of the analyzer crystal, 26 keV, pixel size $8^2 \mu\text{m}^2$) and corresponding section from histologic preparation.

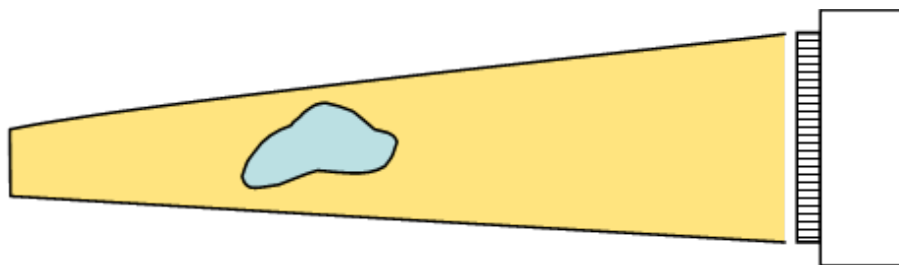
- (A) Portion of an axial CT acquired at the level of the radial zone of the cartilage.
- (B) Coronal plane extracted from the reconstructed CT volume.
- (C) Histologic section (Azan staining), note the original osteochondral cylinder (inset).
- (D) Magnified ROI indicated by inserted rectangle from B.
- (E) Magnified ROI indicated by inserted rectangle from C.

Free-space propagation

Cloetens et al., Appl. Phys. Lett. 75, 2912 (1999)

Snigirev et al., Rev. Sci. Instrum., 66 (12): 5486 (1995)

2D detector

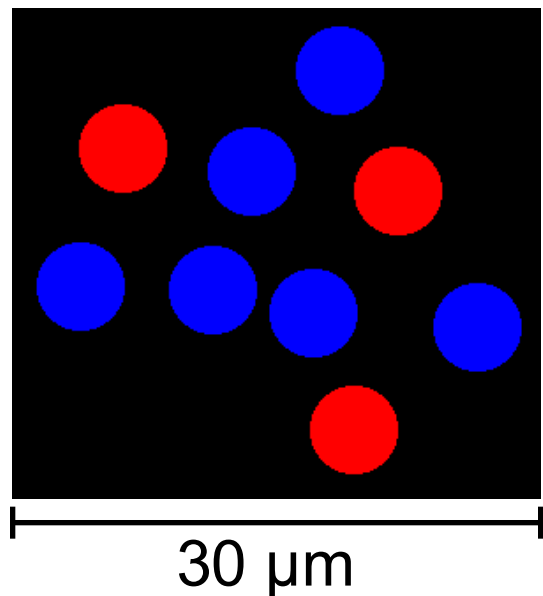


- Propagation turns phase distortions into interference fringes, according to Fresnel diffraction
- The measured quantity is $(\partial^2/\partial x^2 + \partial^2/\partial y^2)\Phi$, or more complicated expressions, depending on the sample-to-detector distance
- **Simple setup (at least in principle)** } +
- **Needs well-defined beam profile** } -
- **Needs high-resolution detector** } -

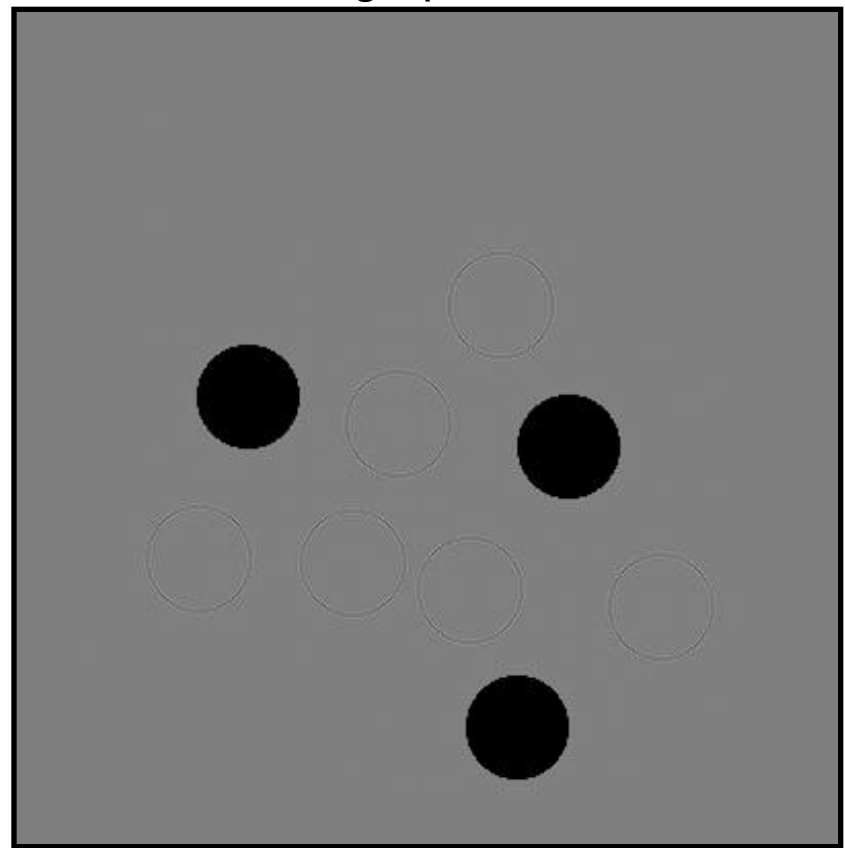
Free-space propagation

“Sample”: cluster of 5-micron spheres.

Red: absorbers, Blue: phase shifters



Simulated radiographs:



Photon energy: 12.4 keV

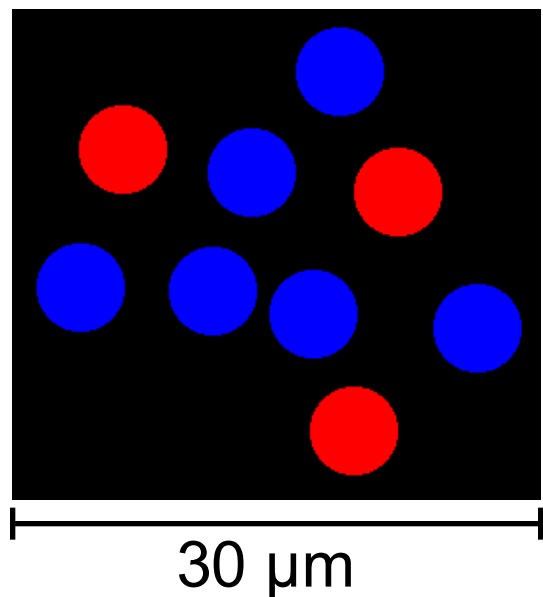
Distance to detector: from 0.3 to 1000 mm

Slide courtesy T. Weitkamp, ESRF

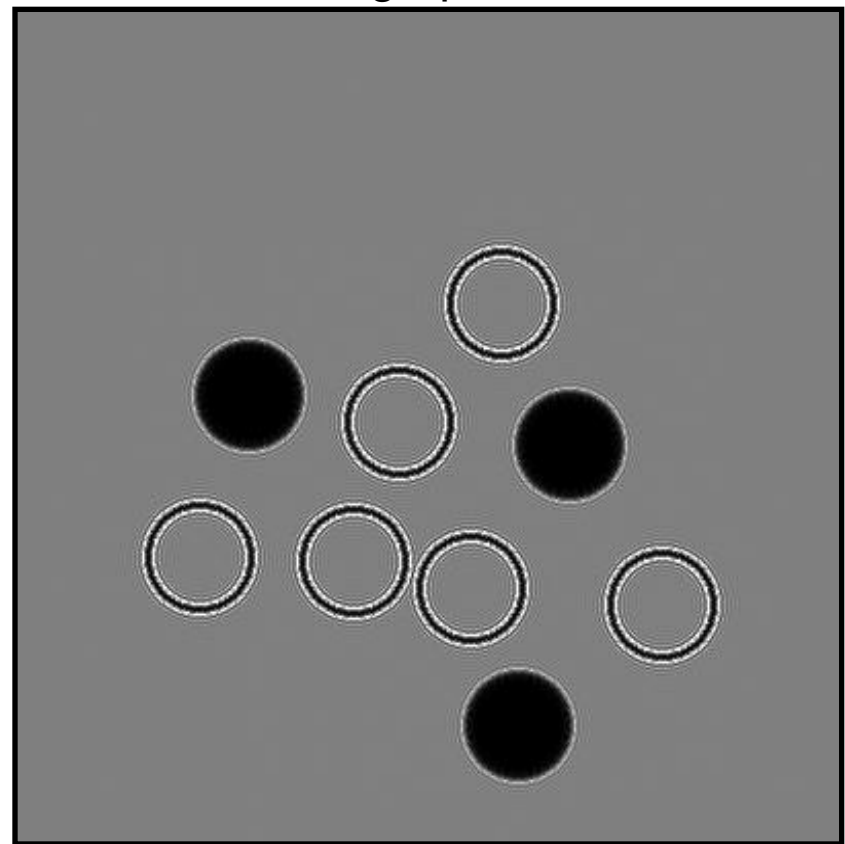
Free-space propagation

“Sample”: cluster of 5-micron spheres.

Red: absorbers, Blue: phase shifters



Simulated radiographs:



Photon energy: 12.4 keV

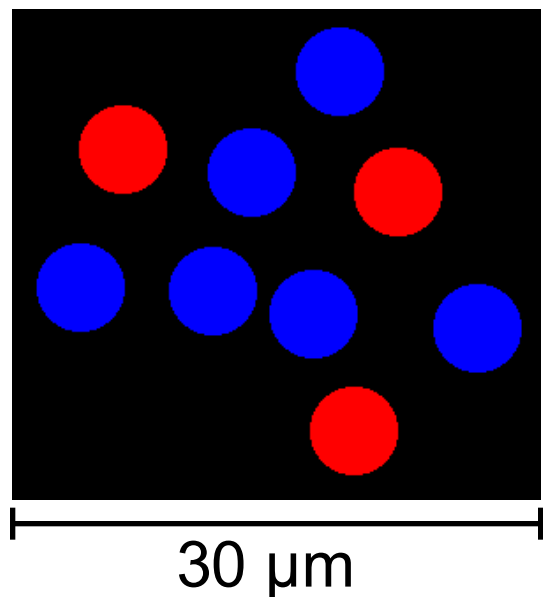
Distance to detector: from 0.3 to 1000 mm

Slide courtesy T. Weitkamp, ESRF

Free-space propagation

“Sample”: cluster of 5-micron spheres.

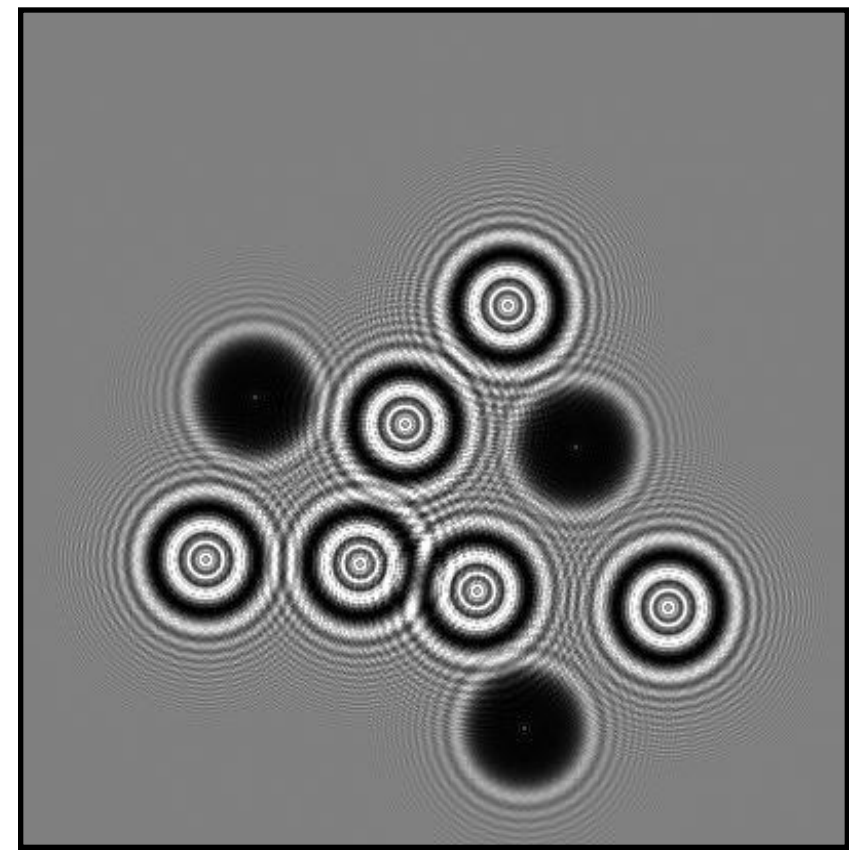
Red: absorbers, Blue: phase shifters



Photon energy: 12.4 keV

Distance to detector: from 0.3 to 1000 mm

Simulated radiographs:



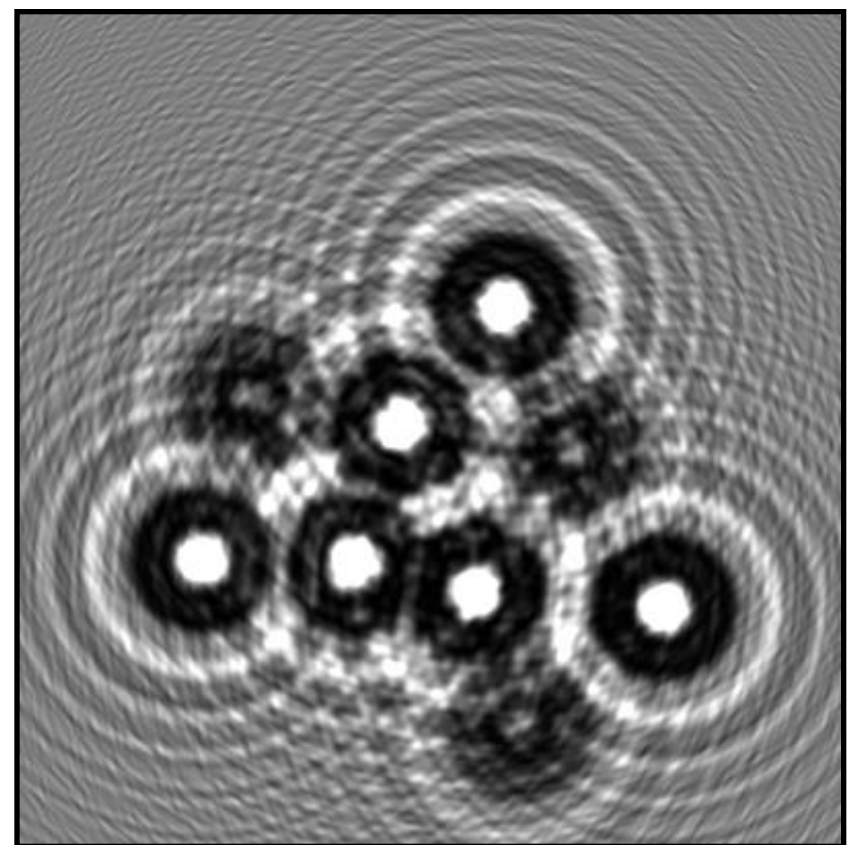
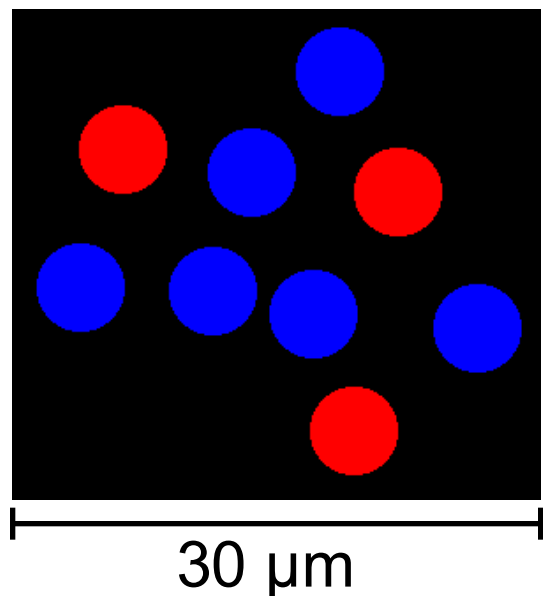
Slide courtesy T. Weitkamp, ESRF

Free-space propagation

“Sample”: cluster of 5-micron spheres.

Red: absorbers, Blue: phase shifters

Simulated radiographs:



Photon energy: 12.4 keV

Distance to detector: from 0.3 to 1000 mm

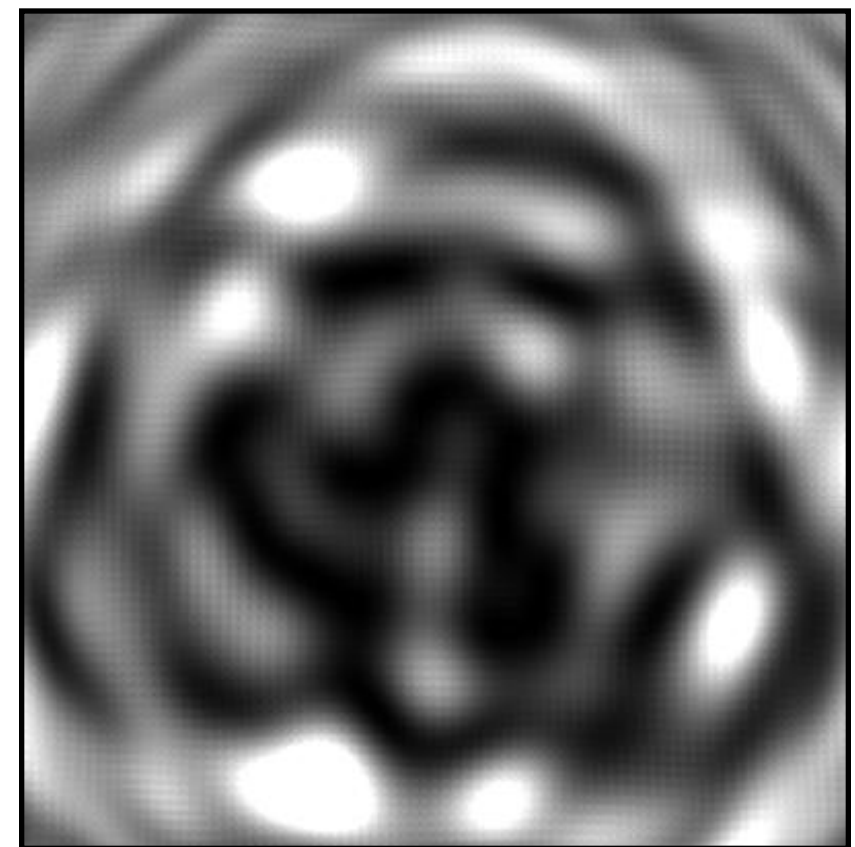
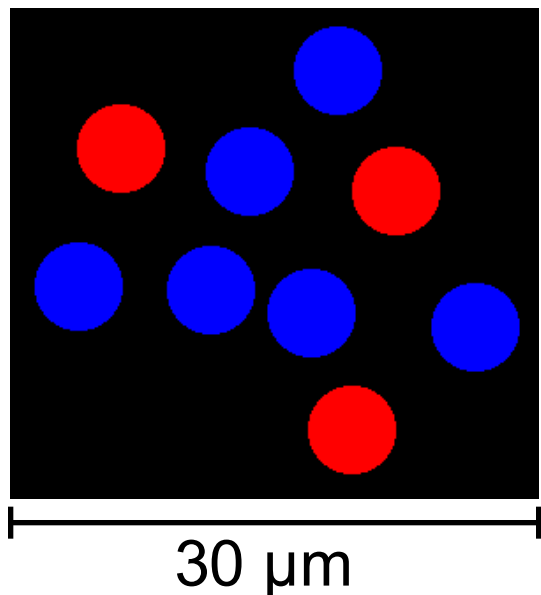
Slide courtesy T. Weitkamp, ESRF

Free-space propagation

“Sample”: cluster of 5-micron spheres.

Red: absorbers, Blue: phase shifters

Simulated radiographs:

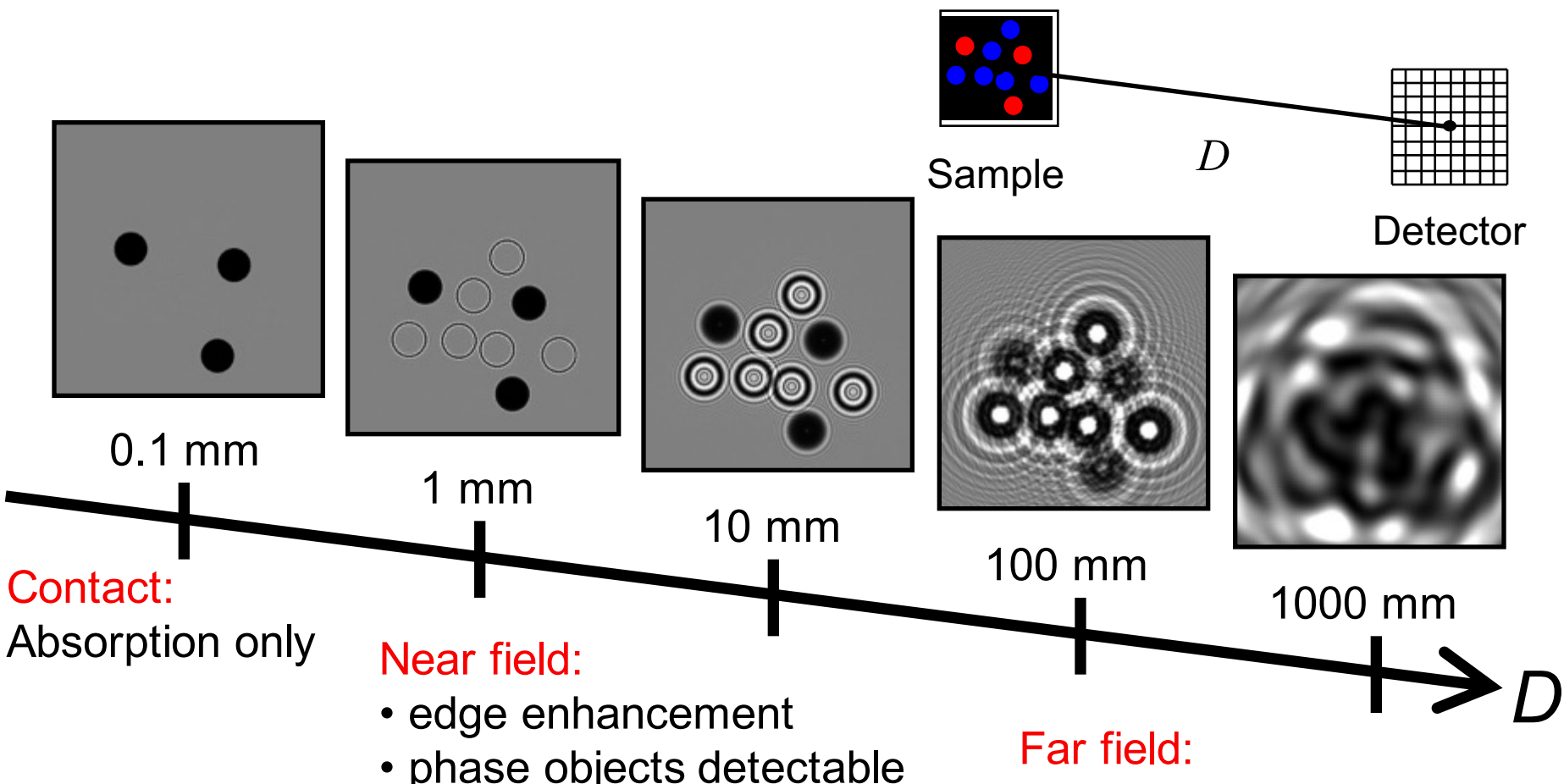


Photon energy: 12.4 keV

Distance to detector: from 0.3 to 1000 mm

Slide courtesy T. Weitkamp, ESRF

Propagation-based phase contrast imaging

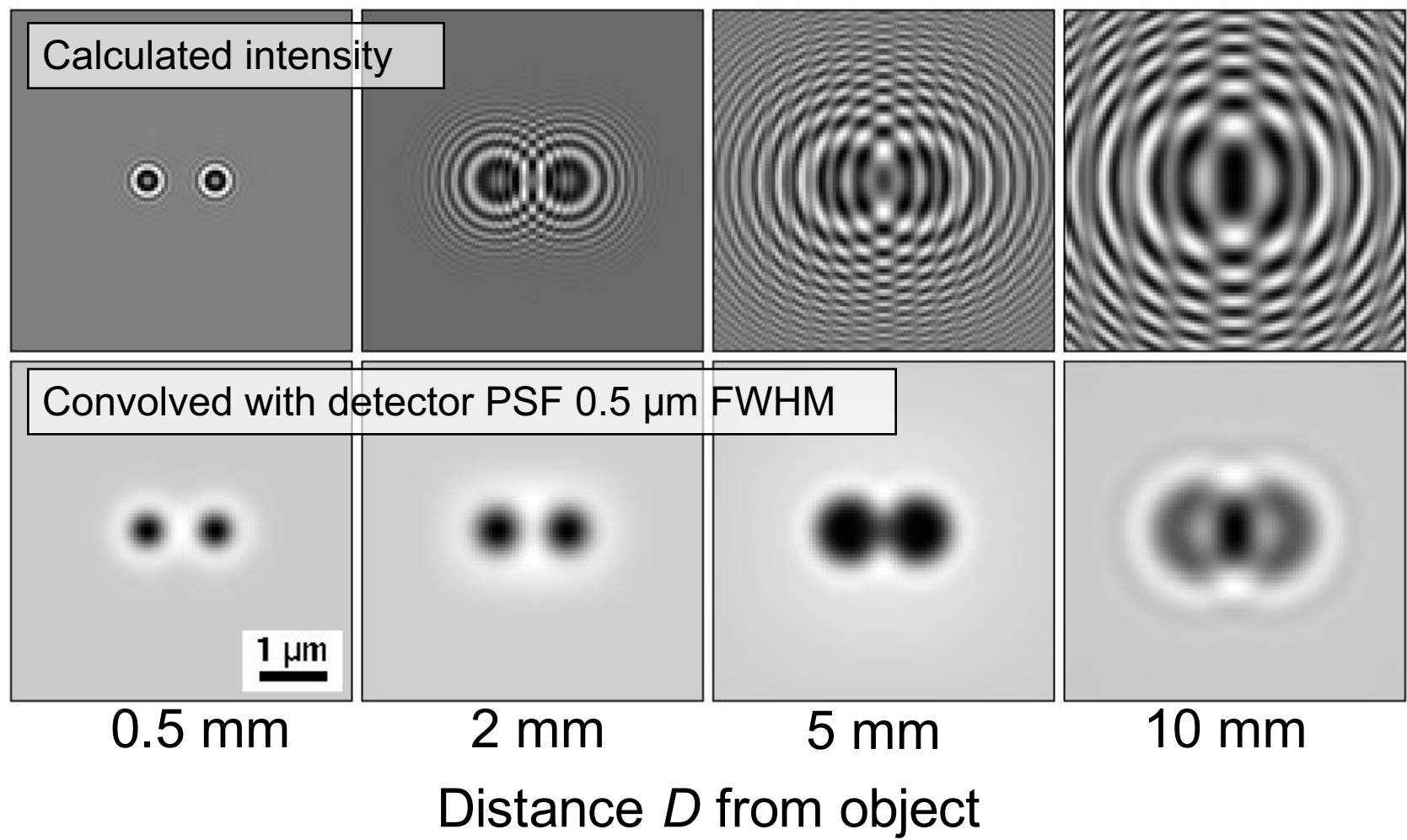


$$H(\nu_x, \nu_y) = \exp \left[-i2\pi \sqrt{\frac{1}{\lambda^2} - \nu_x^2 - \nu_y^2 \cdot d} \right]$$

Transfer function of the free space → Phase factor builds up!

Propagation and resolution: Fresnel diffraction

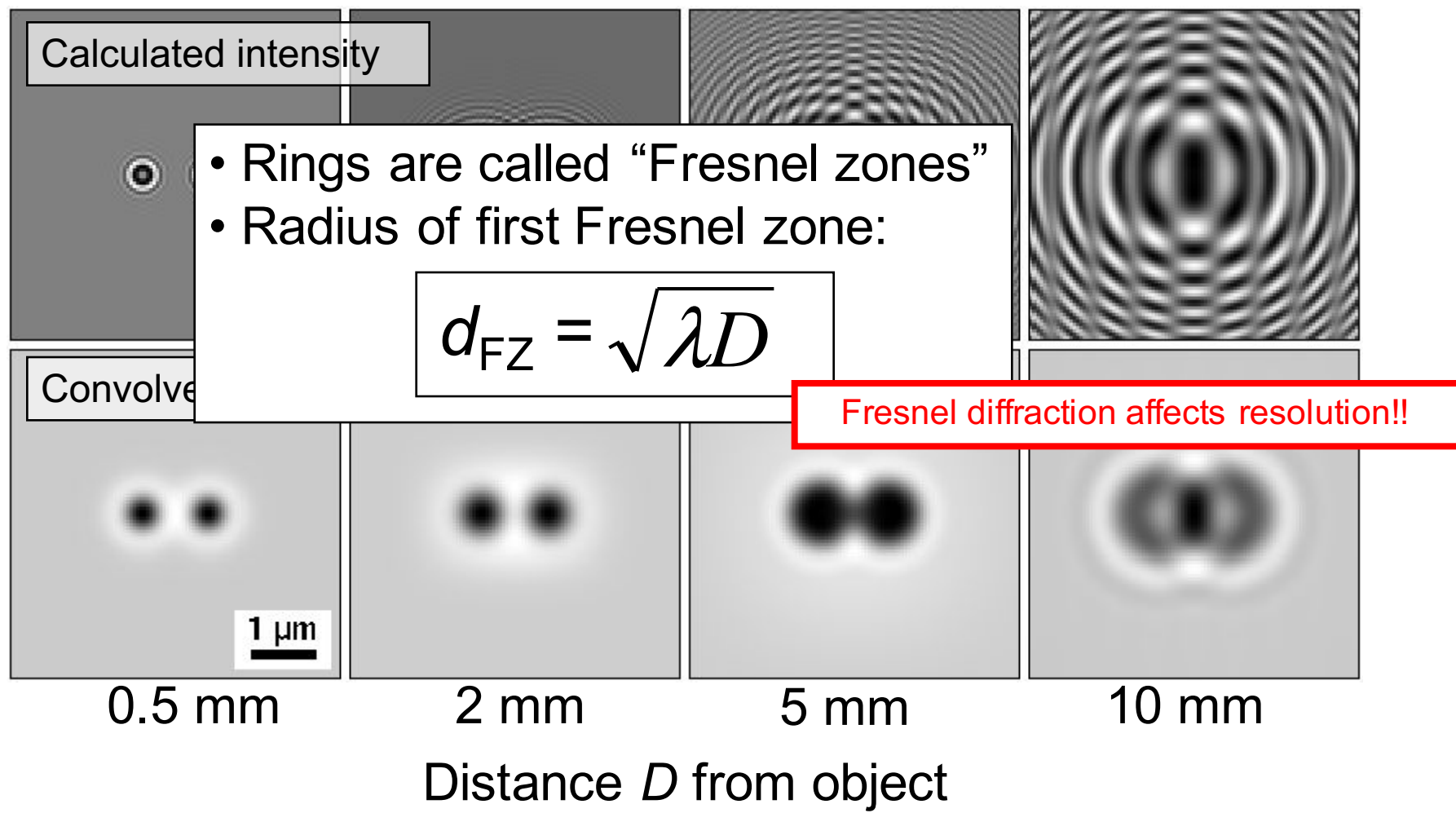
Intensity downstream of two-point object @ 20 keV



Reference: T. Weitkamp, *Imaging and Tomography with High Resolution Using Coherent Hard Synchrotron Radiation*, Cuvillier Verlag, Göttingen, PhD thesis, University Hamburg, 2002

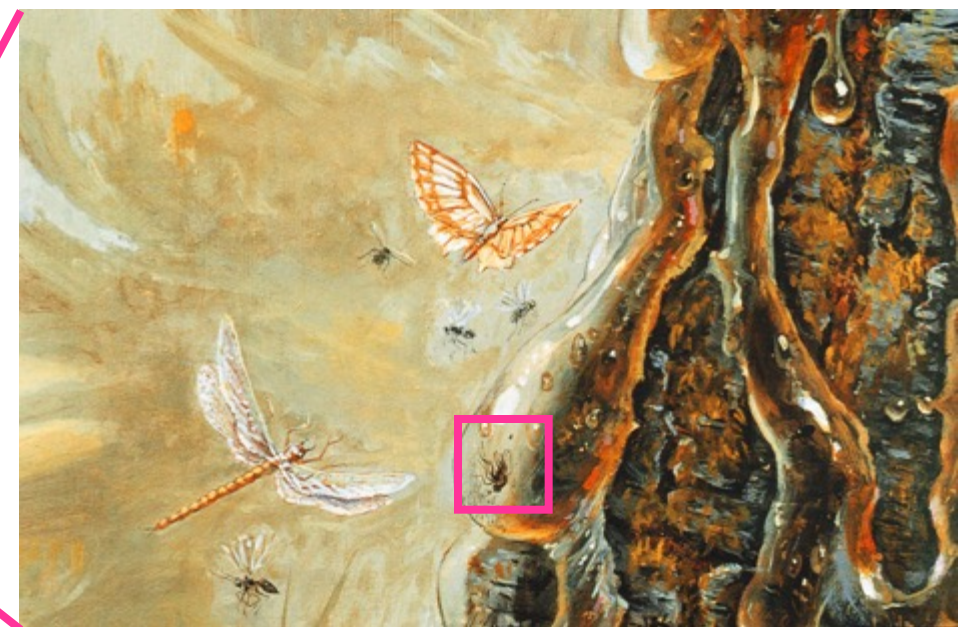
Propagation and resolution: Fresnel diffraction

Intensity downstream of two-point object @ 20 keV



Reference: T. Weitkamp, *Imaging and Tomography with High Resolution Using Coherent Hard Synchrotron Radiation*, Cuvillier Verlag, Göttingen, PhD thesis, University Hamburg, 2002

Revisiting the far past with X-ray phase contrast



40 millions years ago, in the forest...

Courtesy of E.M. Friis,
Swedish Museum of Natural History, Stockholm

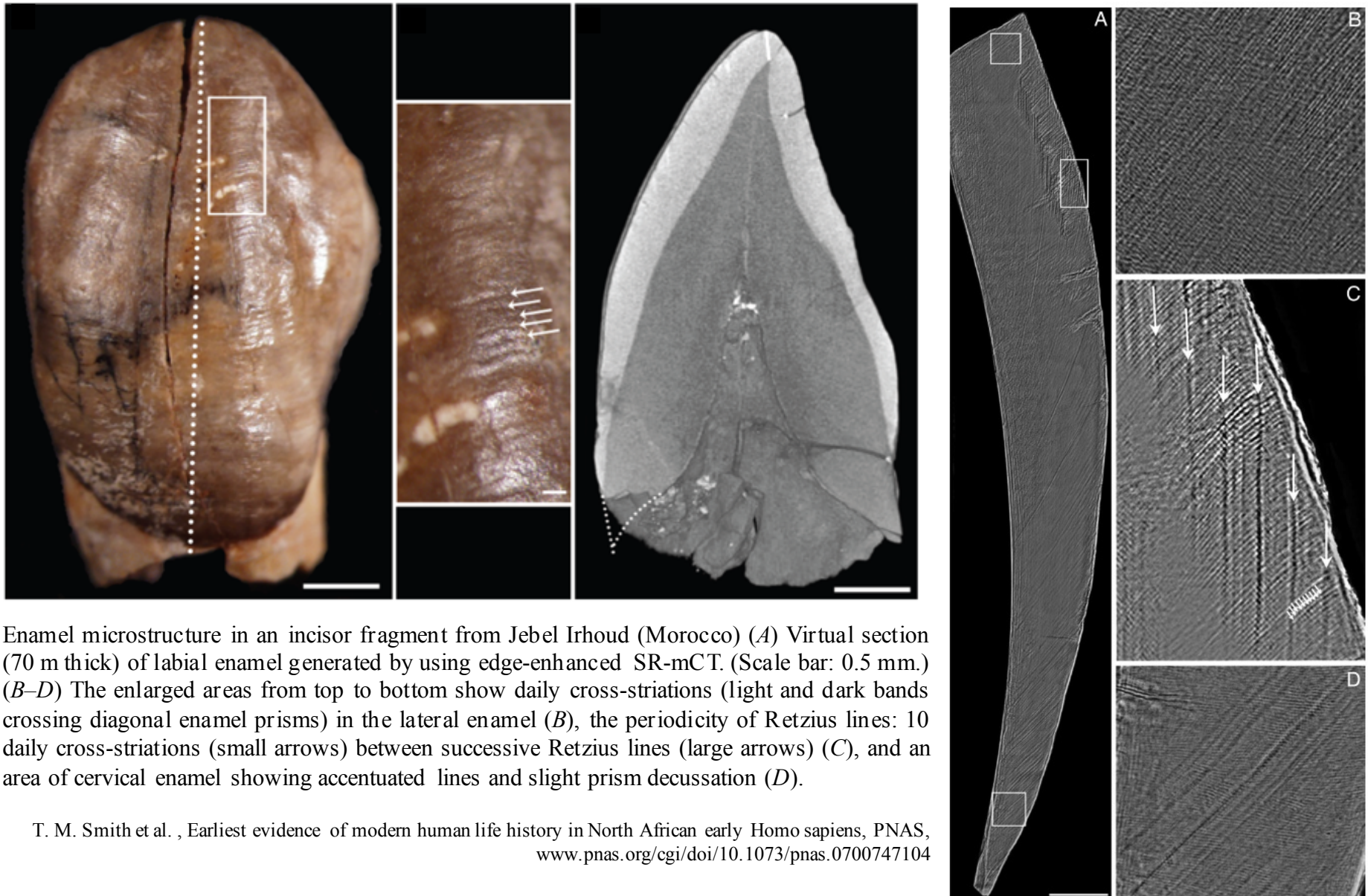
Revisiting the far past with X-ray phase contrast



40 millions years ago, in the forest...

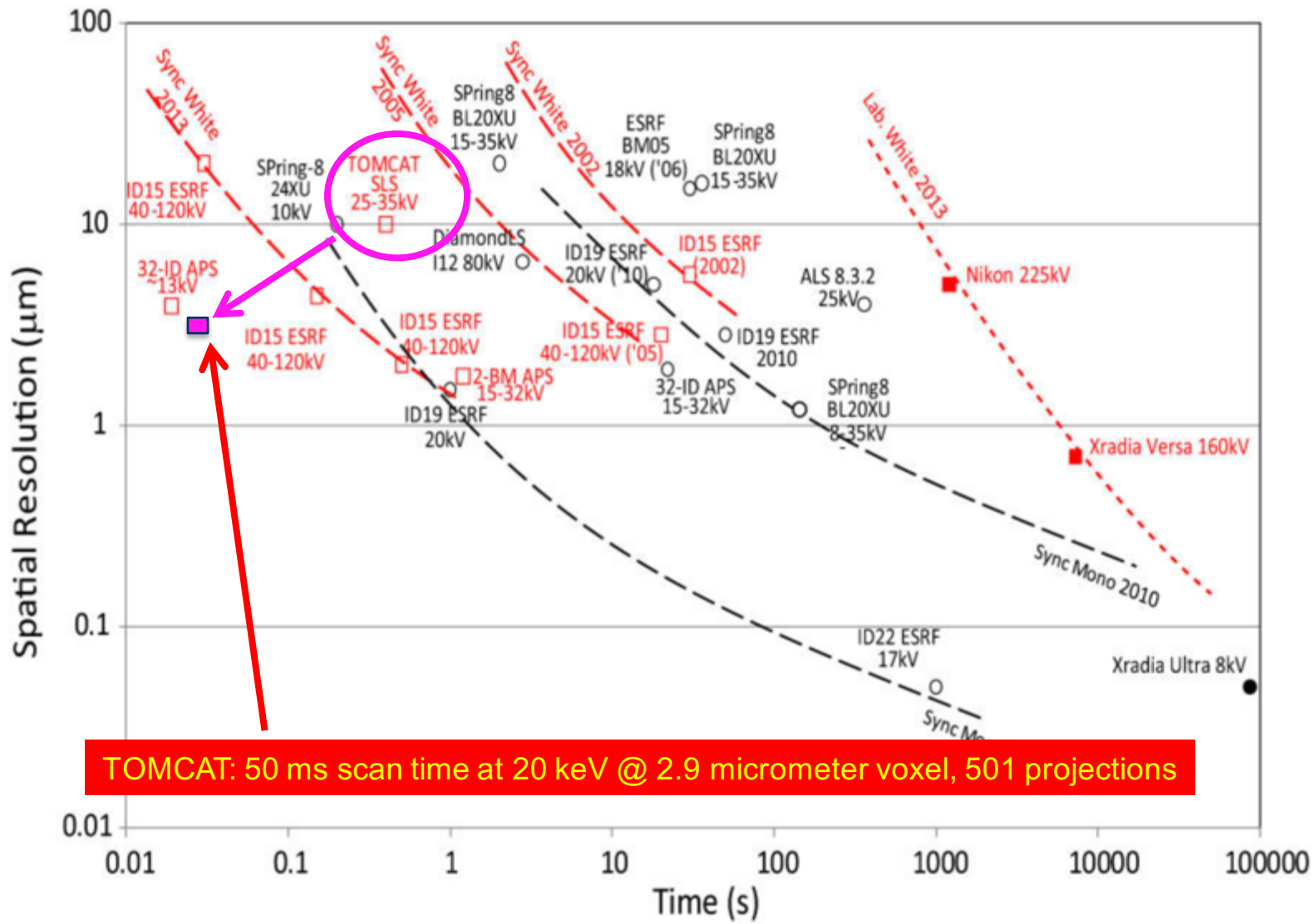
Courtesy of E.M. Friis,
Swedish Museum of Natural History, Stockholm

Edge-enhancement @ work



T. M. Smith et al. , Earliest evidence of modern human life history in North African early *Homo sapiens*, PNAS,
www.pnas.org/cgi/doi/10.1073/pnas.0700747104

Ultrafast imaging: towards 20 Hz imaging

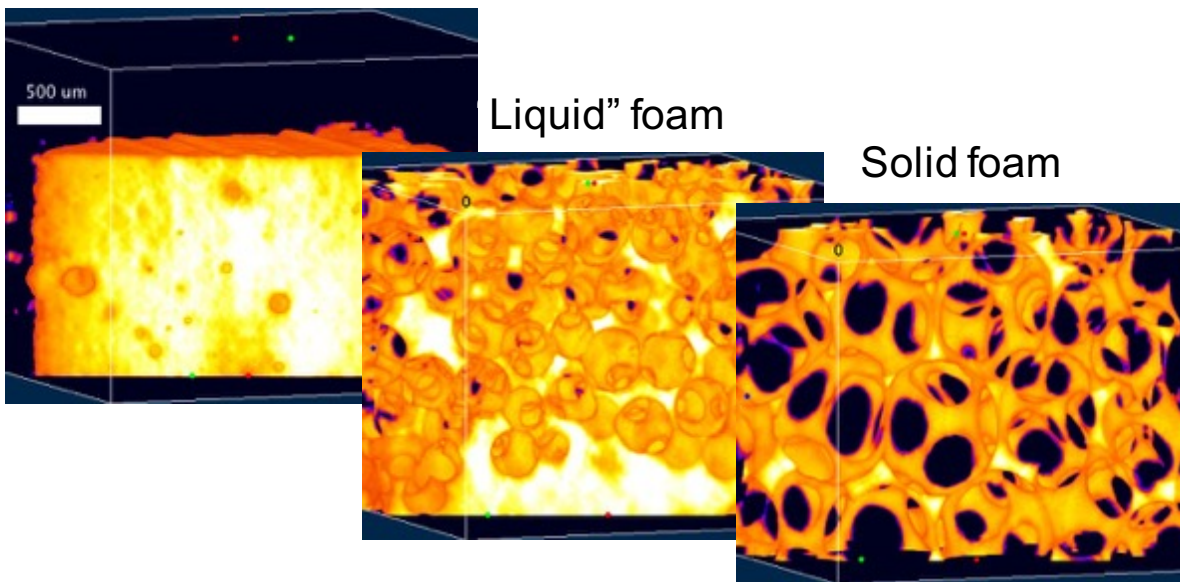


Maire and Whitters, International Materials Review 2014

Nucleation process in polyurethane reactive foam

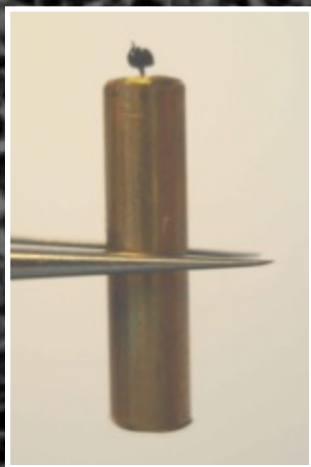


Nucleation

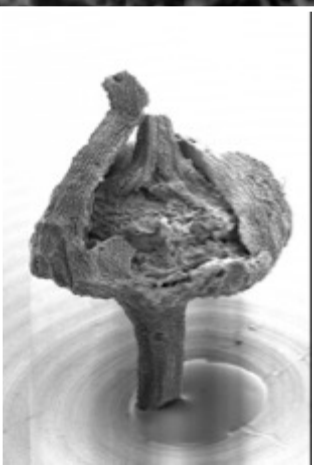


Data courtesy of E. Solorzano and S. Alonso
Univ. Valladolid

Charcoalified flowers imaged with PC-SR-TM



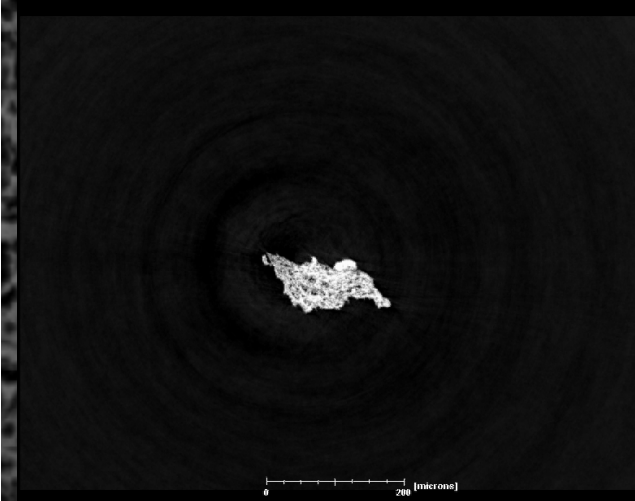
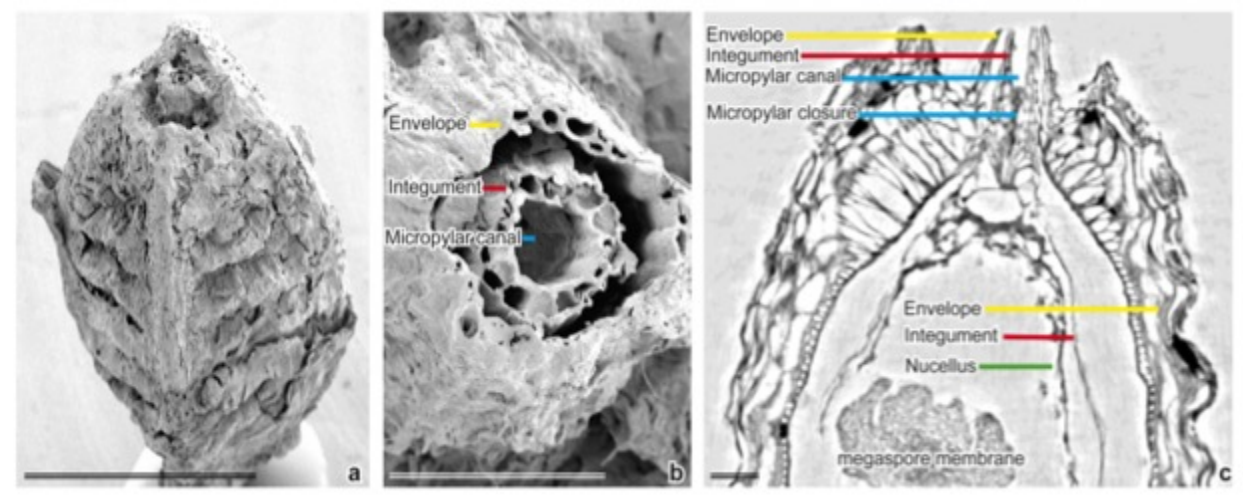
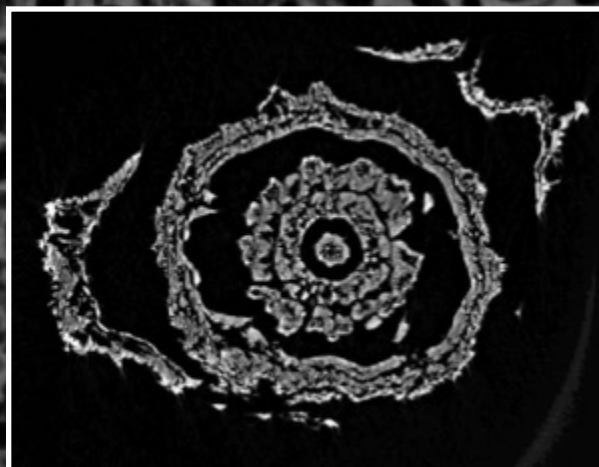
Uncoated flower ready
for PCXTM



SEM



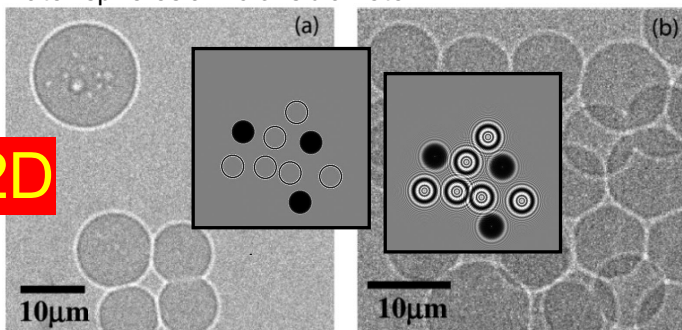
High-resolution (350 nm voxel size) PCXTM views: Sagittal (left) and axial (right)
sections showing internal features of placenta.



Single-step phase retrieval: 2D and 3D

Latex spheres 9 microns diameter

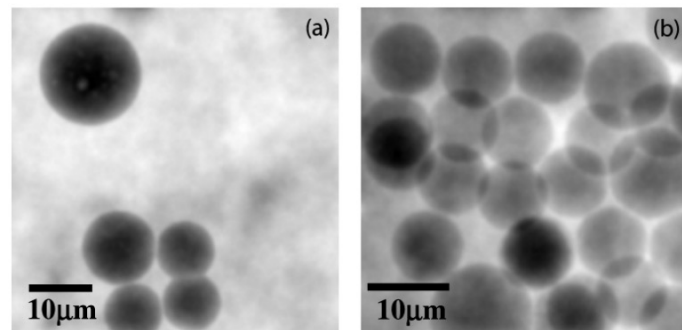
2D



Absorption+ Edge-enhancement

$$T(\mathbf{r}_\perp) = -\frac{1}{\mu} \log_e \left(\mathcal{F}^{-1} \left\{ \mu \frac{\mathcal{F}\{I(\mathbf{r}_\perp, z=R_2)\}/I^{in}}{R_2 \delta |\mathbf{k}_\perp|^2 + \mu} \right\} \right).$$

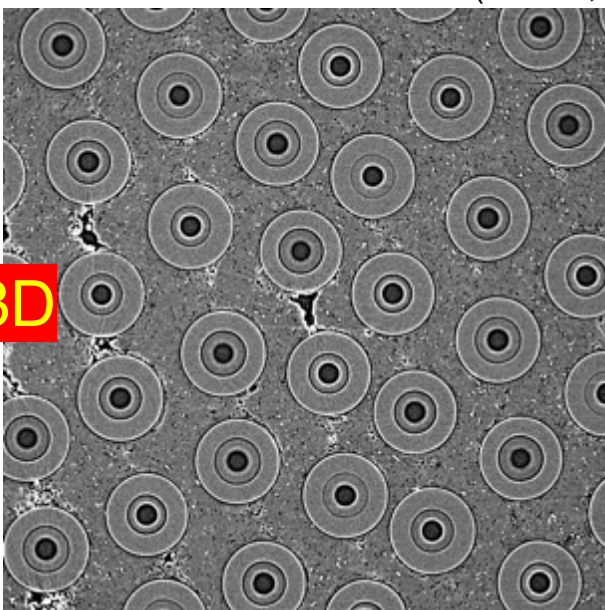
D. Paganin, JoM 206, 33-40, 2002



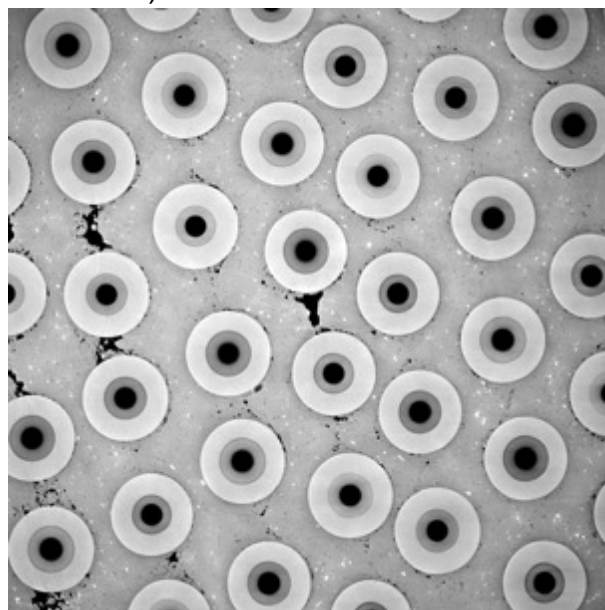
Phase-retrieved projection

Aluminium matrix with SiC fibres (C Core, SiC sheath)

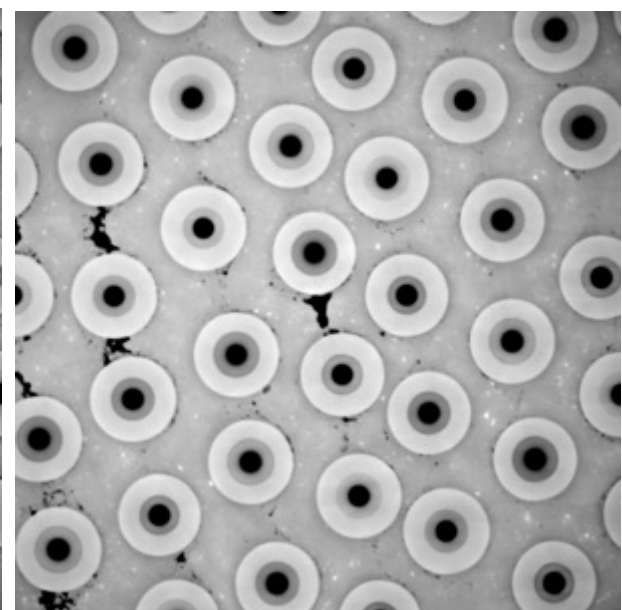
3D



Abs+Edge reconstruction



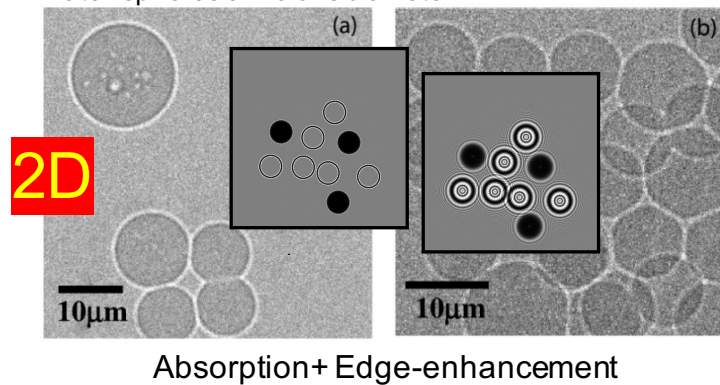
S. Irvine et al., accepted



Phase-retrieved reconstruction

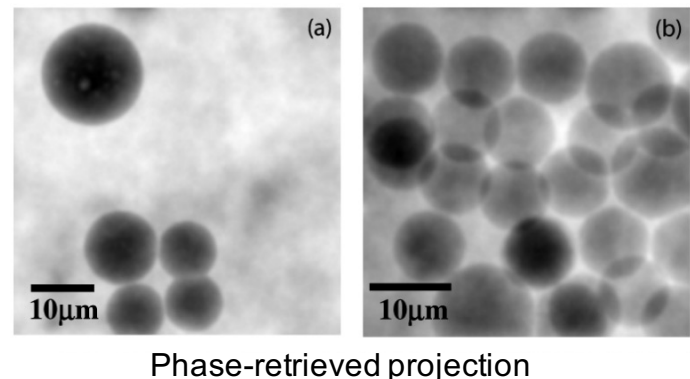
Single-step phase retrieval: 2D and 3D

Latex spheres 9 microns diameter

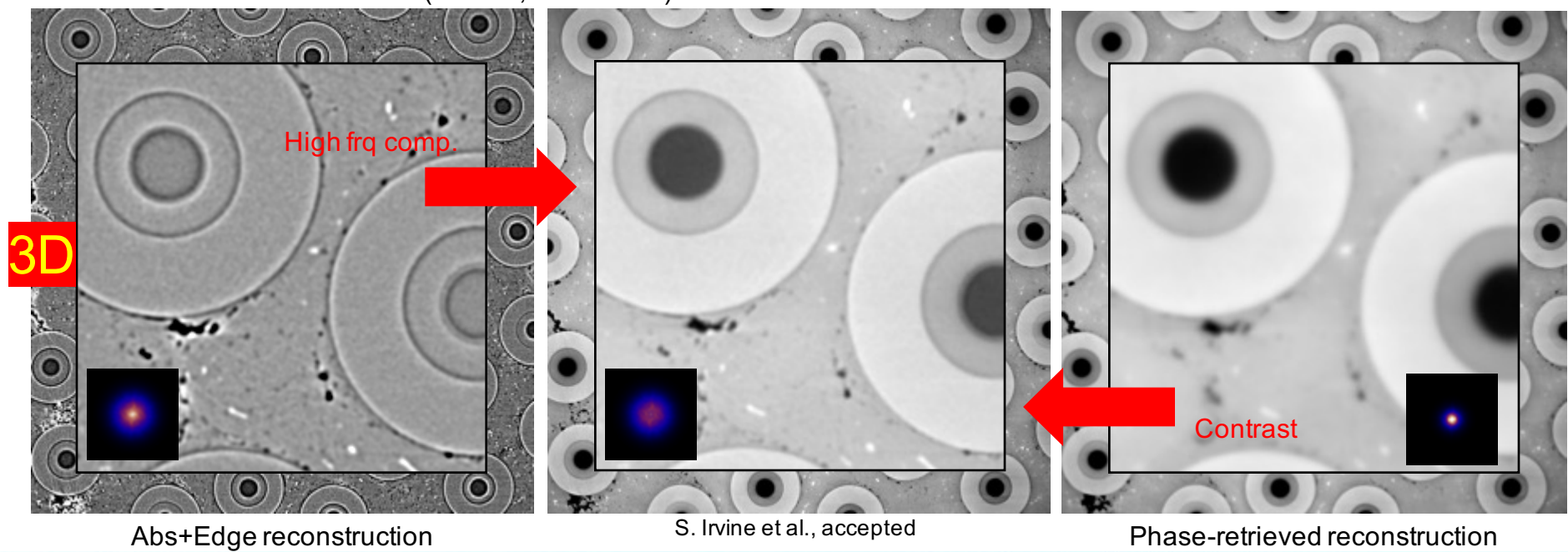


$$T(\mathbf{r}_\perp) = -\frac{1}{\mu} \log_e \left(\mathcal{F}^{-1} \left\{ \mu \frac{\mathcal{F}\{I(\mathbf{r}_\perp, z=R_2)\}/I^{in}}{R_2 \delta |\mathbf{k}_\perp|^2 + \mu} \right\} \right).$$

D. Paganin, JoM 206, 33-40, 2002



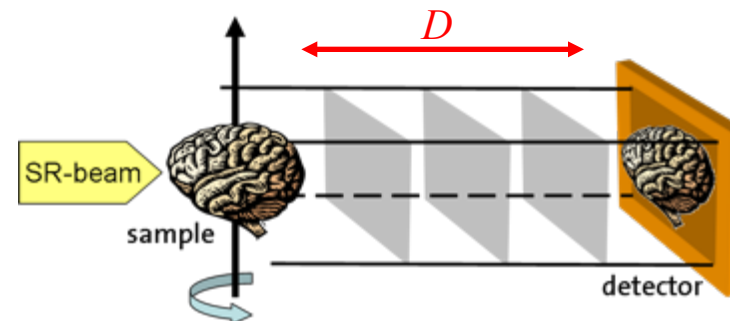
Aluminium matrix with SiC fibres (C Core, SiC sheath)



(Multiple-step) phase retrieval in the near field

Acquire images at multiple detector distances

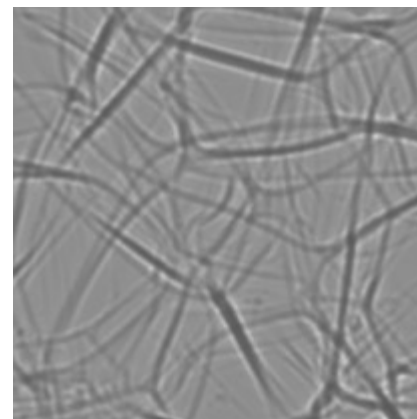
Retrieve the phase considering free-space propagation



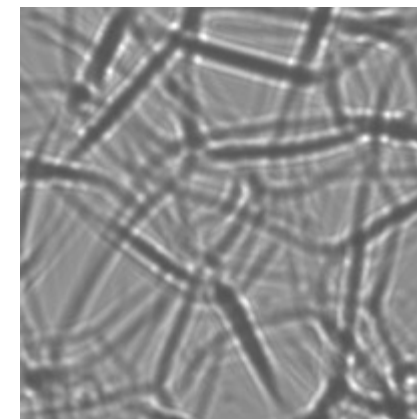
Example: non-absorbing foam @ 18 keV



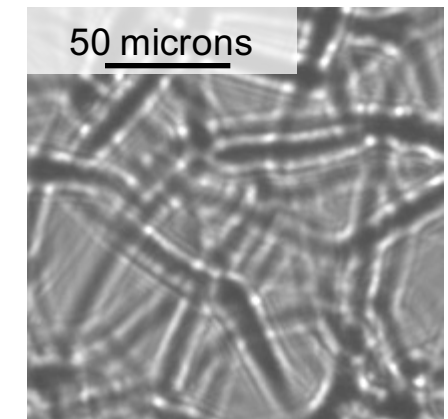
D = 0.03 m



D = 0.21 m



D = 0.51 m

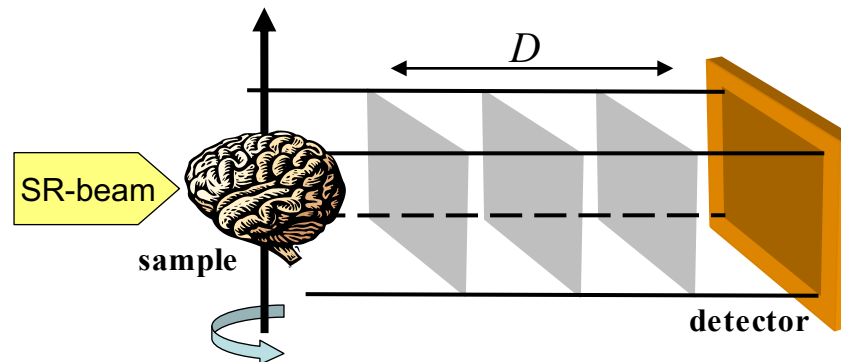


D = 0.90 m

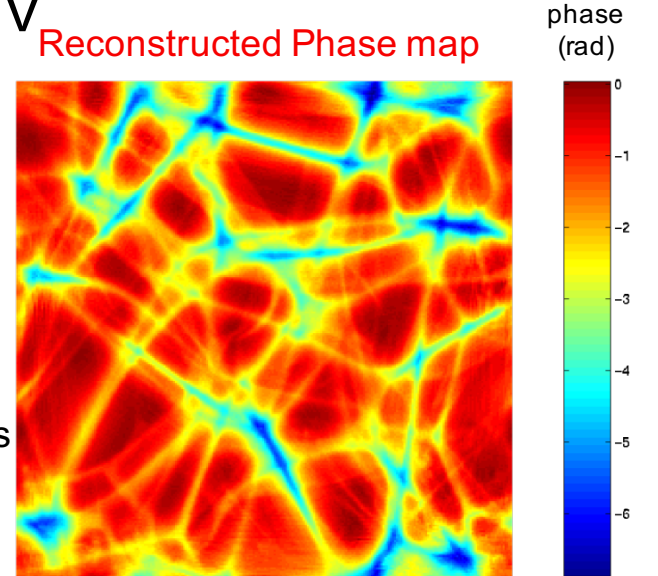
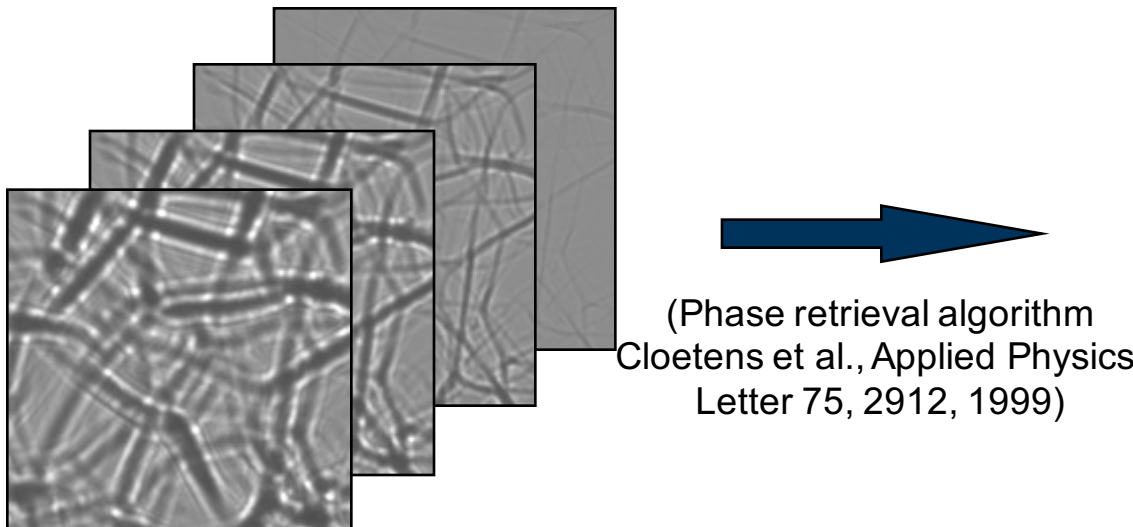
Images courtesy of P. Cloetens, ESRF

(Multiple-step) phase retrieval in the near field

- Acquire images at multiple detector distances
- Retrieve the phase considering free-space propagation



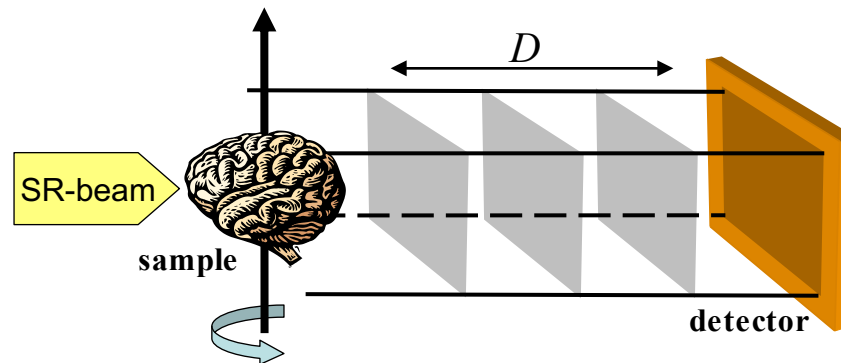
- Example: non-absorbing foam @ 18 keV



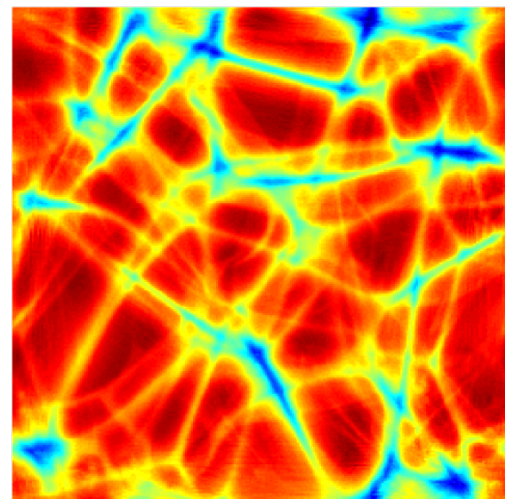
Images courtesy of P. Cloetens, ESRF

(Multiple-step) phase retrieval in the near field

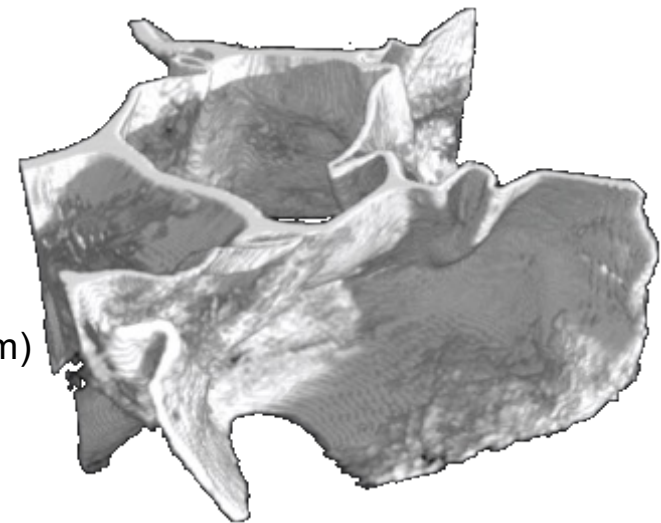
- Acquire images at multiple detector distances
- Retrieve the phase considering free-space propagation



- Example: non-absorbing foam @ 18 keV



(CT reconstruction algorithm)



Images courtesy of P. Cloetens, ESRF

Phase retrieval @ work



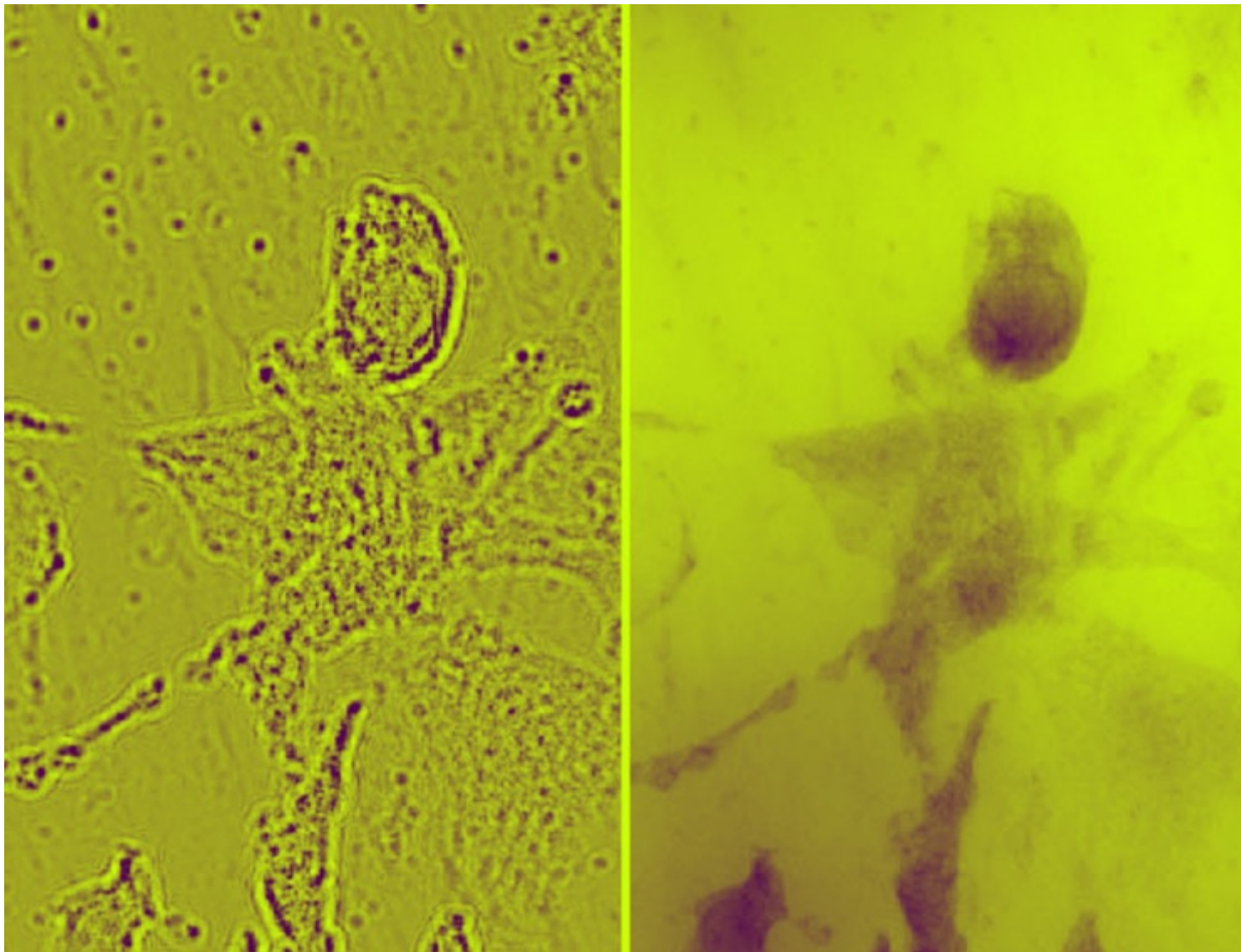
- (a) Absorption radiograph of a *Crossodactylodes bookermanni* frog embedded in a liquid-filled cylindrical glass sample holder.
- (b) Phase map retrieved from radiographs at sample-to-detector distances 18, 83, 283 and 973 mm. The bright areas are due to air bubbles in the liquid.
- (c) Tomographic slice through the frog head using the absorption radio-graphs and...
- (d) ...the retrieved phase maps.

Fine structures in the soft tissue are visible in (d) despite the presence of strongly absorbing structures (bone).

Reference:

J. Guigay et al., Optics Letters, Vol. 32, No. 12, June 15, 2007.

Freeze-dried neuron cell



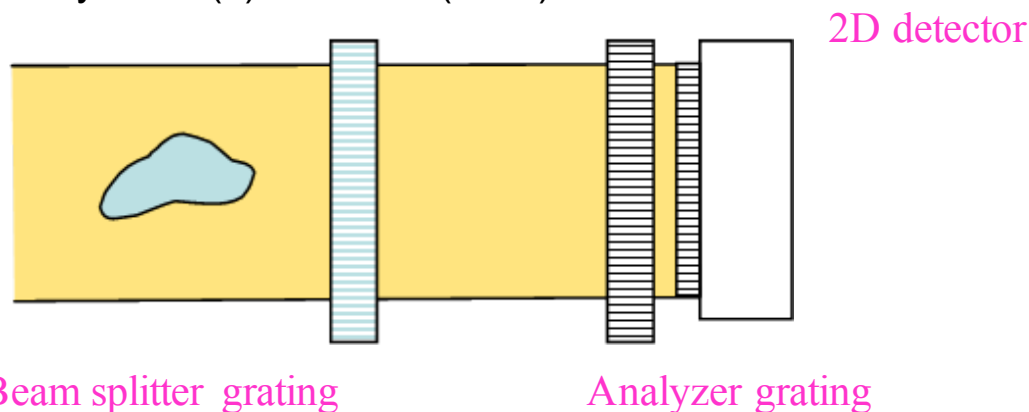
Edge-enhanced radiography

Retrieved phase map

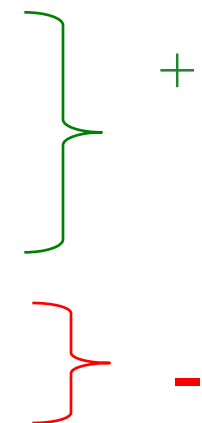
Mokso et al., Appl. Phys. Lett. 90, 144104 2007

Grating interferometry

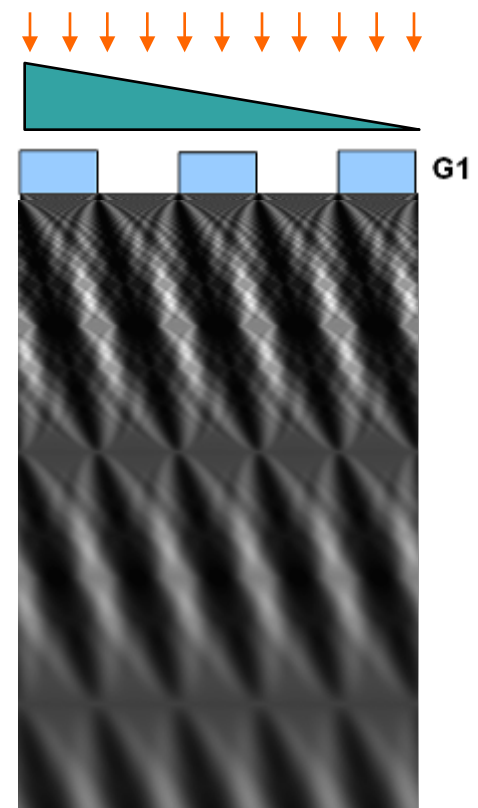
Weitkamp et al., Optics Express (13), 6296 (2005)
Pfeiffer et al., Nature Physics 2 (4): 258-261 (2006)



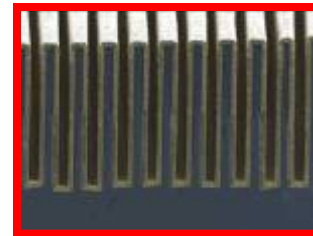
- The measured quantity is $(\partial\Phi/\partial y)$, as in DEI.
- Phase stepping technique followed by integration
- **Simple setup, mechanically robust**
- **Large field of view**
- **Usable with divergent and polychromatic beams**
- **Usable with standard X-ray tubes, low coherence required**
- **Moderate spatial resolution, limited by grid period**



Phase contrast recorded with grating interferometry

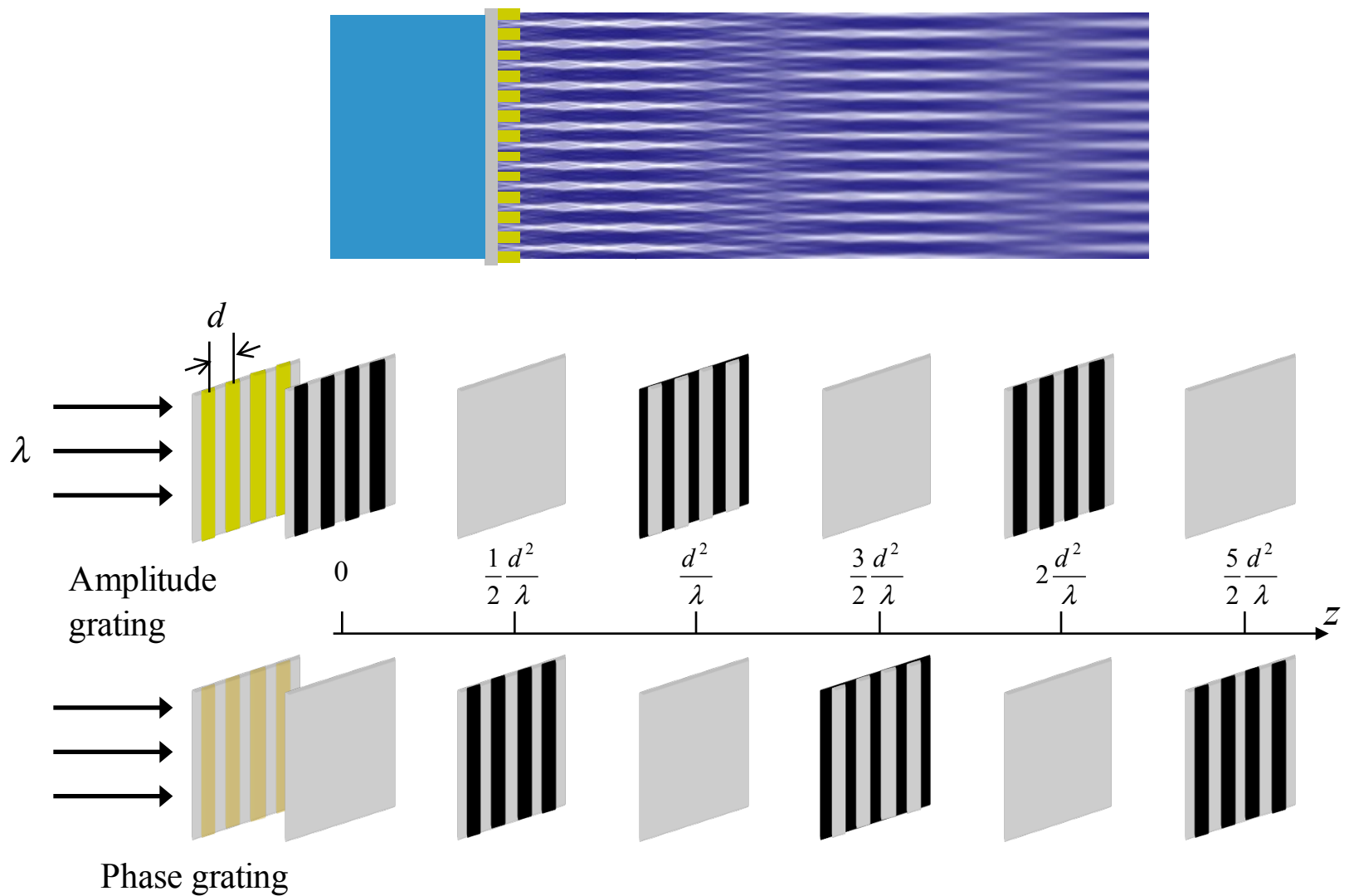


We „measure“ an interference → Interferometer



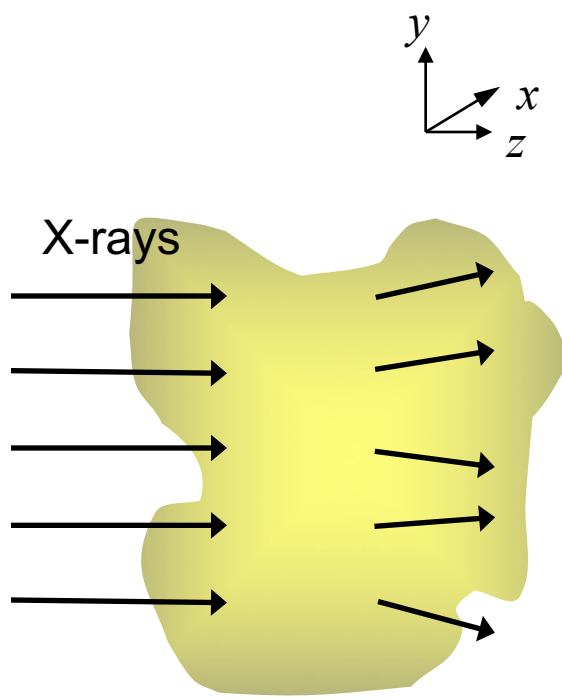
→ We transform an interference signal into an „readable“ image

Talbot Self Imaging Effect

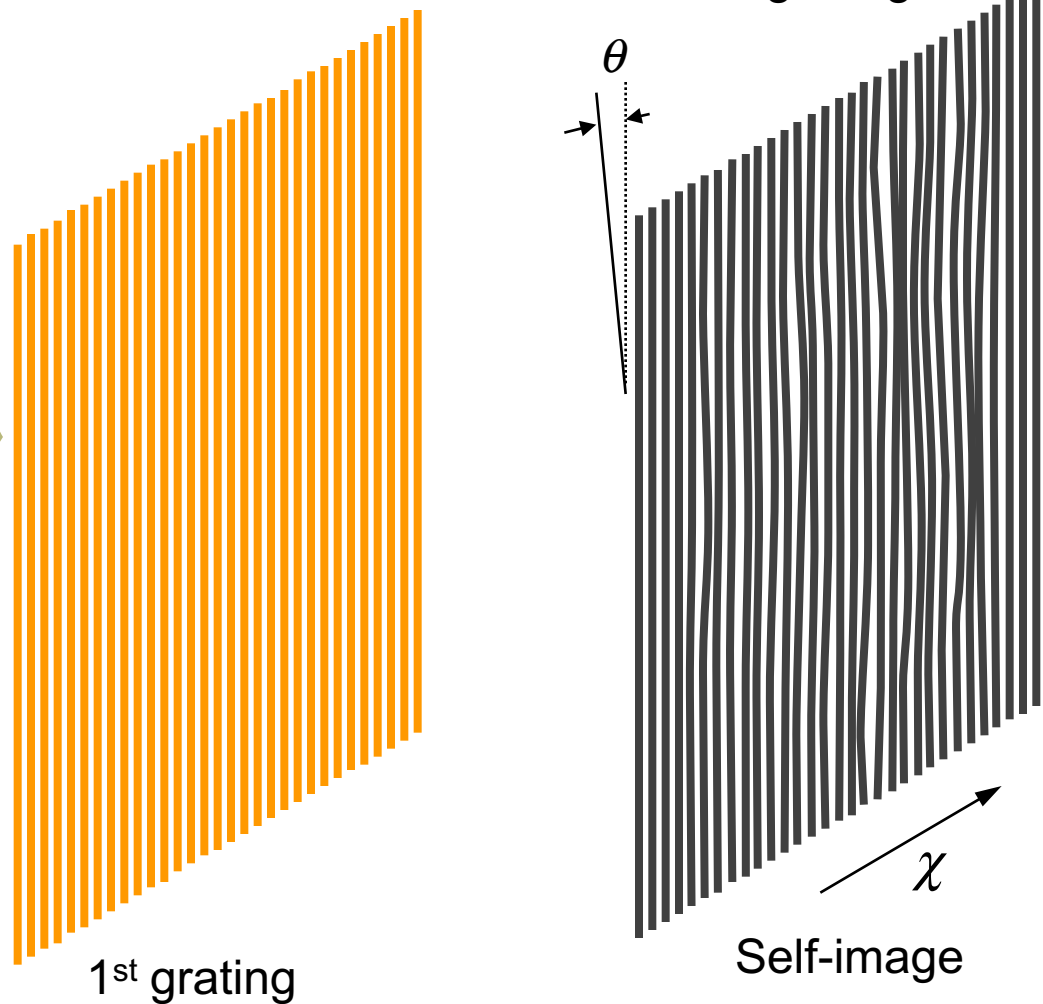


Slide courtesy of A. Momose, University of Tokyo, Japan

Talbot Interferometer: Moiré Pattern 2nd grating



Phase object
Phase shift: $\Phi(x, y)$



1st grating

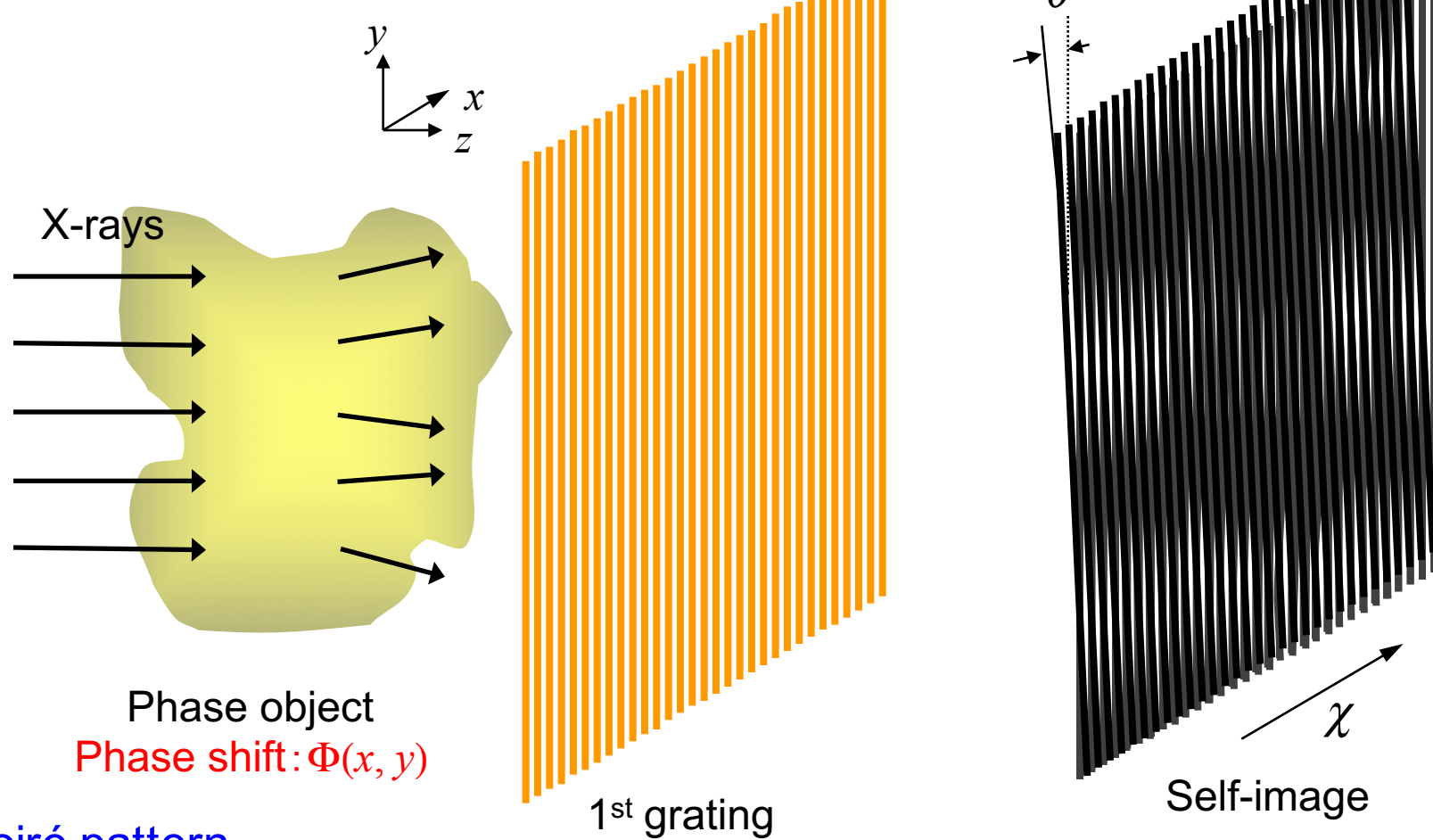
Self-image

Deformed self-image

$$\sum_n b_n \exp\left[i2\pi \frac{nx}{d}\right] \Rightarrow \sum_n b_n \exp\left[i2\pi \frac{n}{d} \left(x - z \frac{\partial \Phi}{\partial x}\right)\right]$$

Slide courtesy of A. Momose, University of Tokyo, Japan

Talbot Interferometer: Moiré Pattern 2nd grating

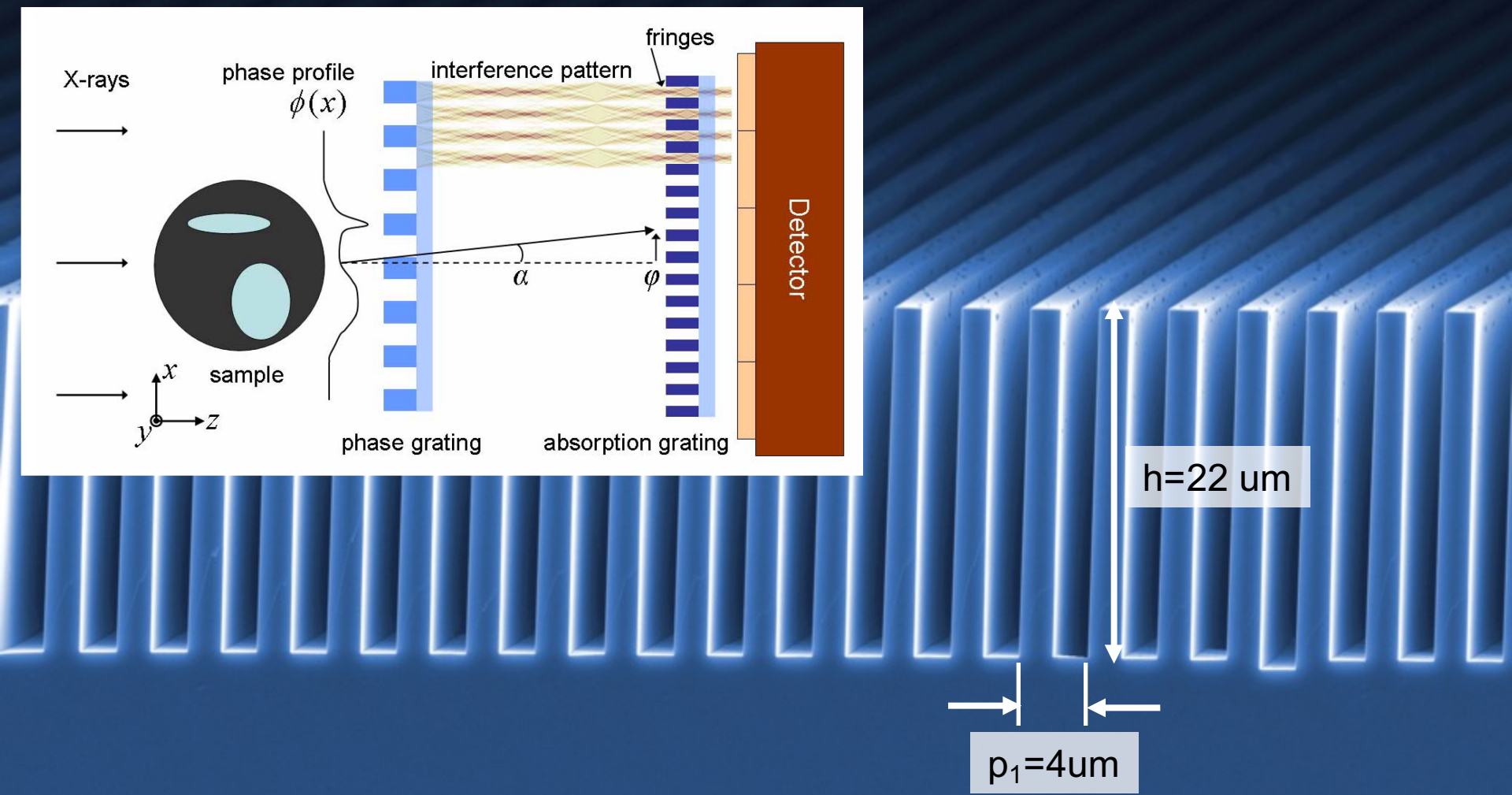


Moiré pattern

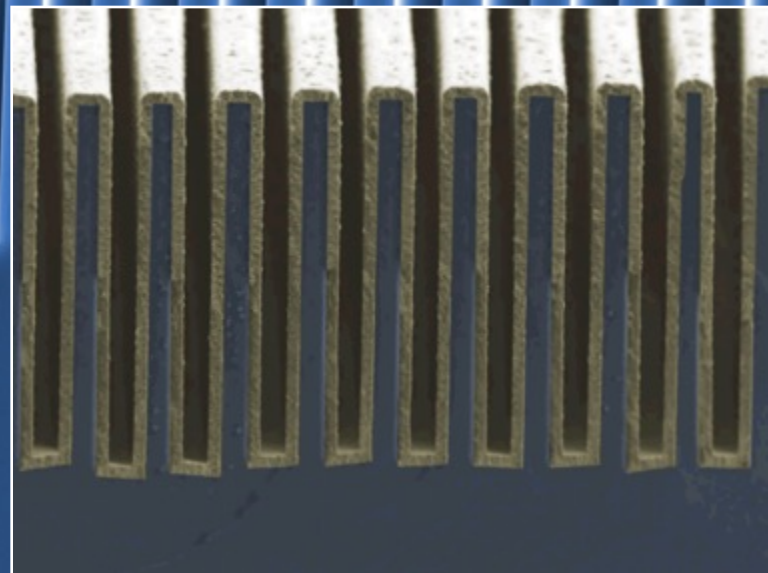
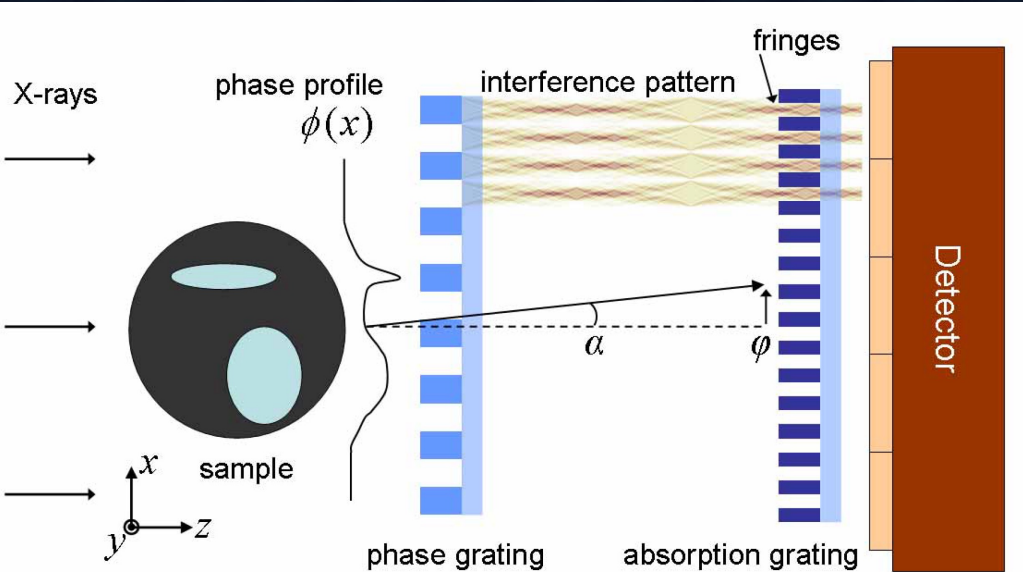
$$I(x, y, z) = b_0 c_0 + 2 \sum_{n>0} b_n c_n \cos \left[2\pi \frac{n}{d} \left(y\theta + z \frac{\partial \Phi}{\partial x} + \chi \right) \right]$$

Slide courtesy of A. Momose, University of Tokyo, Japan

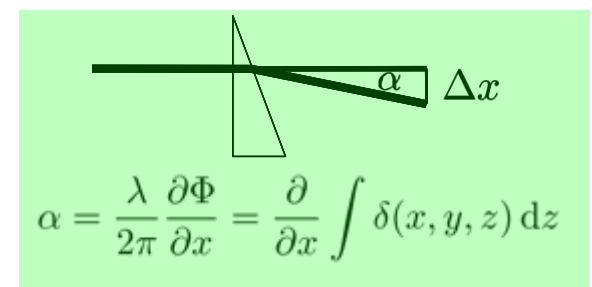
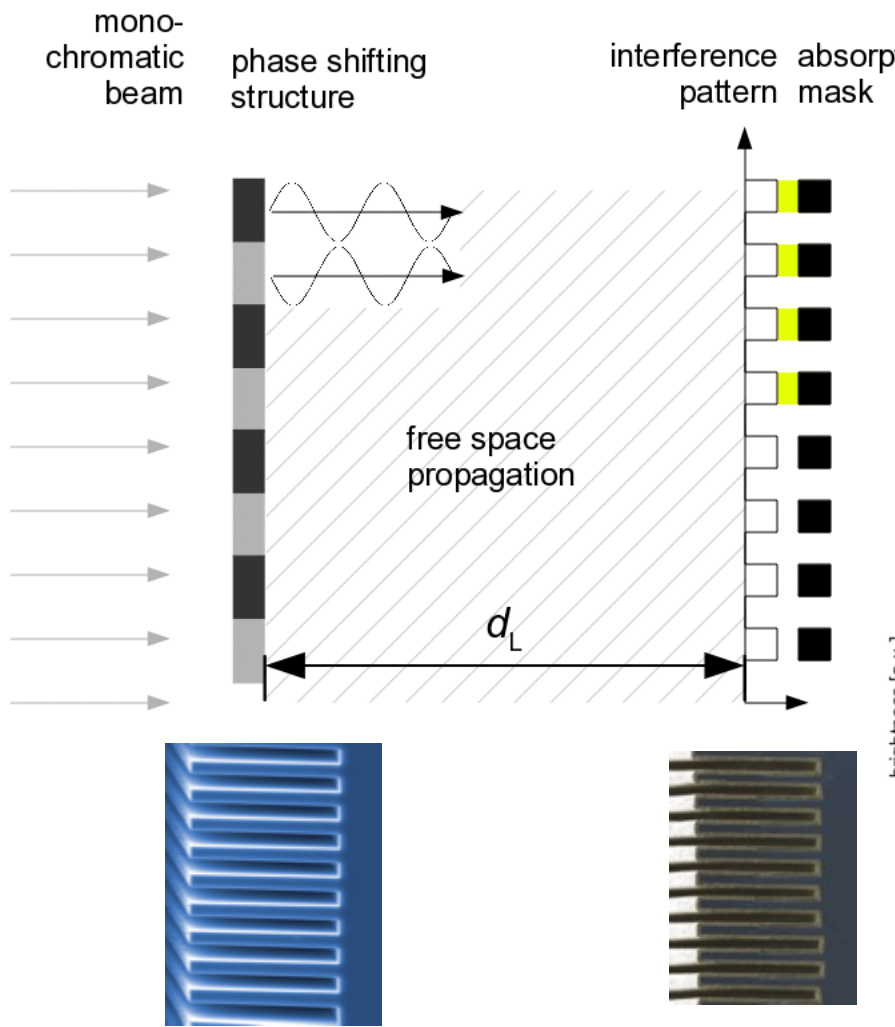
Sensing the wavefront with grating interferometry



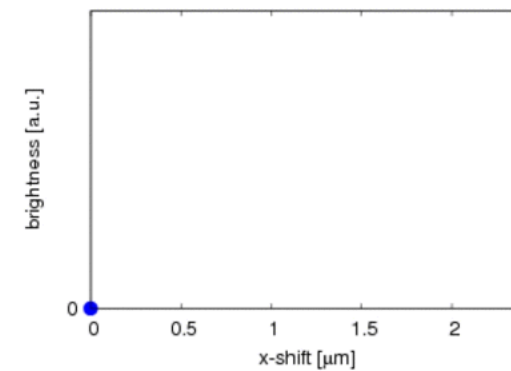
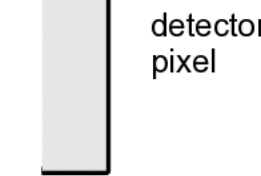
Sensing the wavefront with grating interferometry



A finer look into the working mechanism of a GI

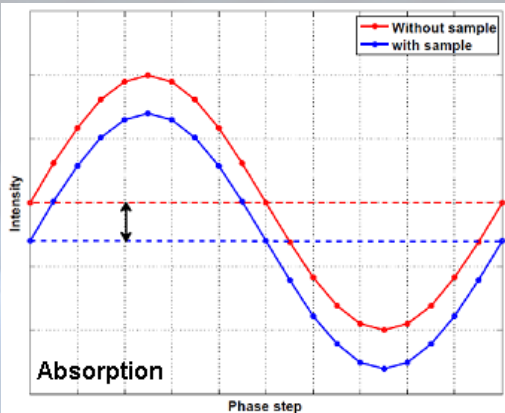


Refractive angles are microradians



Sensing the wavefront with grating interferometry

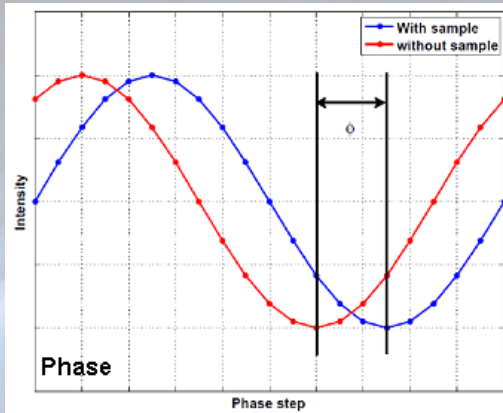
Absorption contrast



$$-\log\left(\frac{I_s}{I_b}\right)$$



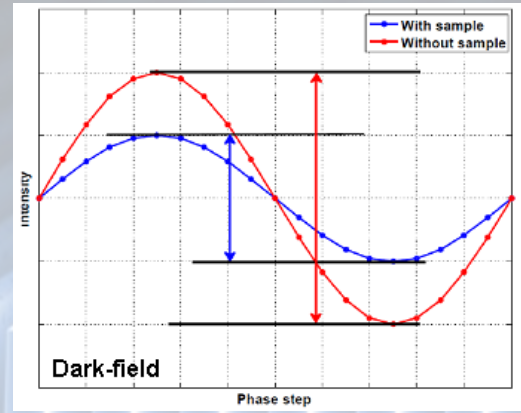
Differential phase contrast



$$\Phi_s - \Phi_b$$



Dark-field contrast

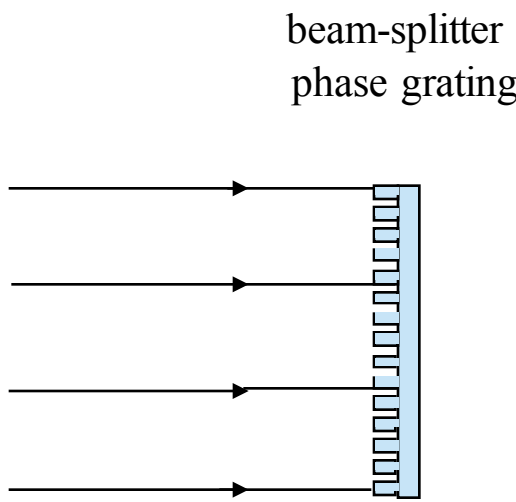


$$-\log\left(\frac{V_s}{V_b}\right)$$

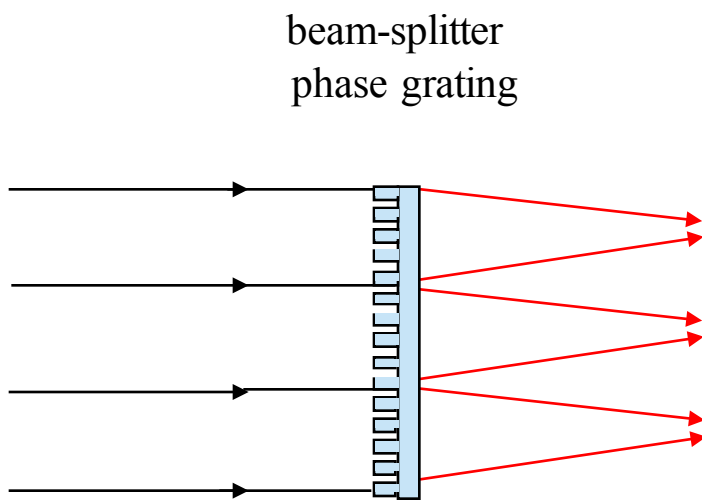
$$V = \frac{I_{\max} - I_{\min}}{I_{\max} + I_{\min}}$$



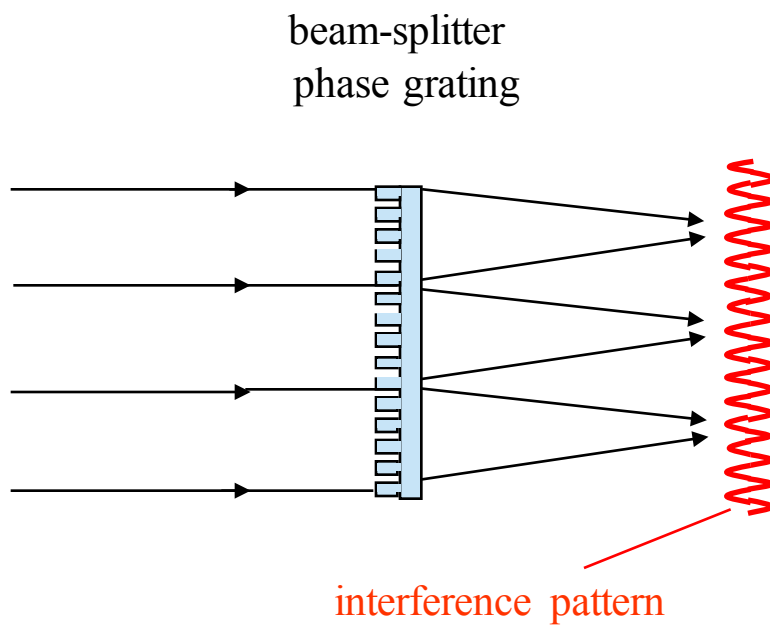
Grating interferometry: how does this work?



Grating interferometry: how does this work?

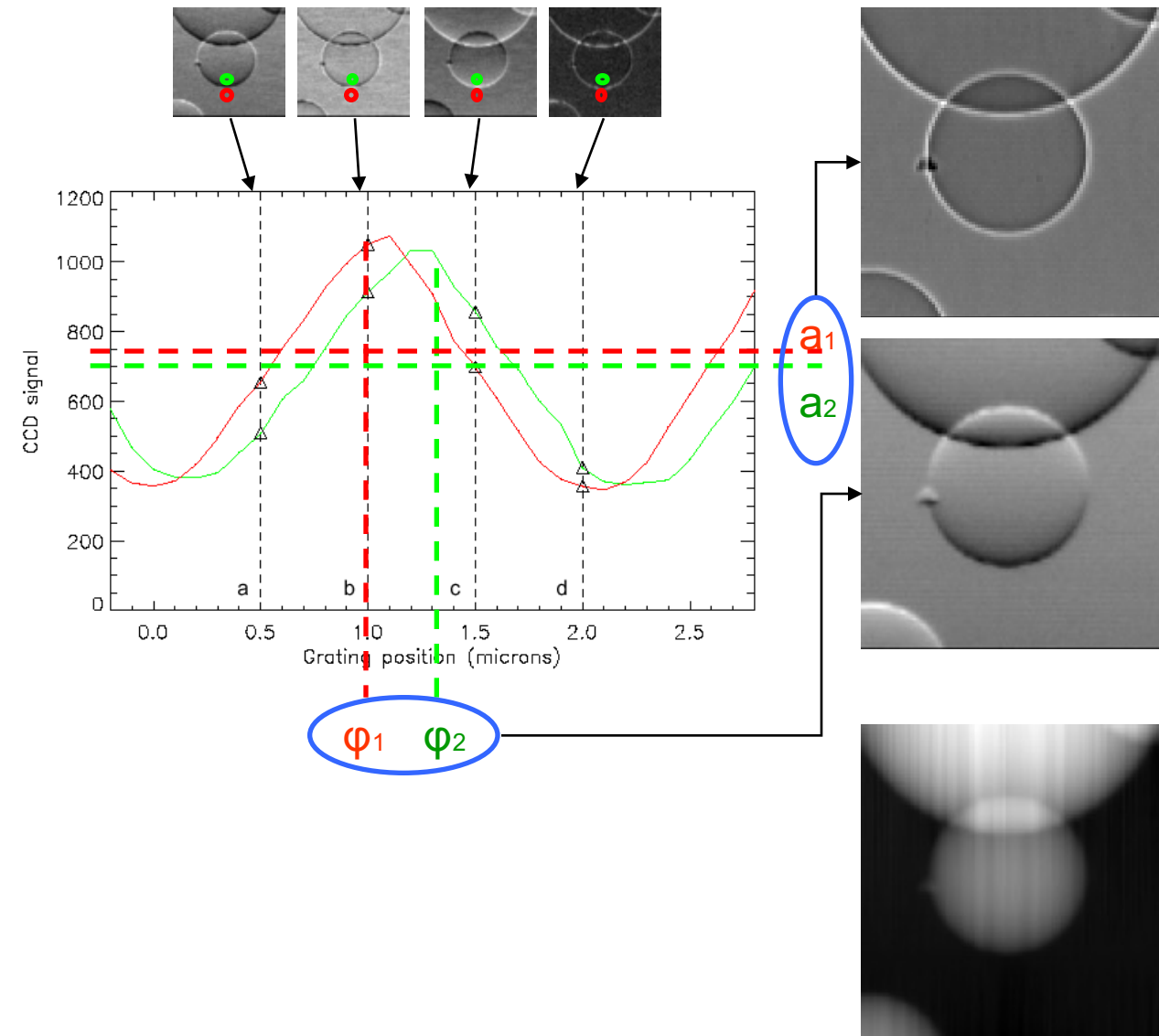


Grating interferometry: how does this work?



Talbot effect...

Phase-stepping interferometry



a_{ij} : mixture of absorption and inline phase

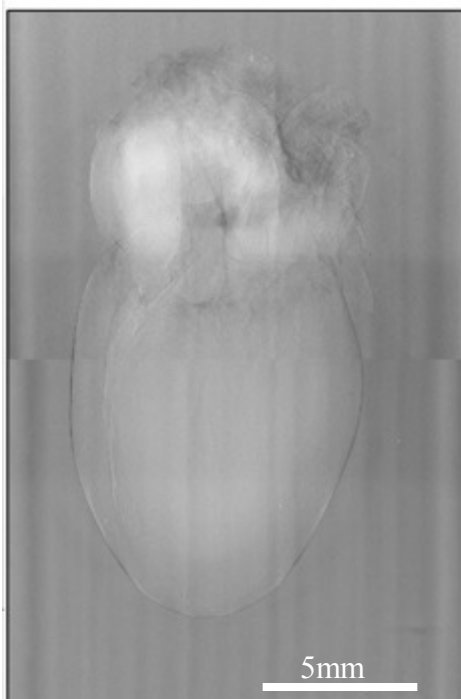
- same image that would be observed without the interferometer in the beam
- an amplitude flat-field image corrects for inhomogeneous illumination

Φ_{ij} : phase gradient image

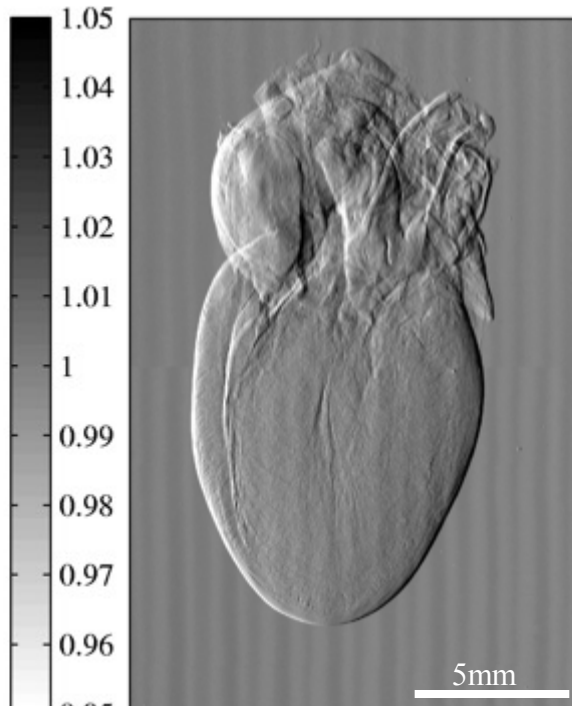
- all absorption contributions eliminated
- a phase flat field removes all wavefronts or grating distortions

Can be integrated to yield the projected phase shift of the sample

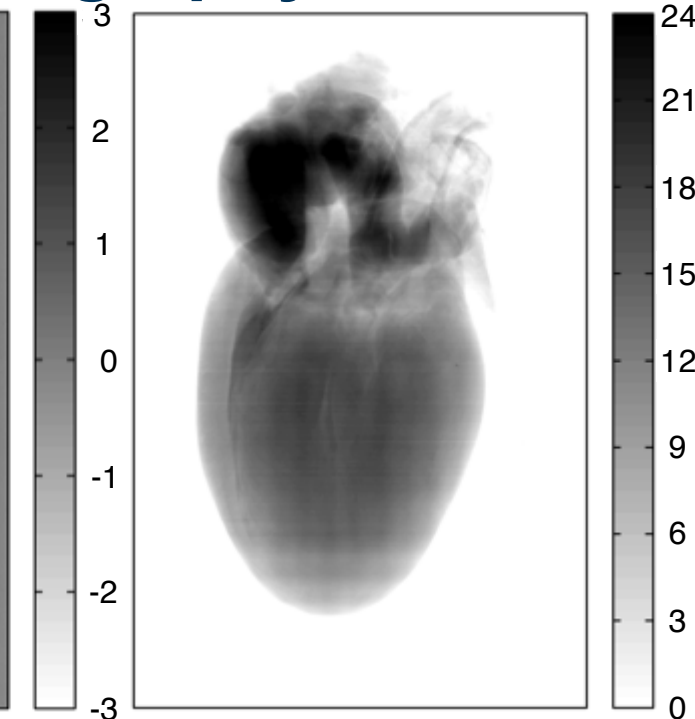
Phase contrast radiography



Absorption



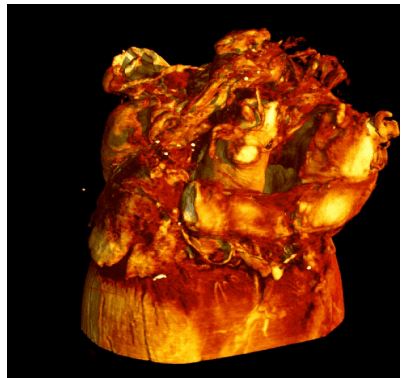
Phase gradient [mrad/μm]



Phase [rad]

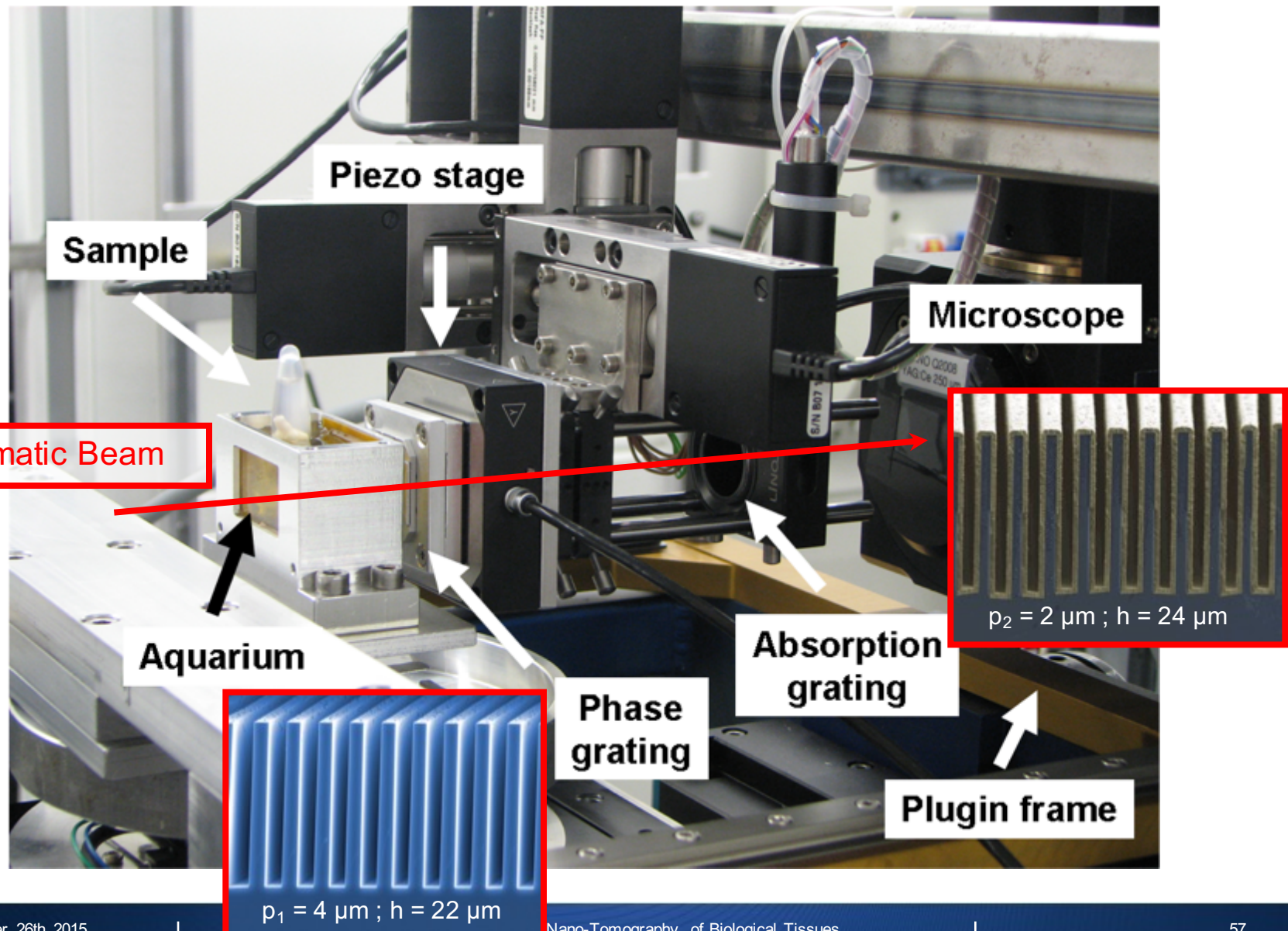


Integration

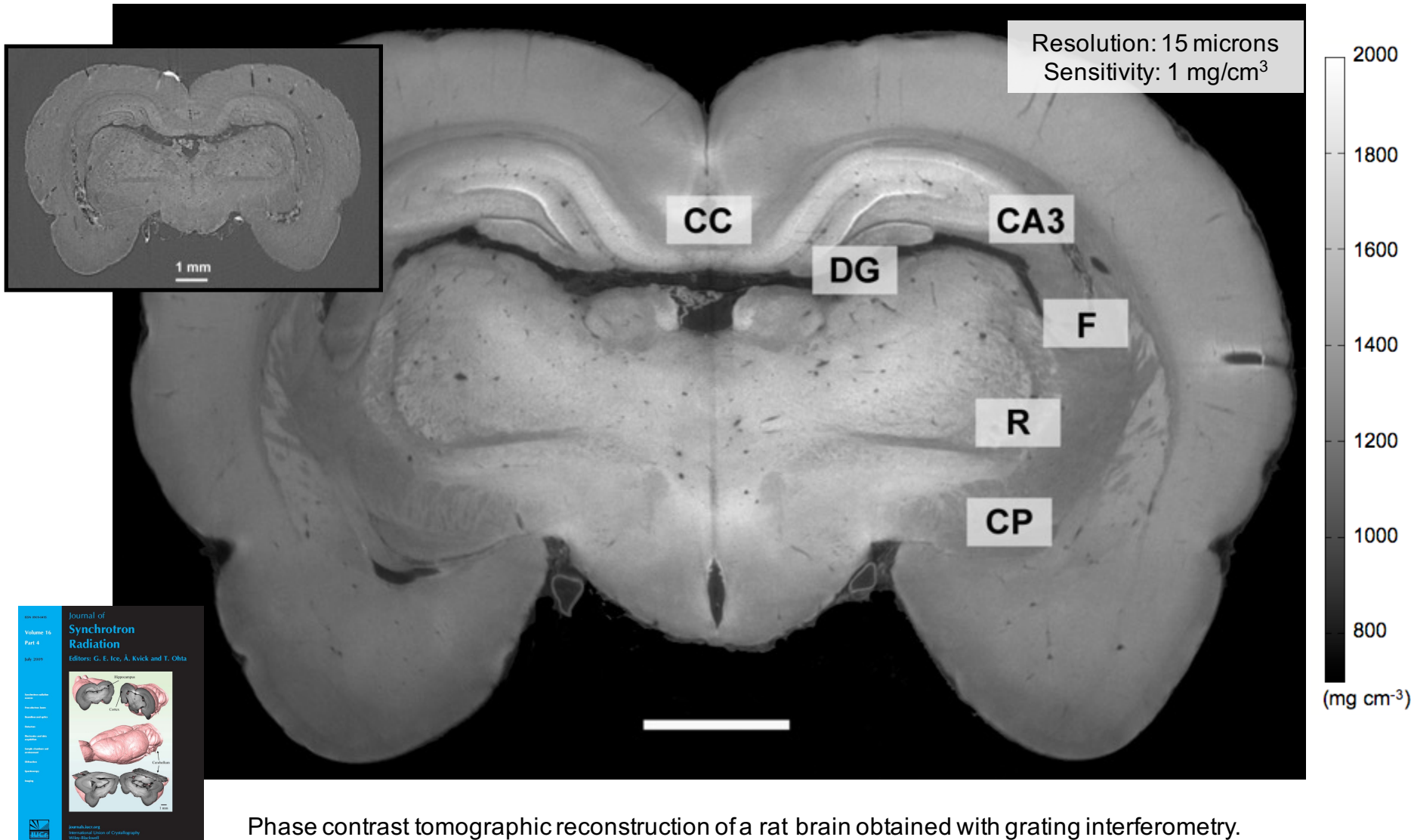


Rat heart in formalin solution, ESRF, ID19, 17.8 keV.
Images courtesy of T. Weitkamp

Grating interferometry at TOMCAT

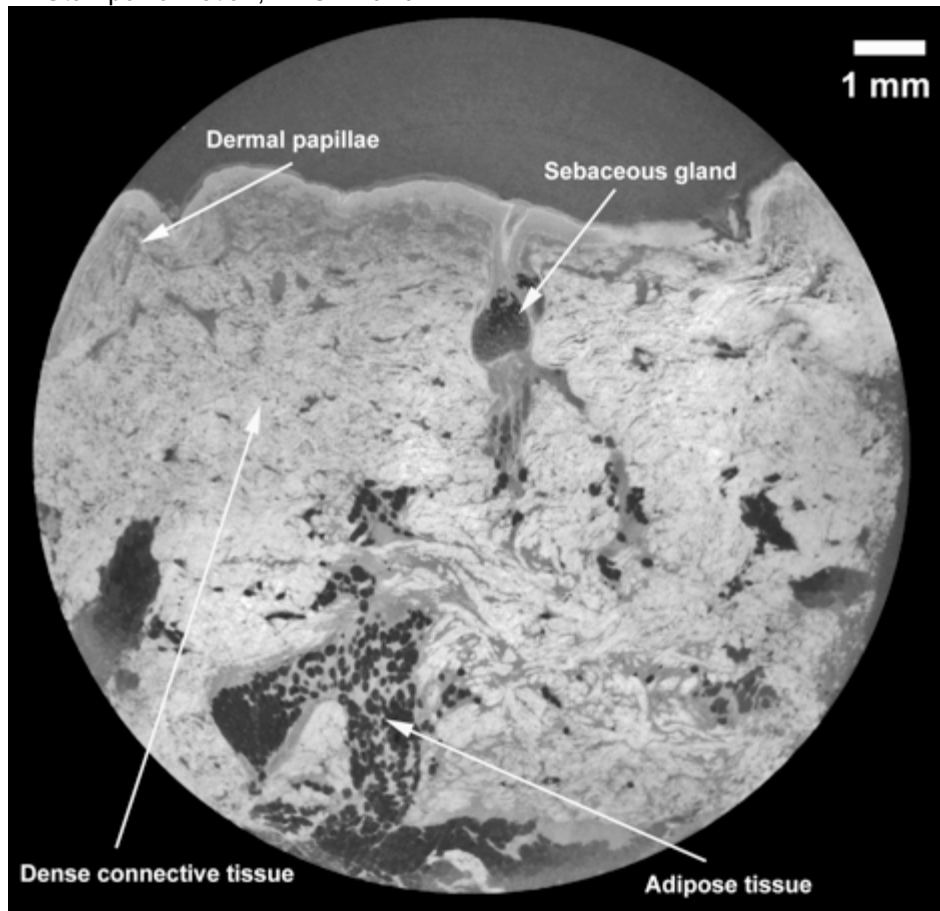


High sensitivity at isotropic, high resolution



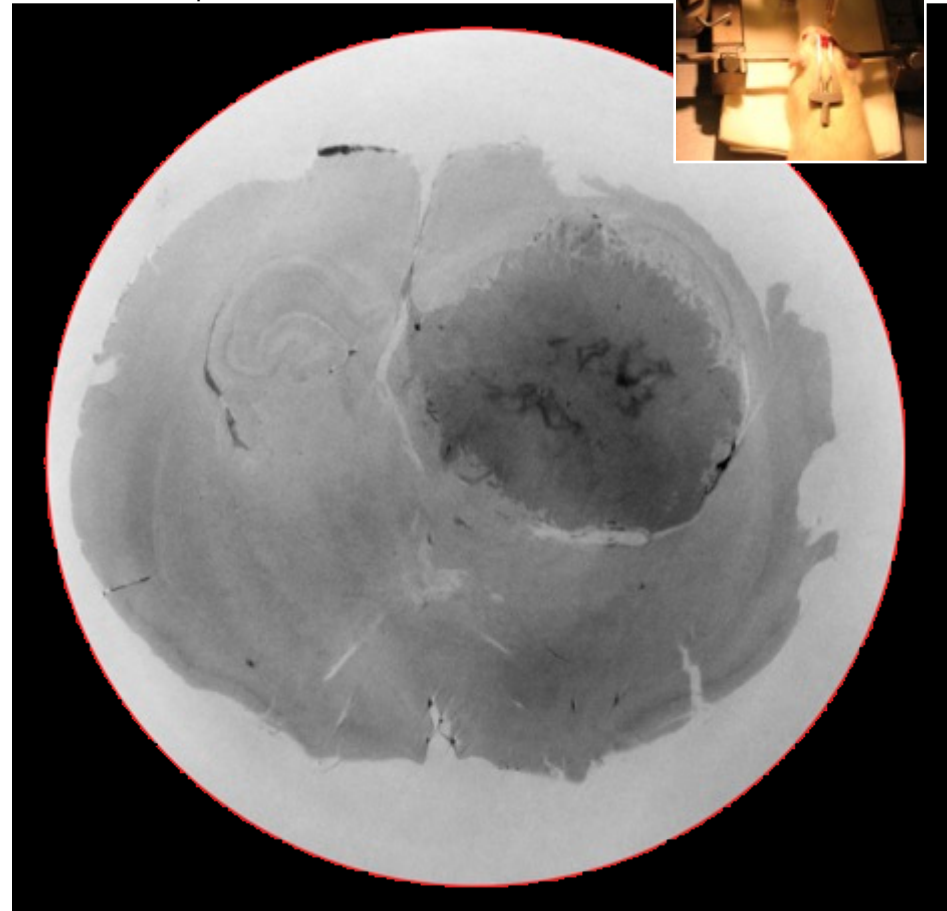
Soft-tissue sensitivity

M. Stampanoni et al., MASR 2010



Human skin tissue biopsy

E. Schültke, unpublished data

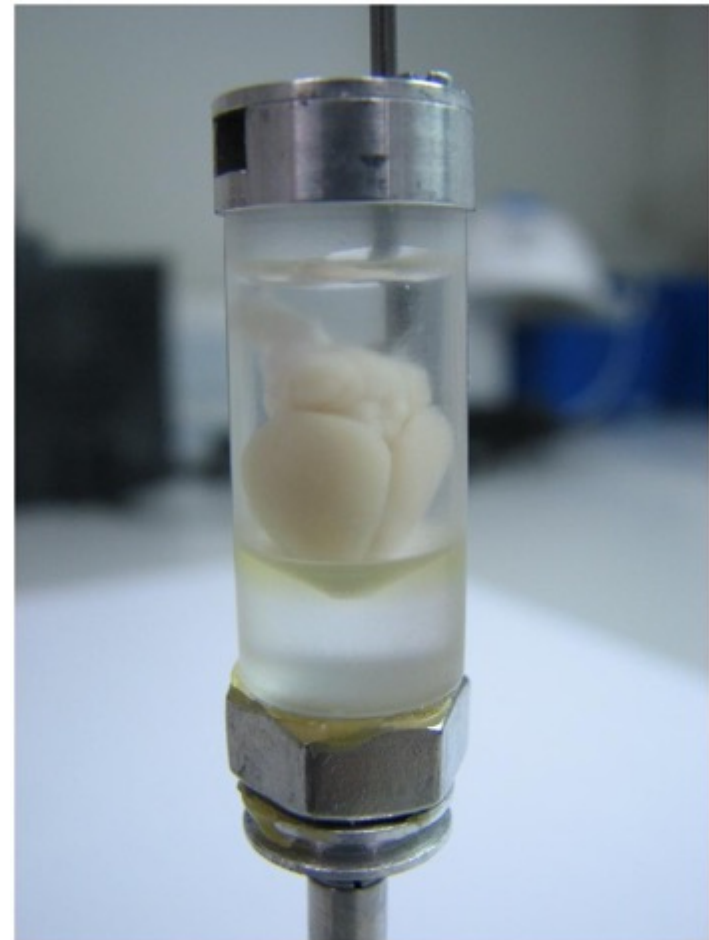


Inoculated GNP-F98 glioma

TOMCAT Interferometer: 25 keV, 3rd Talbot Distance

Pathogenesis of Alzheimer's plaques

5x FAD Mouse Model



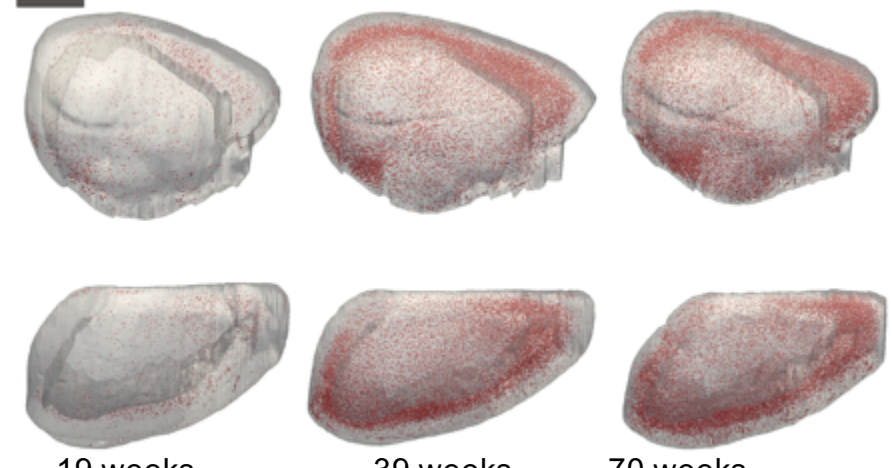
B. R. Pinzer et al., Neuroimage 2012

Pathogenesis of Alzheimer's plaques

5x FAD Mouse Model



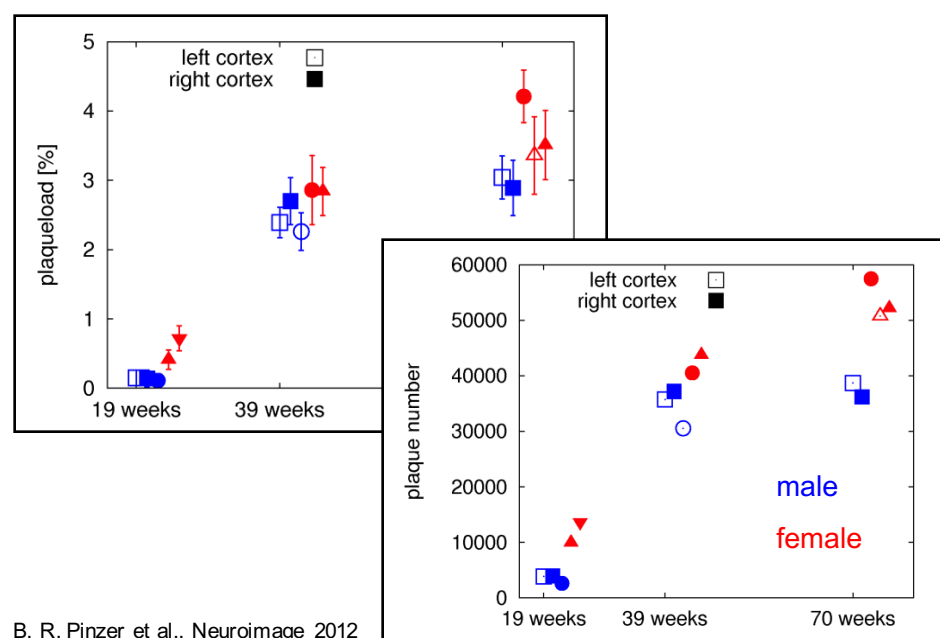
2 mm



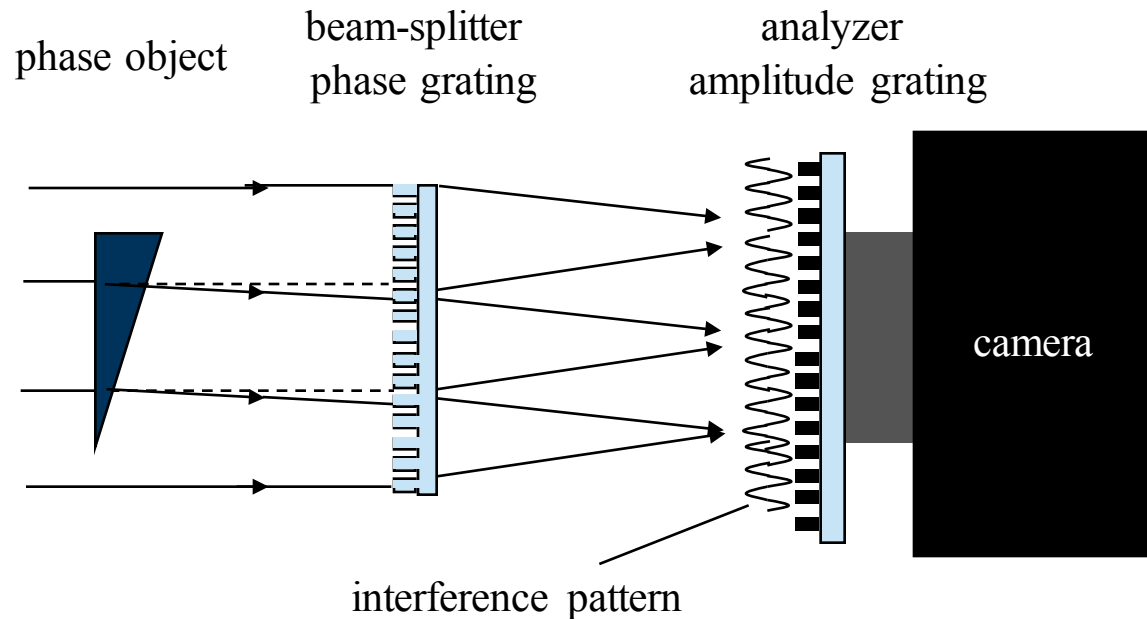
19 weeks

39 weeks

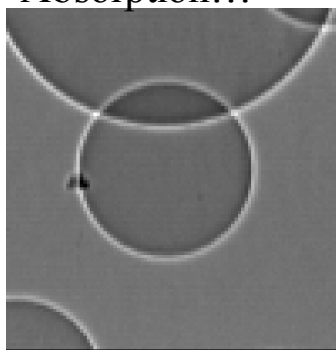
70 weeks



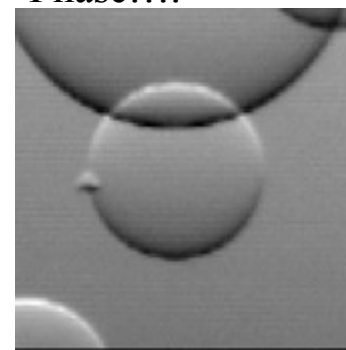
Grating interferometry: absorption + phase + ??



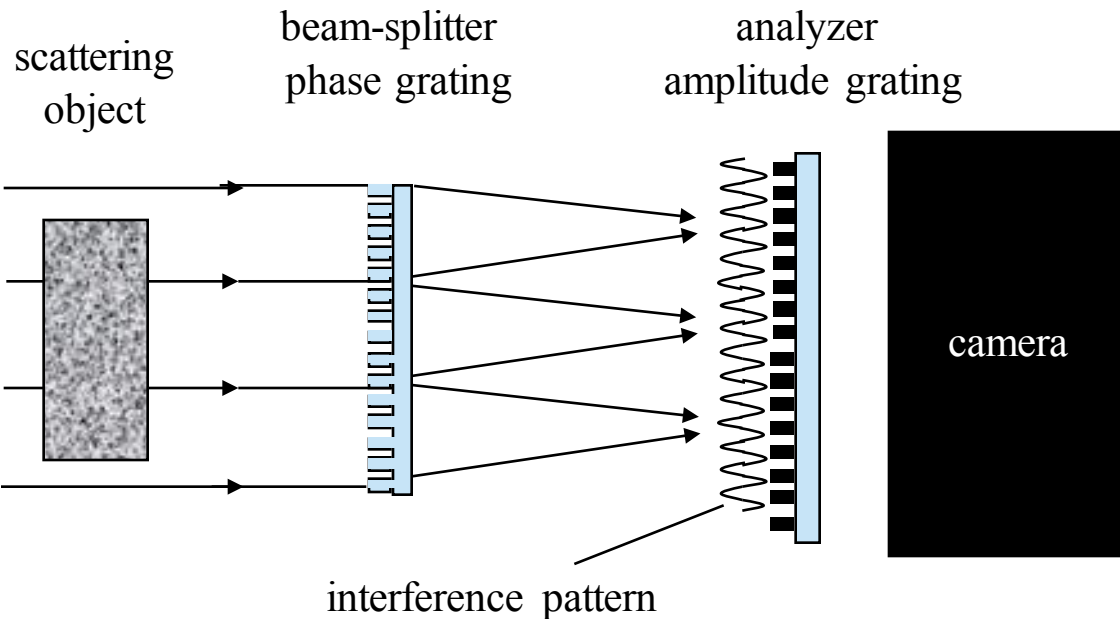
Absorption...



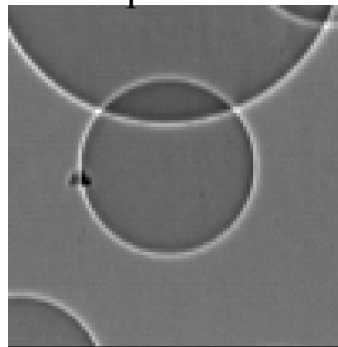
Phase....



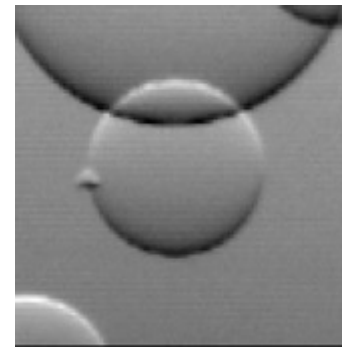
Grating interferometry: absorption + phase + ??



Absorption...

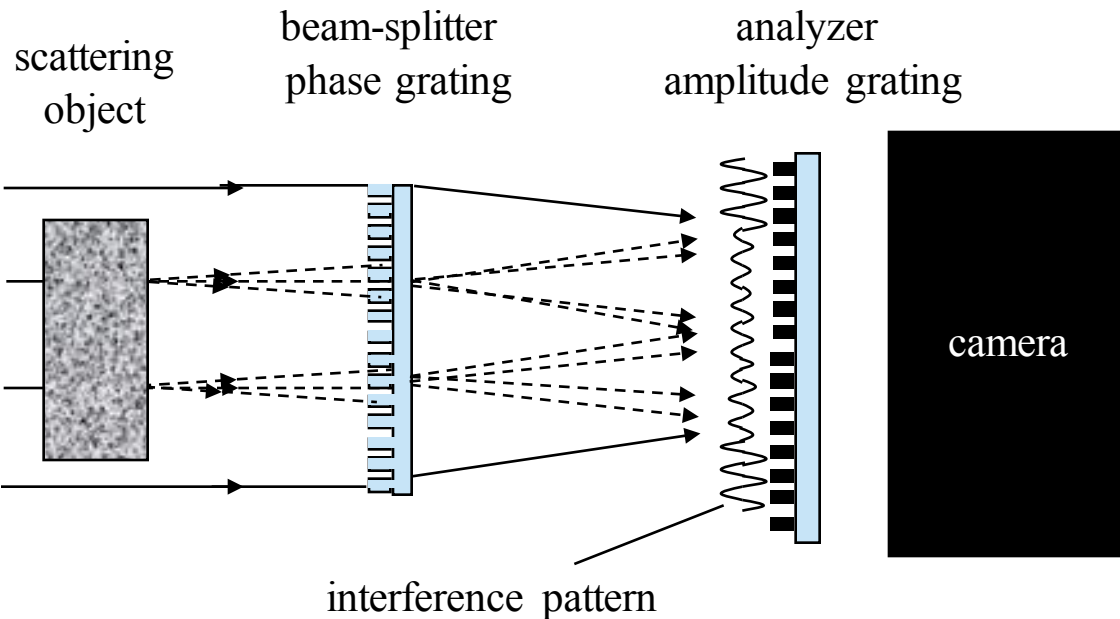


Phase....

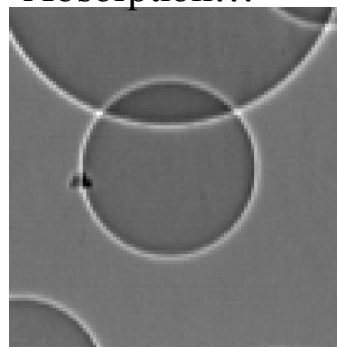


?

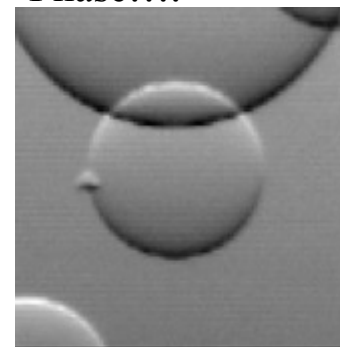
Grating interferometry: absorption + phase + ??



Absorption...

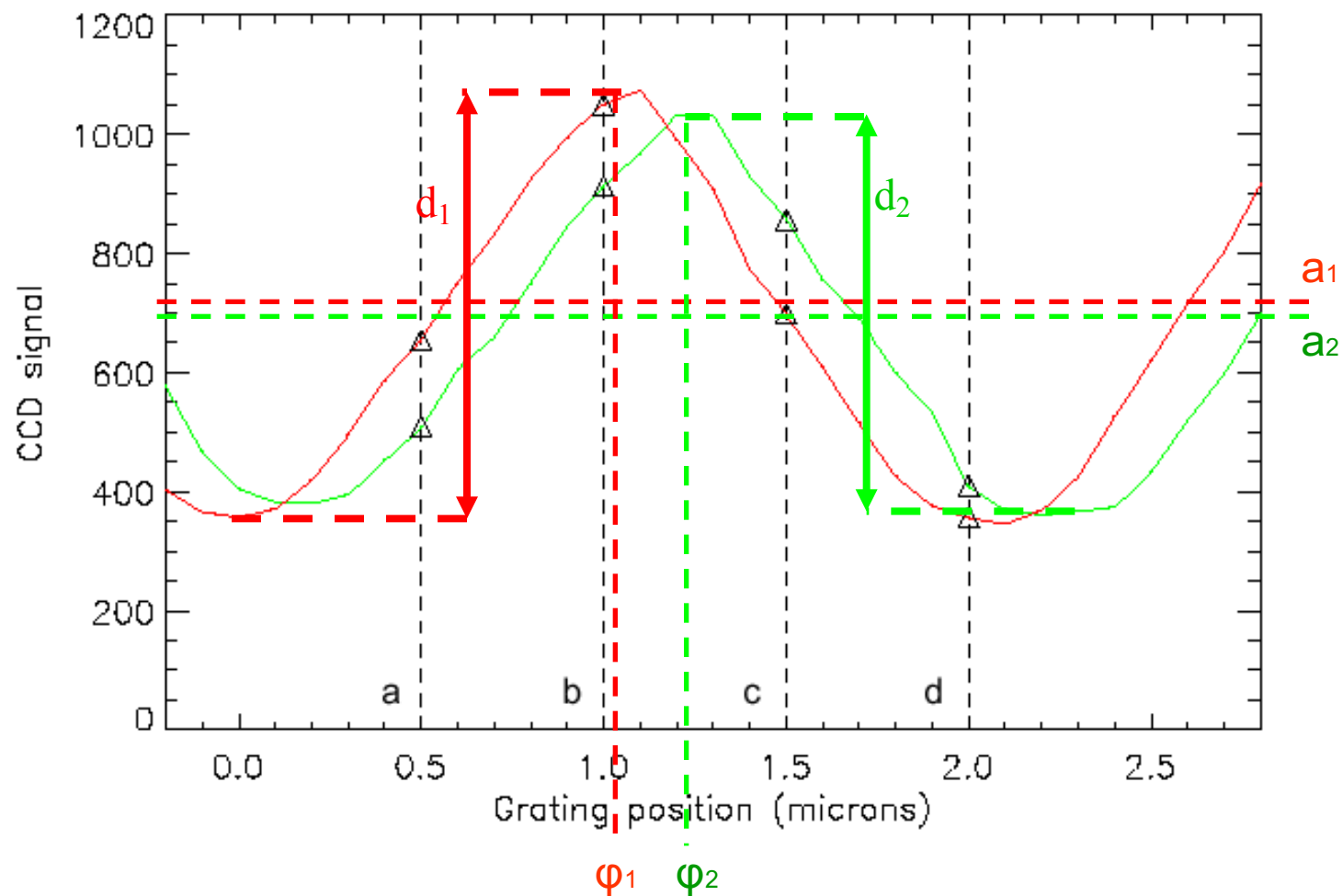


Phase....



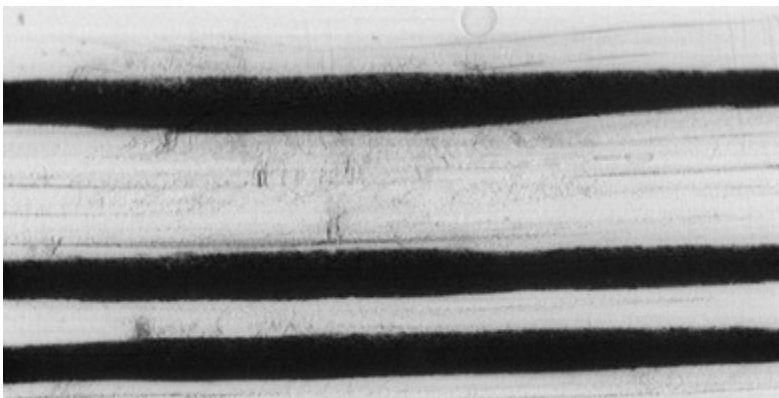
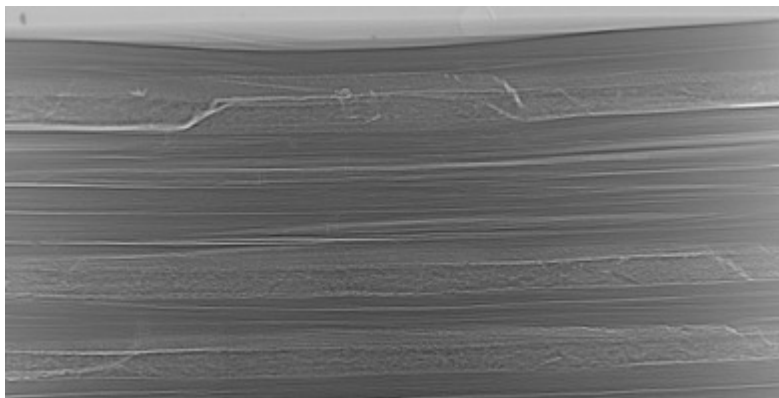
?

Visibility reduction – Dark field imaging

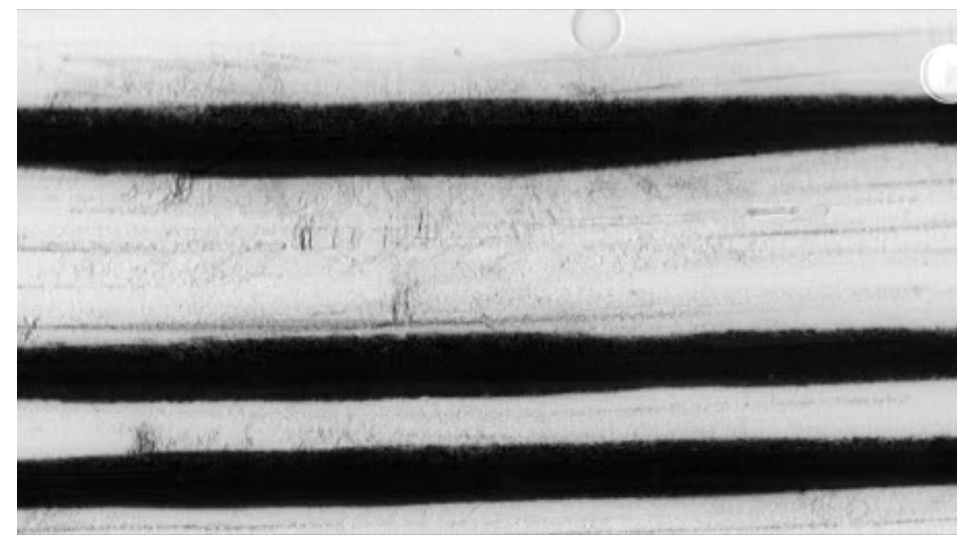


Darkfield radiology

CFRP laminated structure consisting of alternate layers of plastic matrix and fiber reinforcement



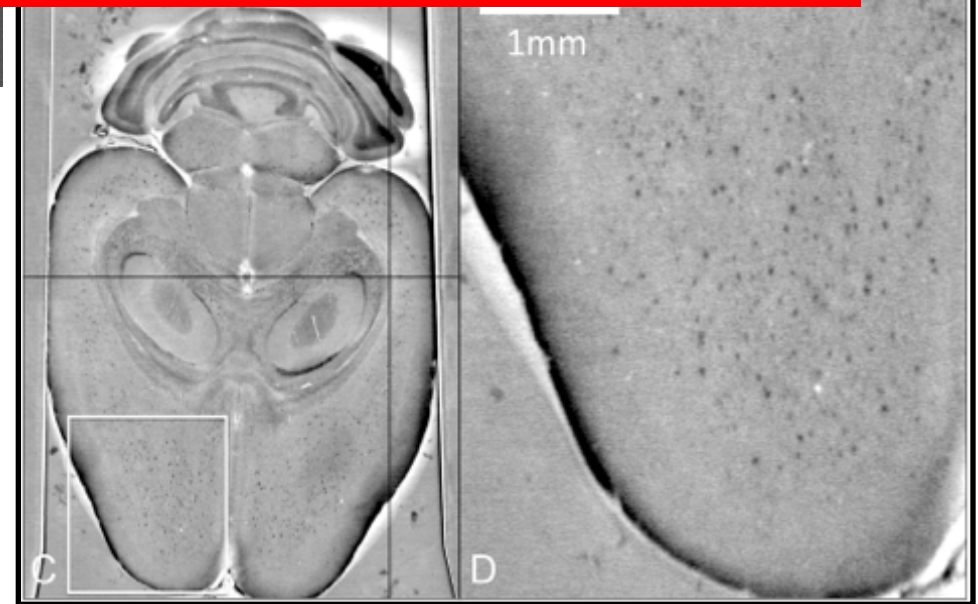
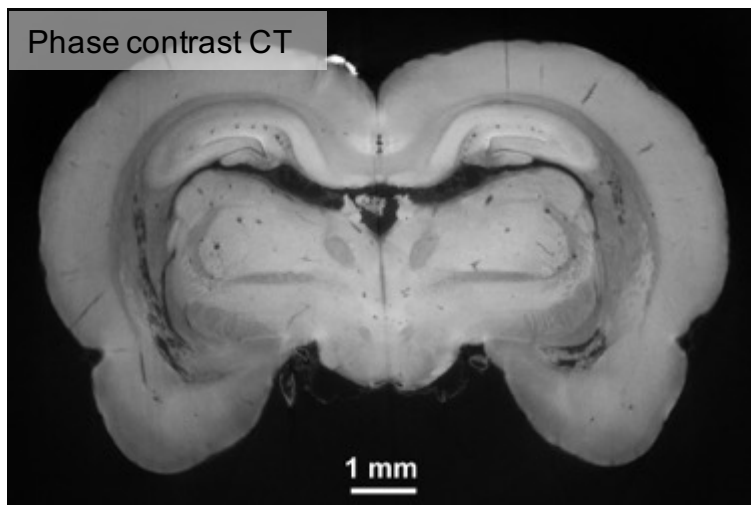
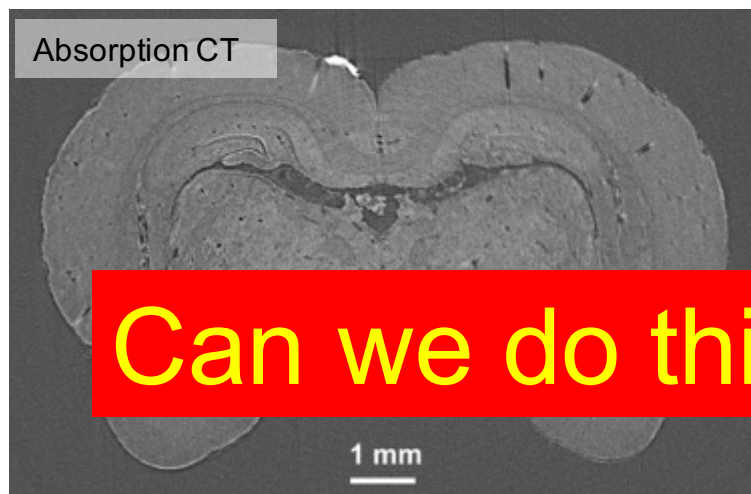
← 10 mm →



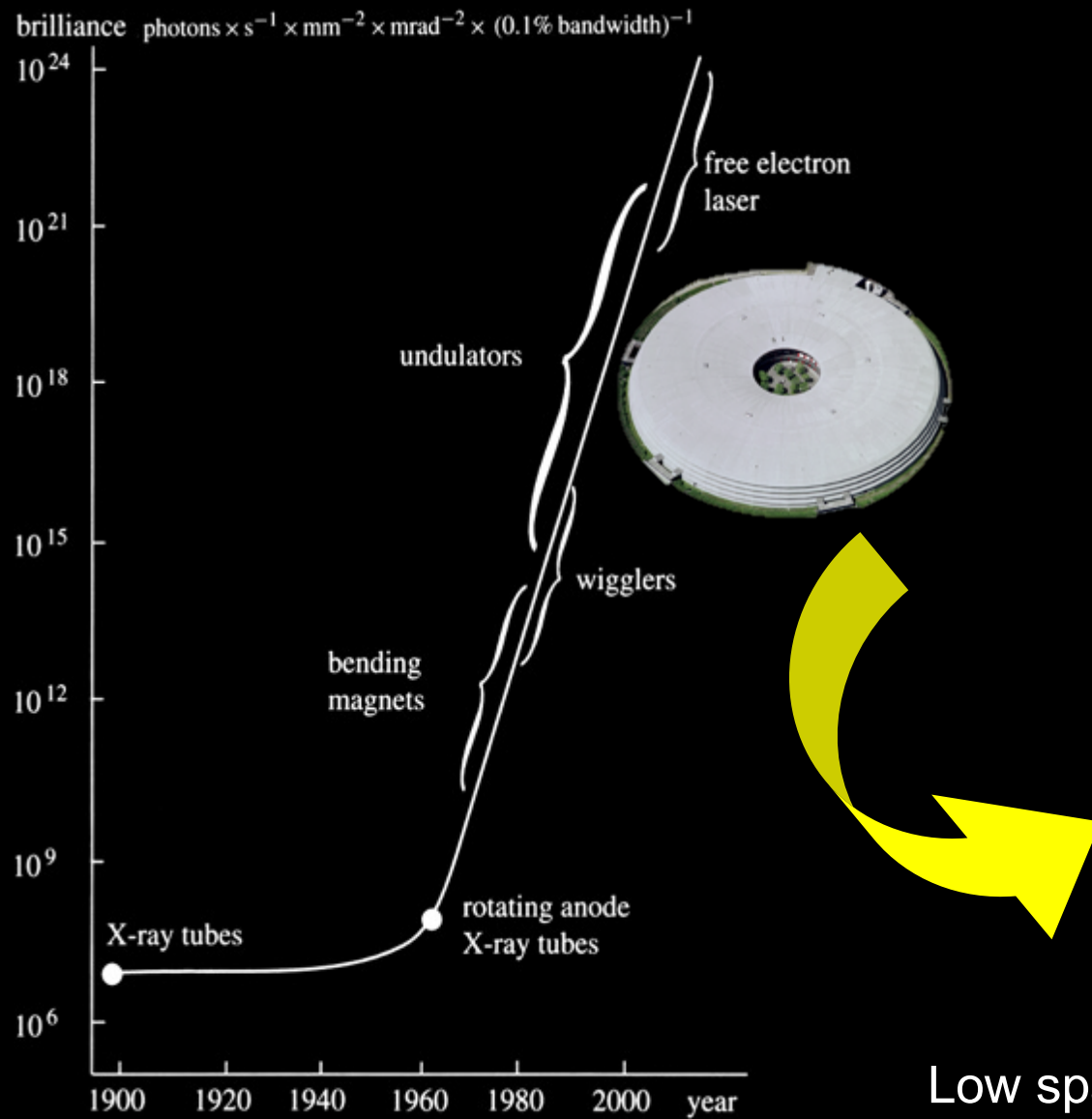
Directional dependency of the darkfield signal.
Issues with the tomographic reconstruction...

S. McDonald, M. Stampanoni et al., Journal of Synchrotron Radiation 16, 562-572,(2009)

Phase contrast imaging (CT) at synchrotron (10 microns isotropic resolution)

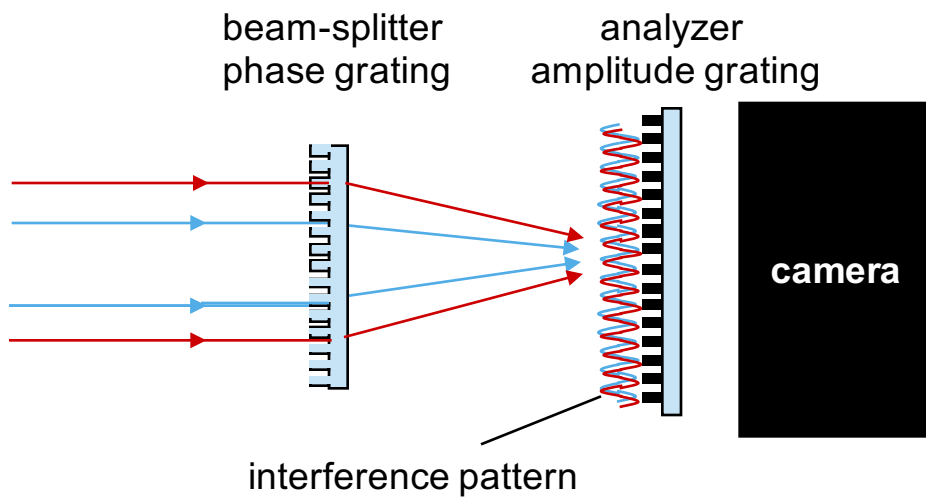


Moving back to the “origins”...



Low spatial and temporal coherence!!

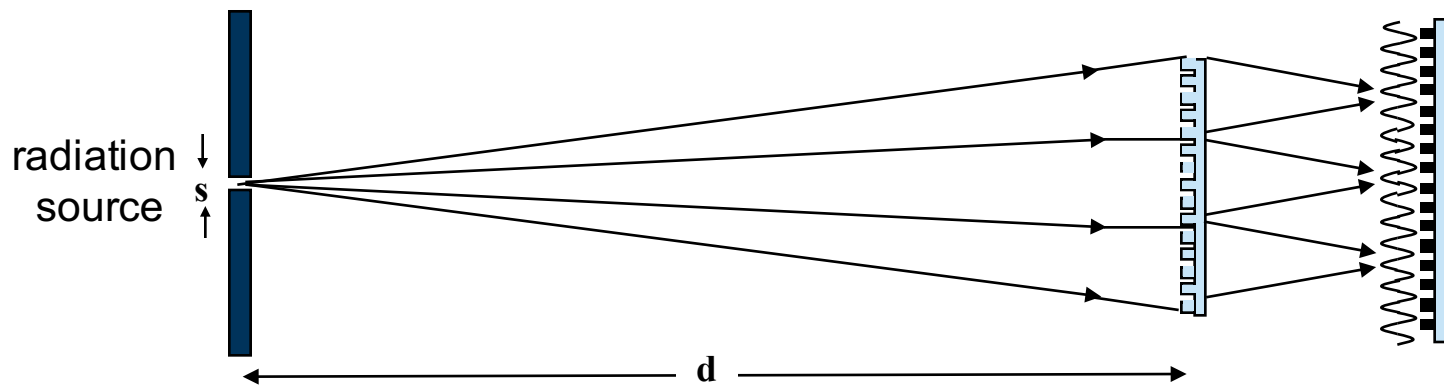
Temporal (longitudinal) coherence requirements



The position and pitch of the interference pattern does not depend on the wavelength!

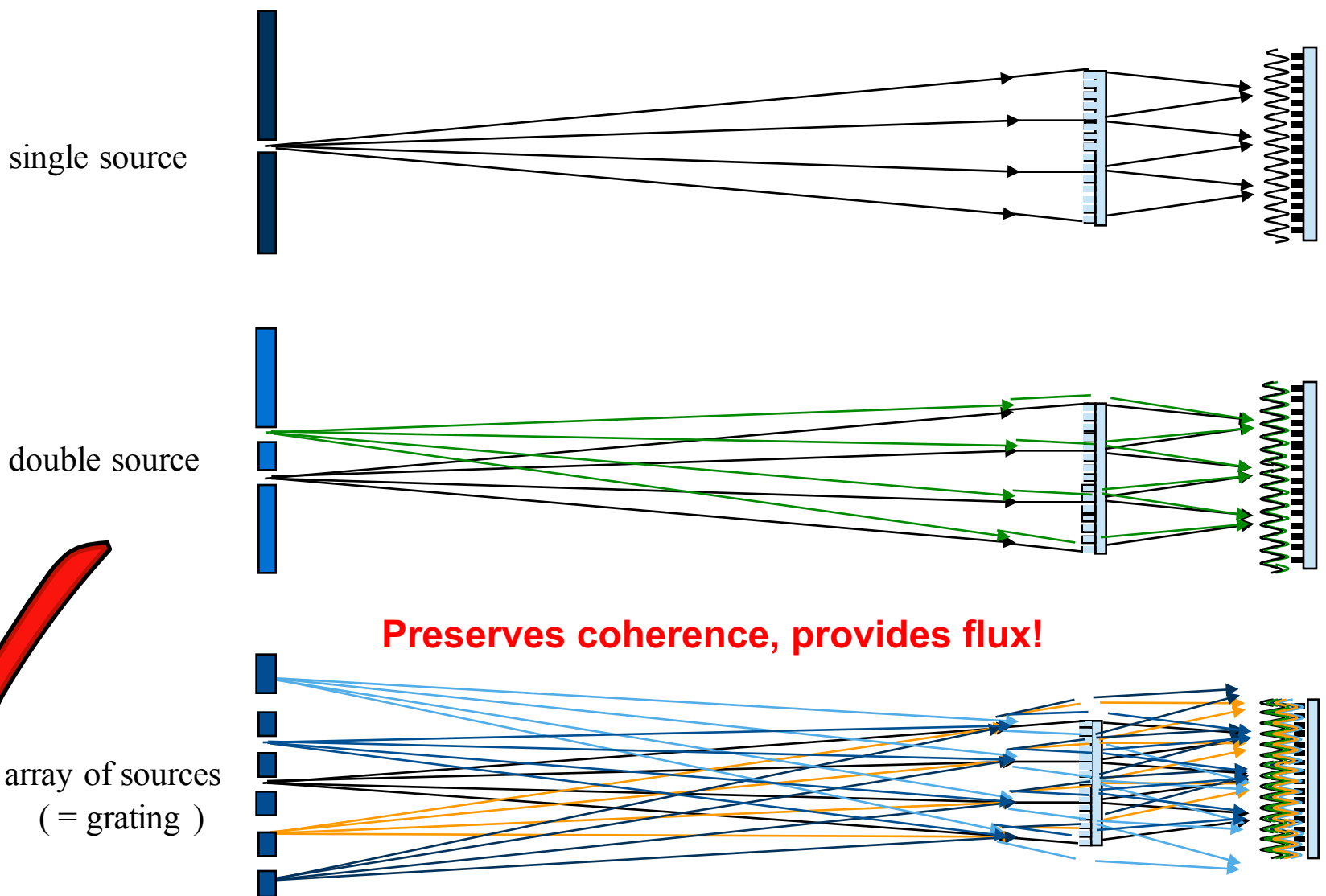
10-20% bandwidth is OK

Spatial (transverse) coherence requirements



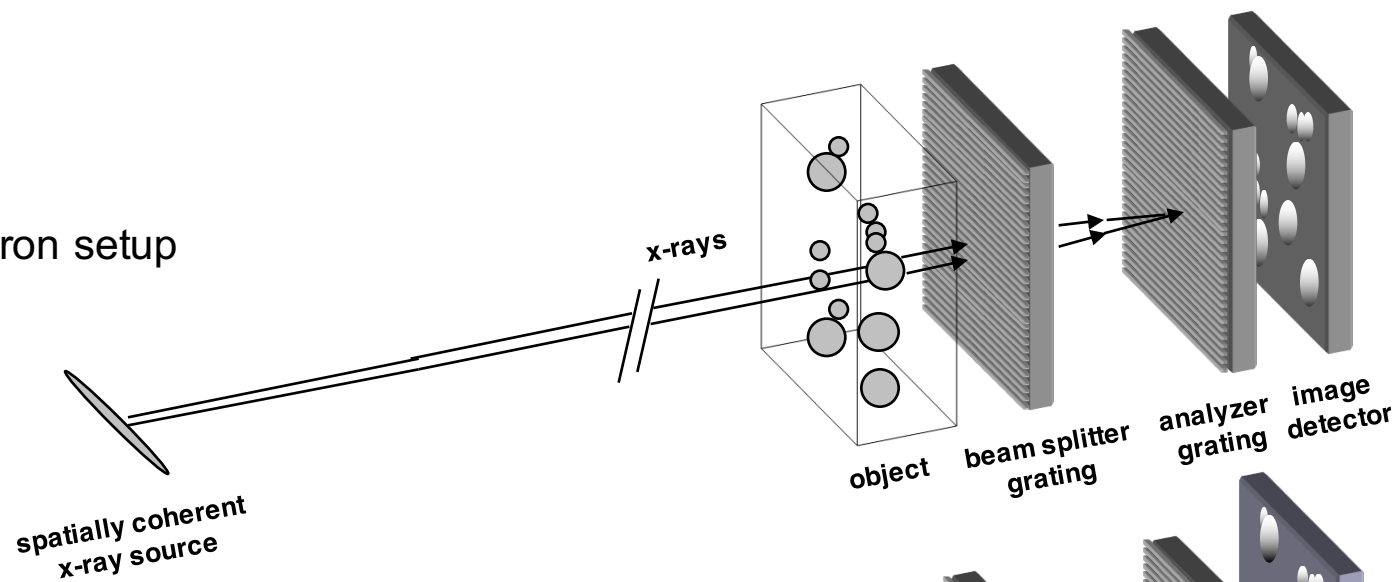
- Required in one direction
 - Depends on wavelength, geometry,
 - For Energy = 20 keV, $d=1\text{m}$, $\rightarrow \text{s} < 10\text{-}20 \mu\text{m}$
- LOW FLUX !!**

The Talbot-Lau interferometer

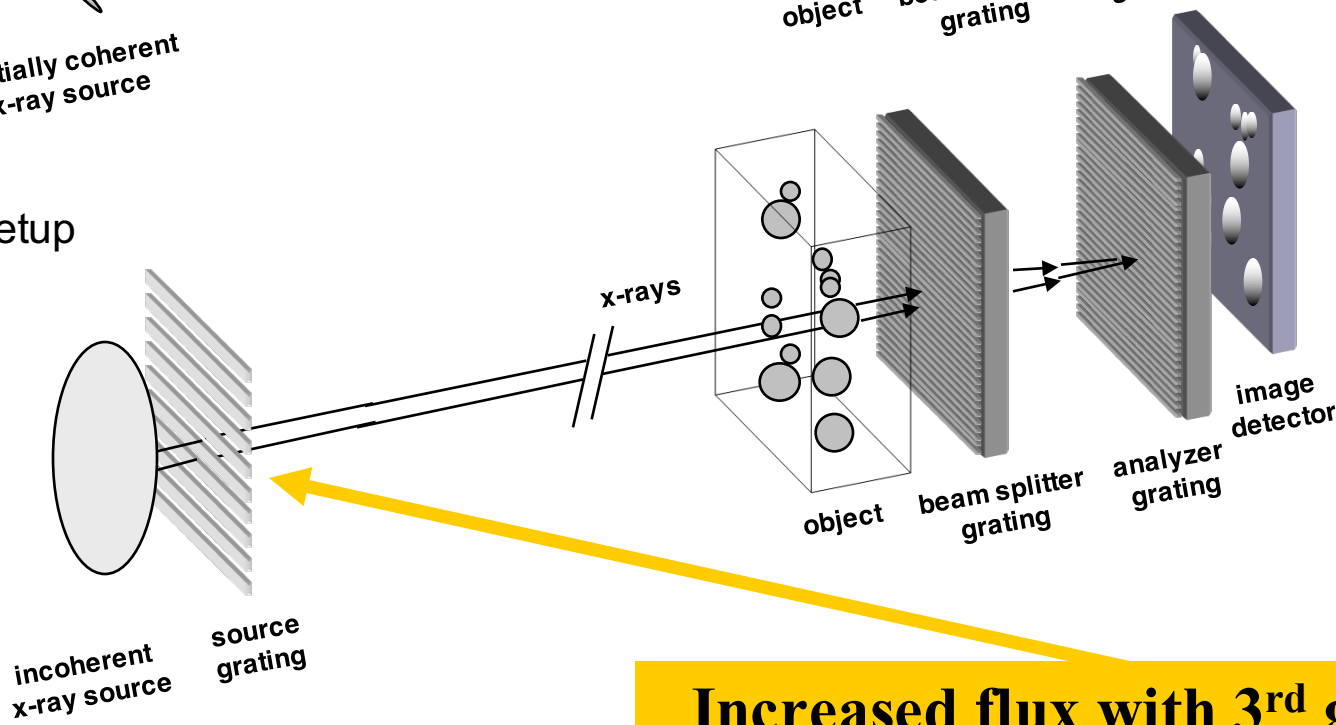


The Talbot-Lau interferometer

Synchrotron setup



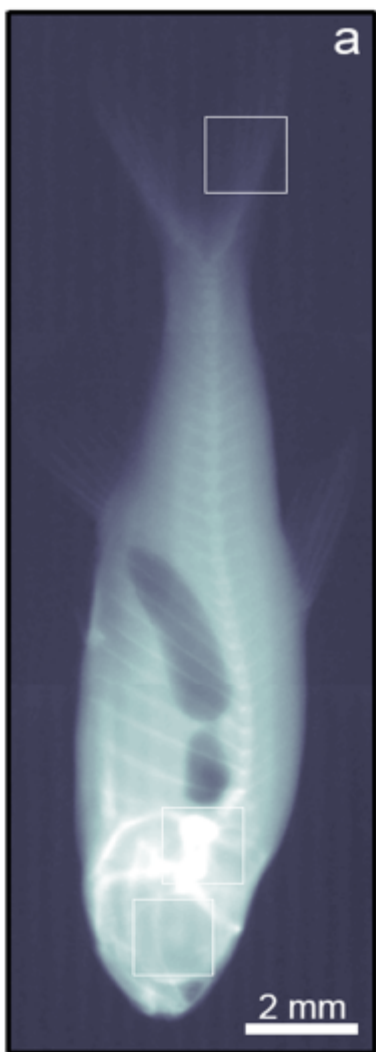
X-ray tube setup



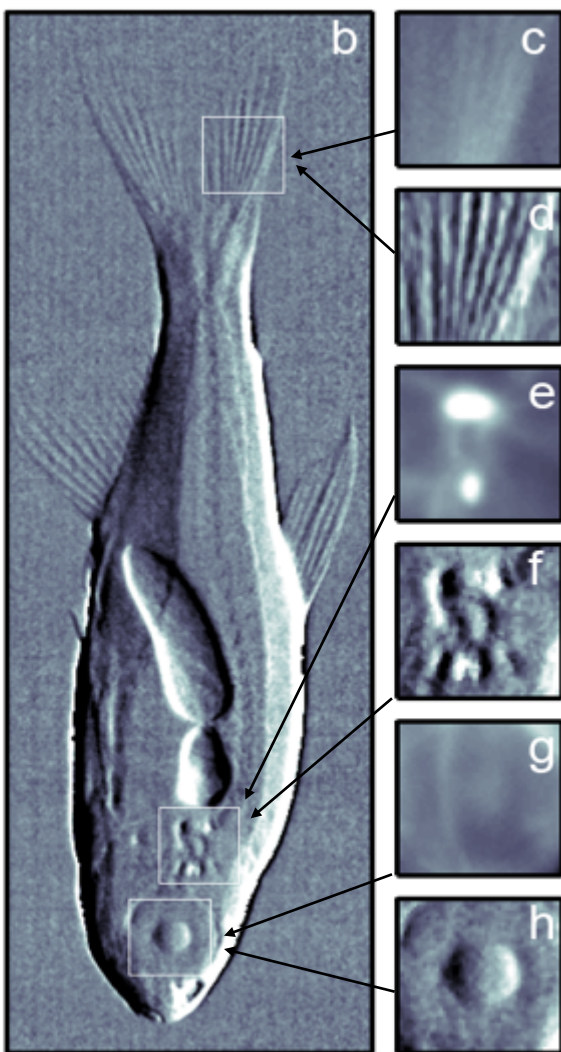
Increased flux with 3rd grating

DPC on a X-ray tube

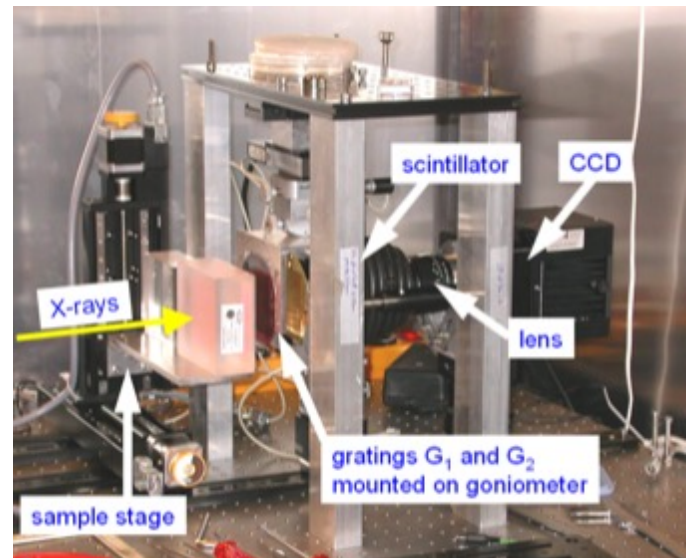
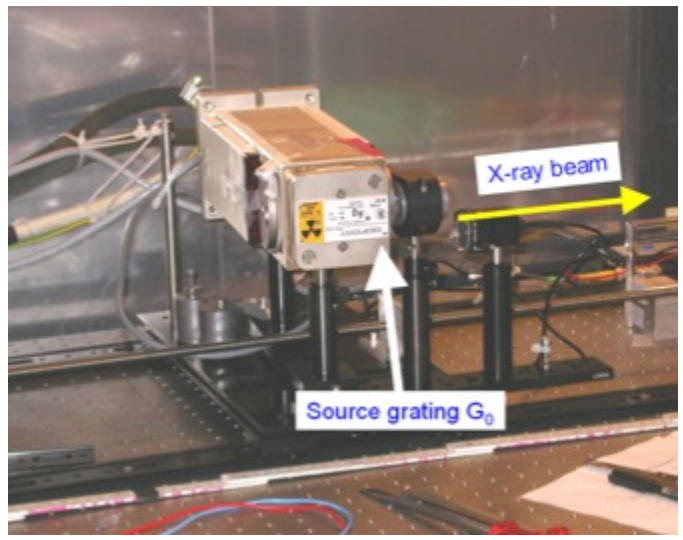
Amplitude



Phase (gradient)



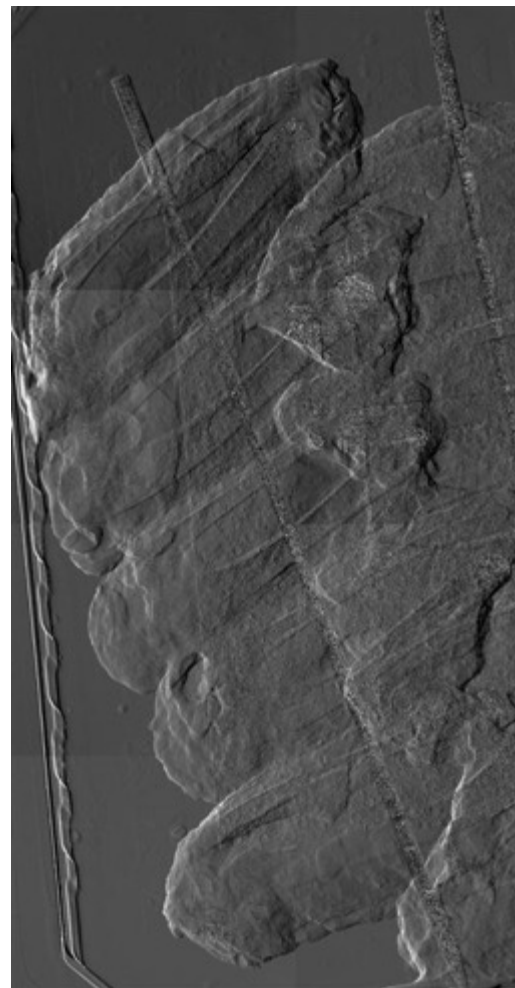
F. Pfeiffer et al., NATURE PHYSICS 2, (2006)



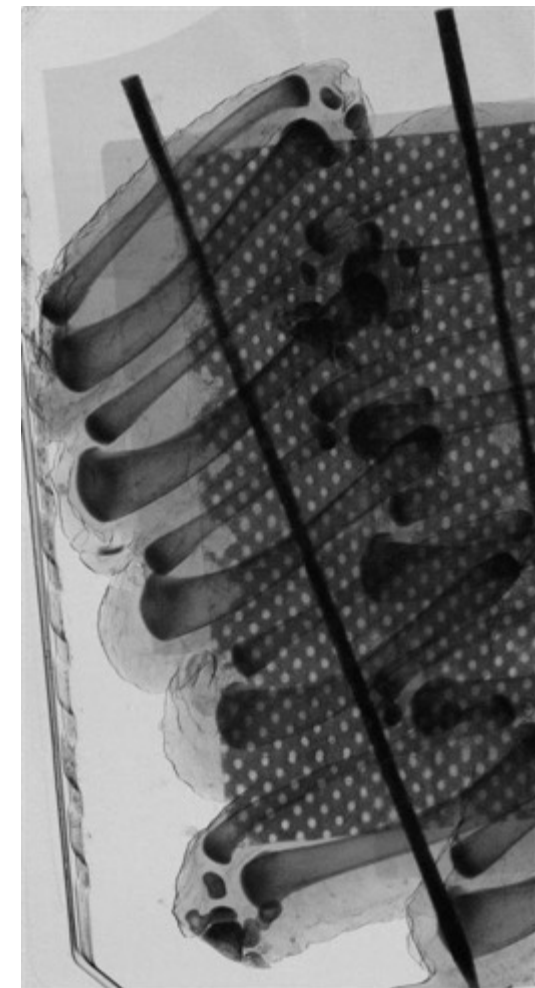
Advanced imaging of large samples



Absorption



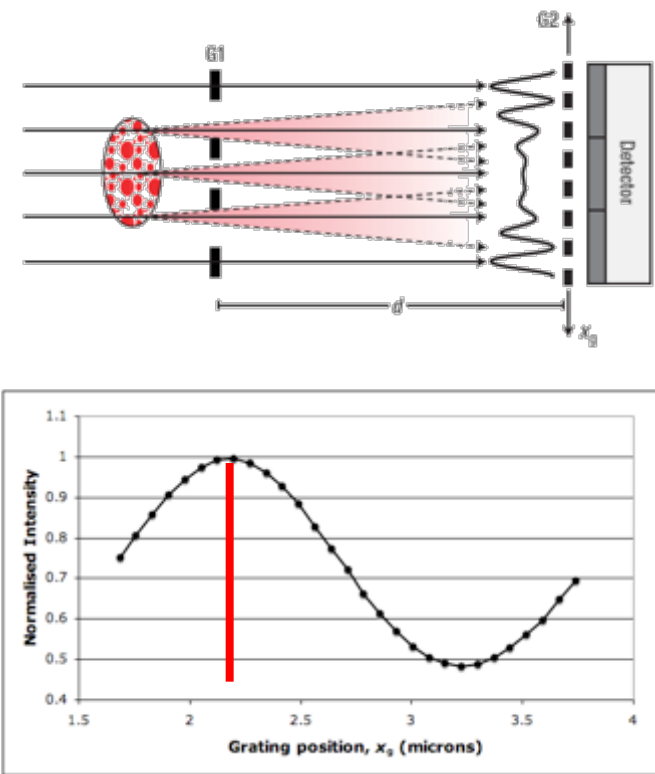
Differential Phase contrast



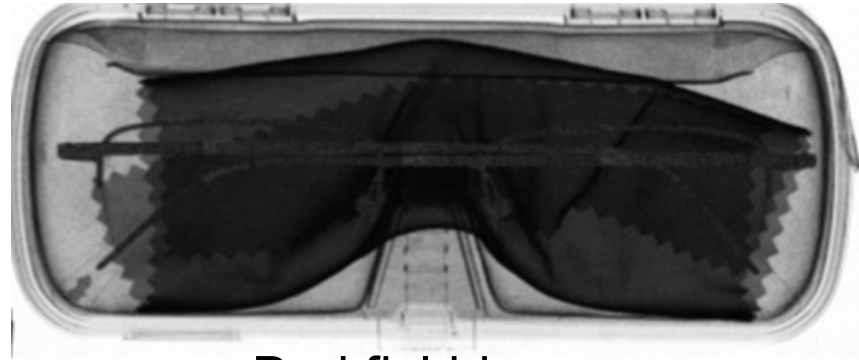
Dark Field

Data courtesy of Z. Wang, TOMCAT Group

Absorption vs. dark-field imaging



Transmission image

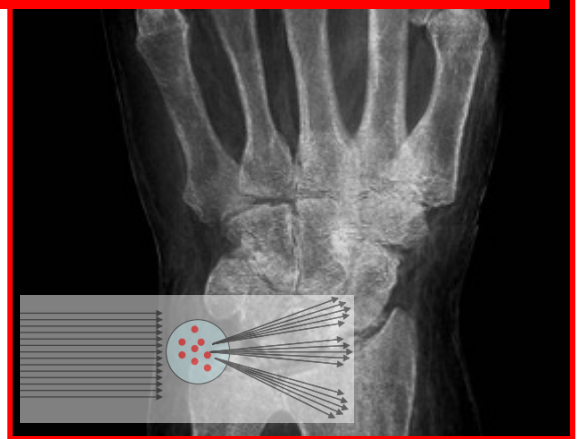
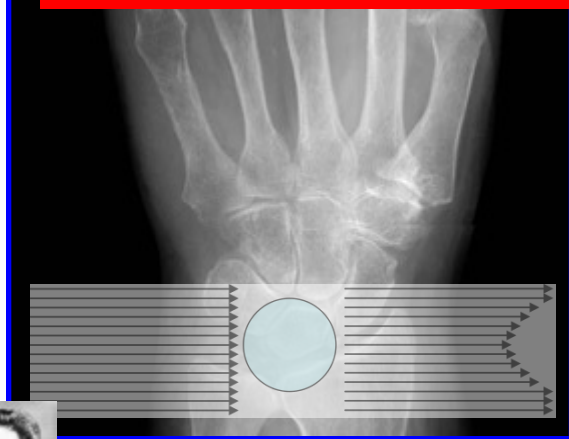


Darkfield image

New radiological capabilities



Exploit these additional physical signals
to improve (early) breast cancer detection



Absorption image
Conventional radiography
(since 1895...)

"Differential Phase image"

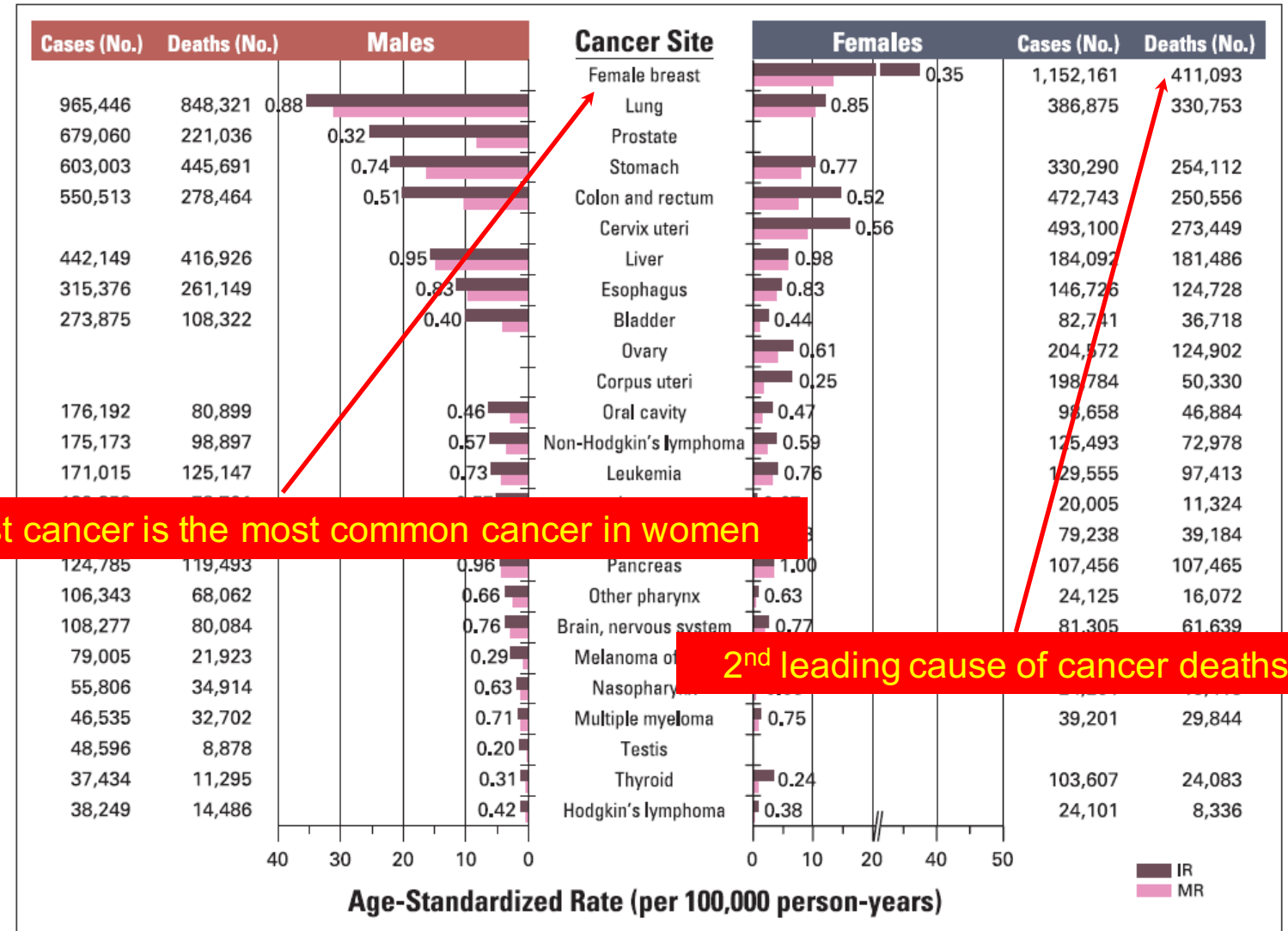
"Scatter image"

$$\text{Index of refraction: } n = 1 - \frac{\delta}{\lambda} + i\frac{\beta}{\lambda}$$

Phase Absorption

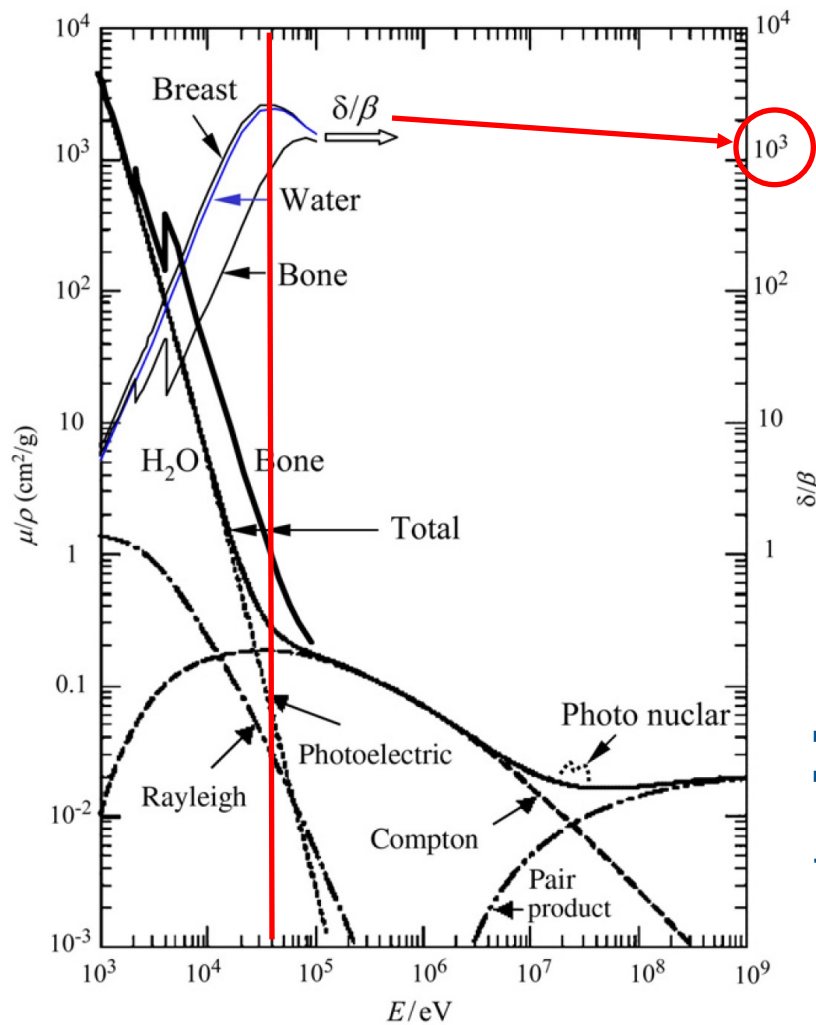
Phase contrast mammography: why?

Worldwide annual number of cancer cases and cancer deaths, incidence rates and mortality rates



F. Kamangar et al., Journal of Clinical Oncology, 24(14), 2137-2150 (2006)

Towards clinical phase contrast mammography



Zhou et al., Physica Medica (2008) 24, 129-148

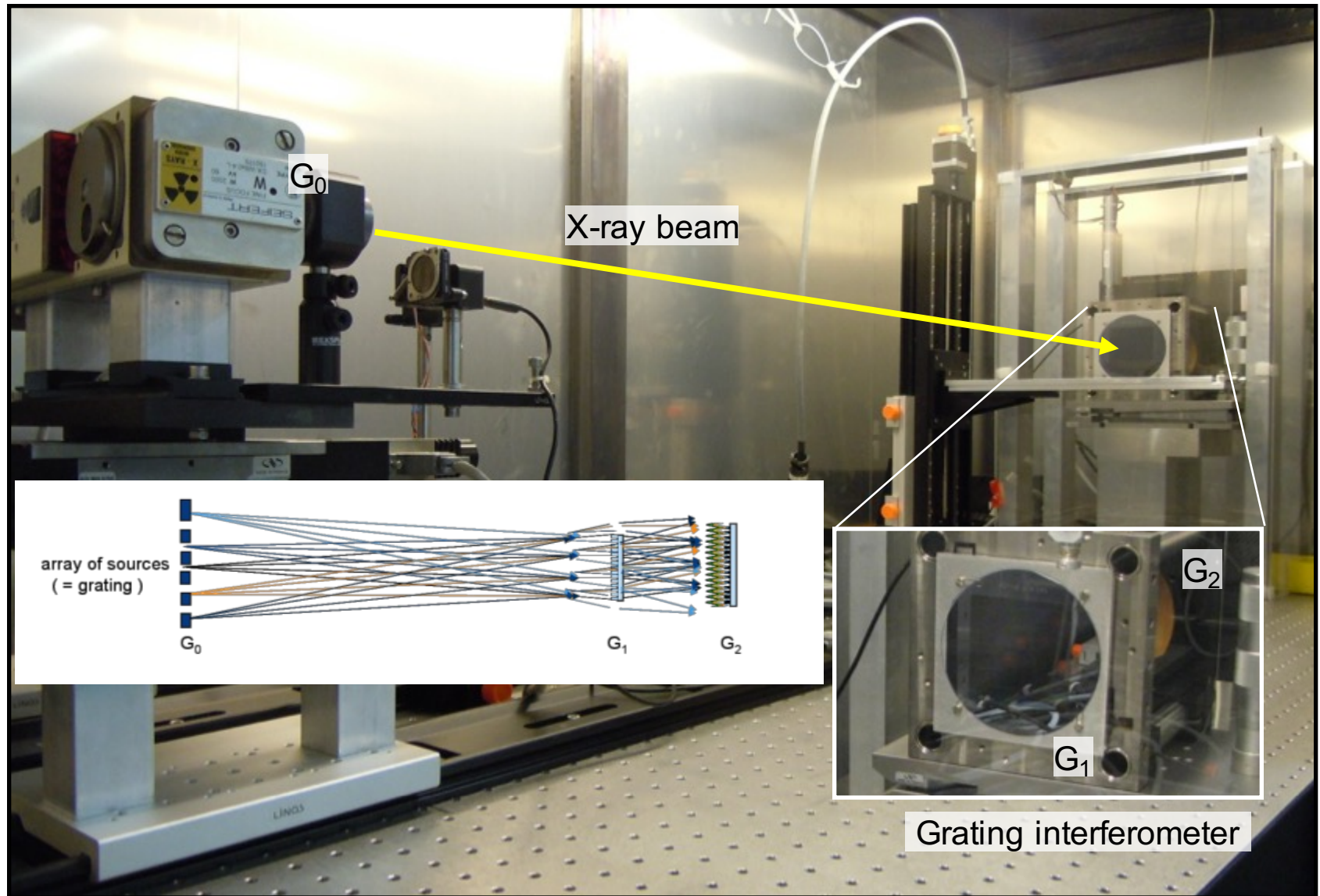
Index of refraction: $n = 1 - \delta + i\beta$

Phase Absorption



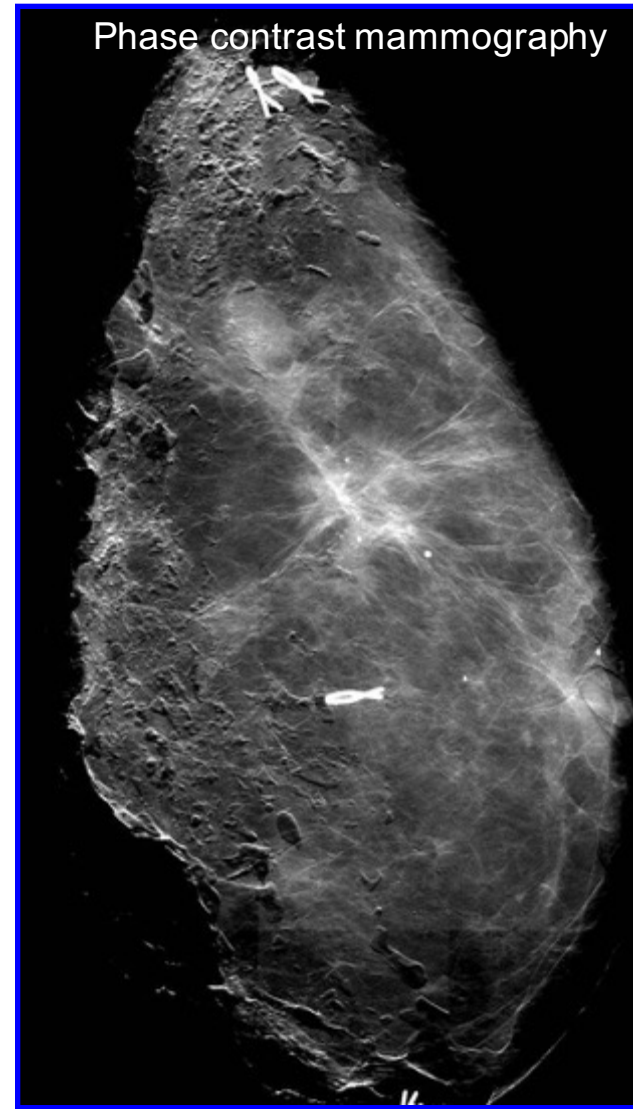
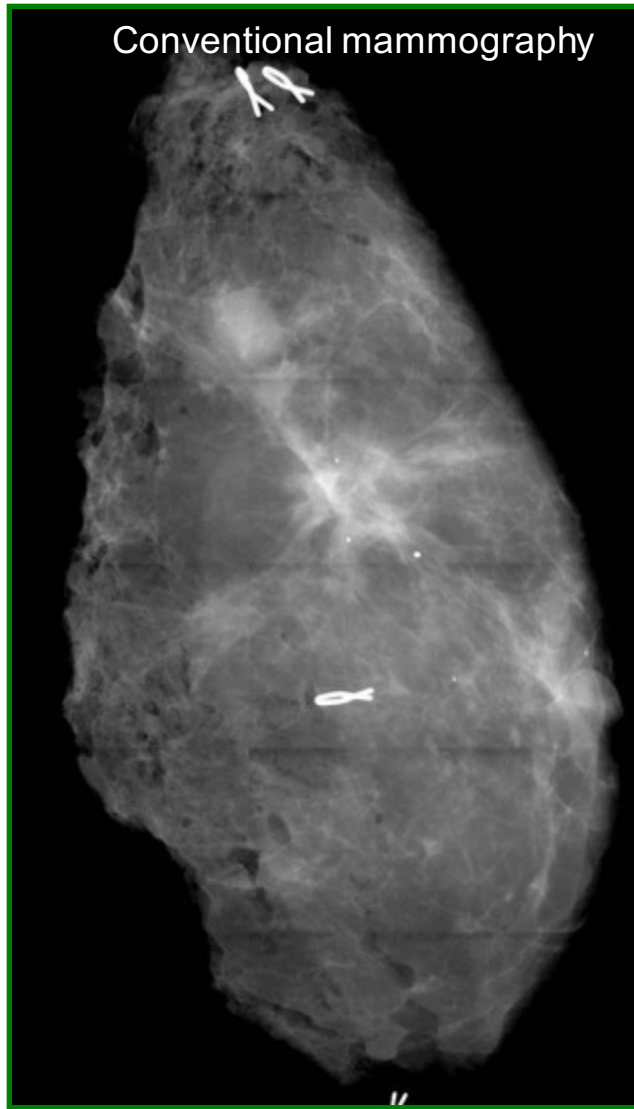
- Working energy for mammography: 20-30 keV
- For 20-30 keV, $\delta/\beta > 1000$
- When comparing various tissue samples, relative differences in angular deviations are larger than the corresponding relative changes in attenuation
- We expect improved diagnostic capabilities when compared to conventional methods

Phase contrast mammography demonstrator



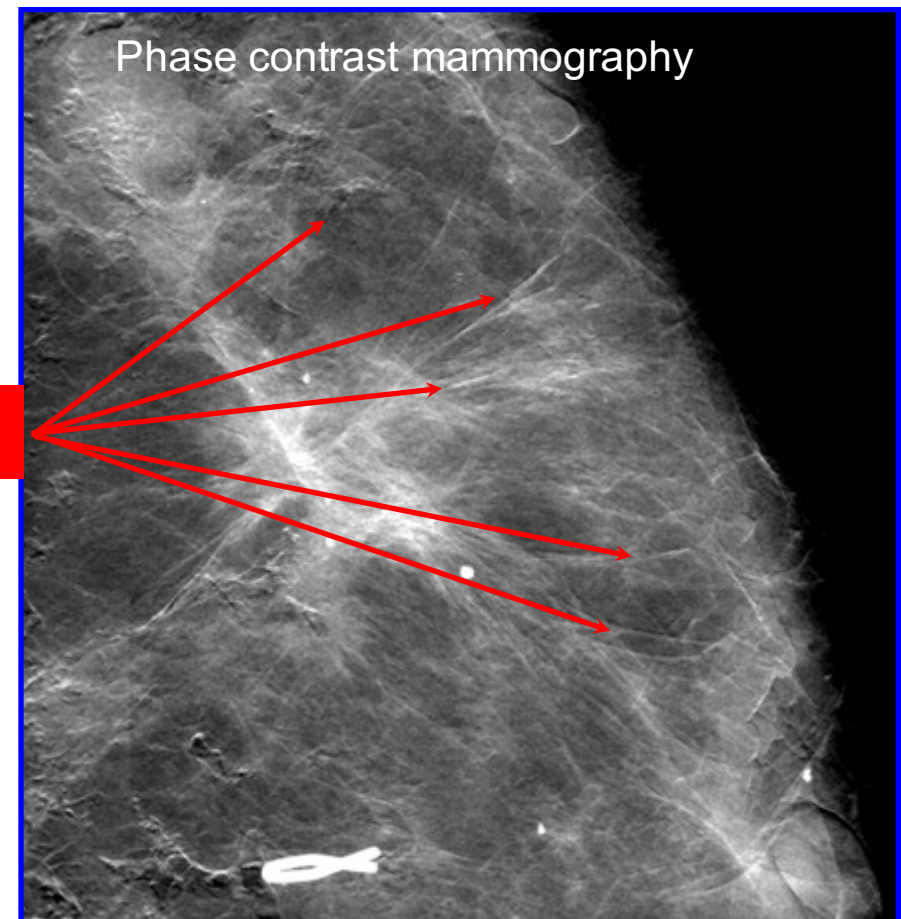
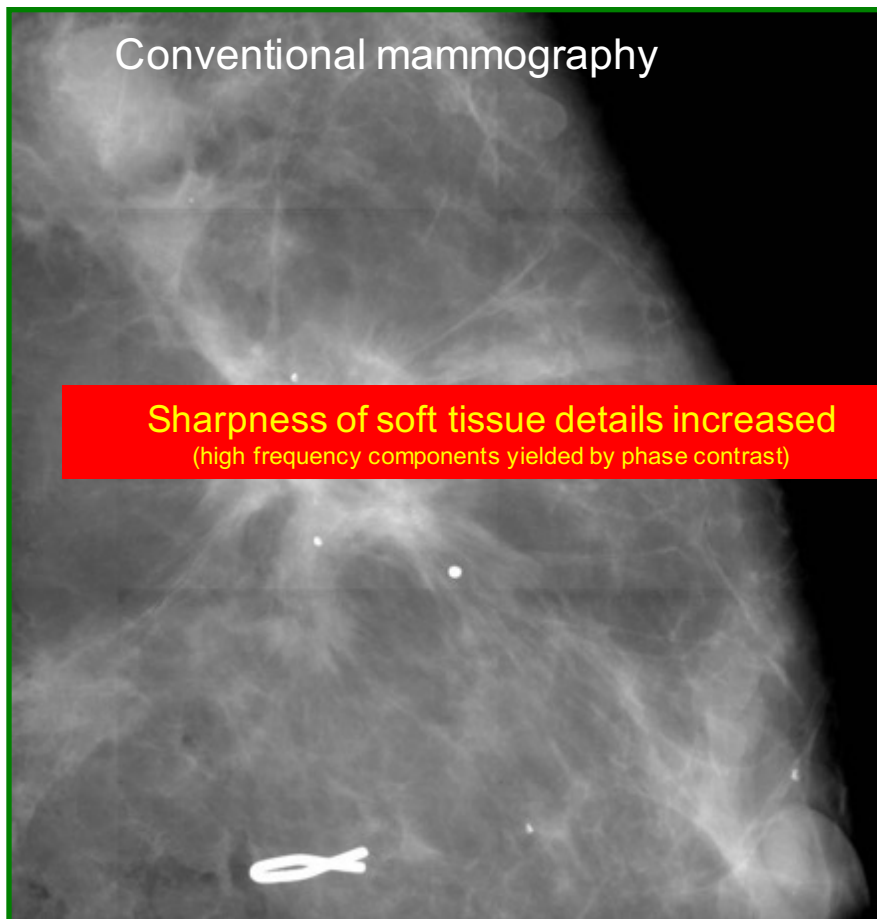
M. Stampanoni et al., Investigative Radiology, 46,801, (2011)

Differential phase signal enhances *spiculations* visibility



M. Stampanoni et al., Investigative Radiology, 46,801, (2011)

Differential phase signal enhances *spiculations* visibility



M. Stampanoni et al., Investigative Radiology, 46,801, (2011)

Phase contrast enhanced mammography

ORIGINAL ARTICLE

A Study on Mastectomy Samples to Evaluate Breast Imaging Quality and Potential Clinical Relevance of Differential Phase Contrast Mammography

TABLE 2. Statistical Outcome Showing the Criteria Under Which mammoDPC Is Superior to Absorption-Based Mammography

Evaluated Criteria (mammoDPC Is Superior)	P*	IQR
General quality of image	<0.001	2–3†
Sharpness and lesion delineation	<0.001	2–3
Delineation of surface structures	<0.001	2–3
Sharpness of microcalcifications	<0.001	2–2
General visibility of microcalcifications	<0.001	2–3
Potentially clinically relevant information	<0.001	4–5‡
Identification of spiculations	<0.015§	

*P < 0.005 is considered to be significant with Bonferroni correction.

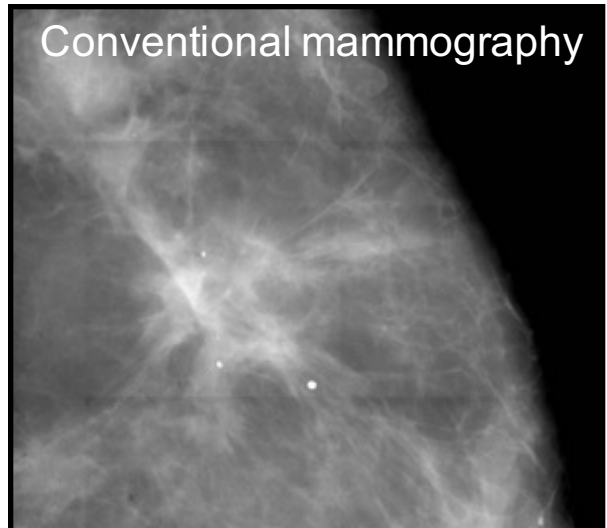
†2 being “superior” and 3 being “equivalent” quality.

‡4 being “11% to 20% superior” and 5 being “1% to 10% superior.”

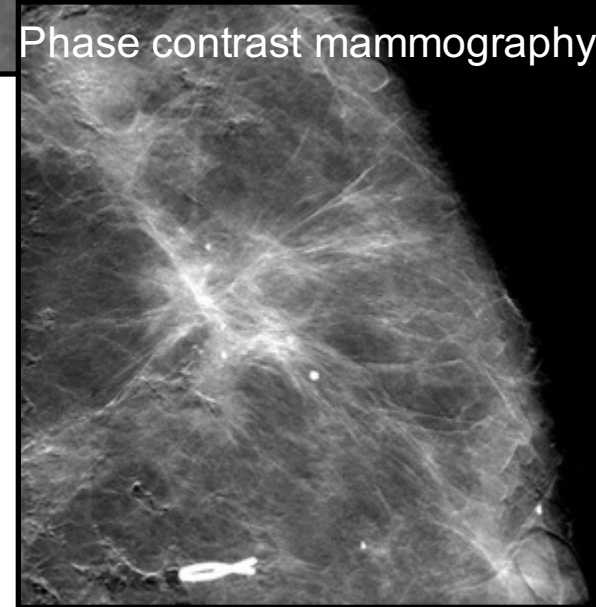
§This criterion was evaluated in study 2. P < 0.025 is significant with the Bonferroni correction.

IQR indicates interquartile range; mammoDPC, phase contrast-enhanced mammography.

Conventional mammography



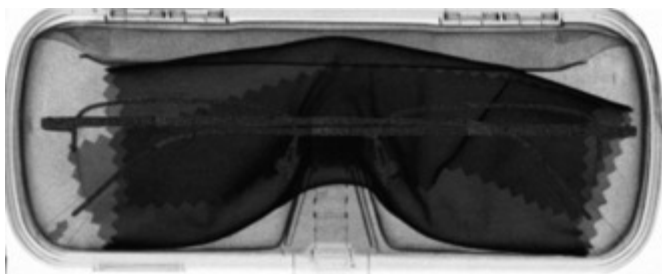
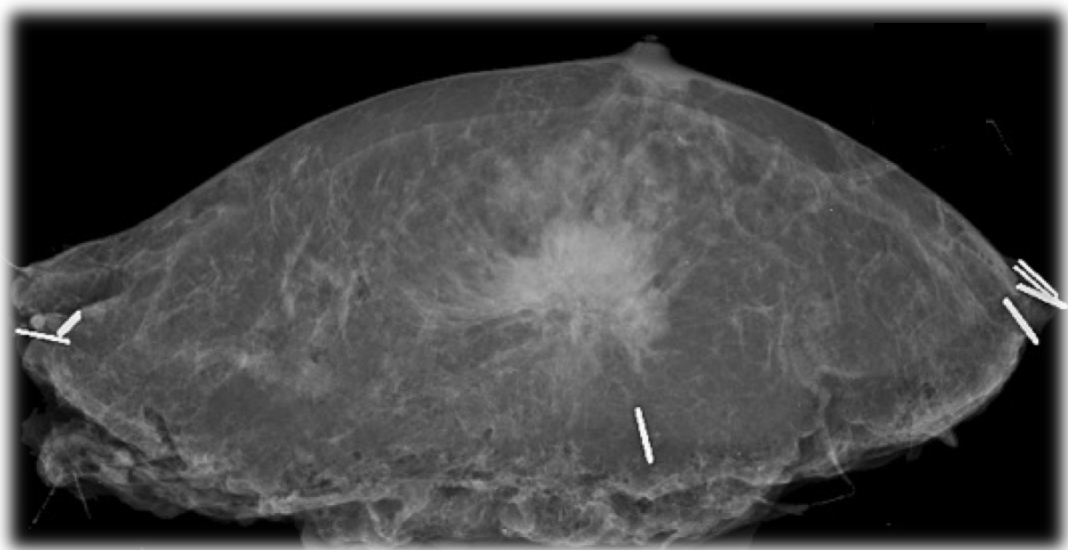
Phase contrast mammography



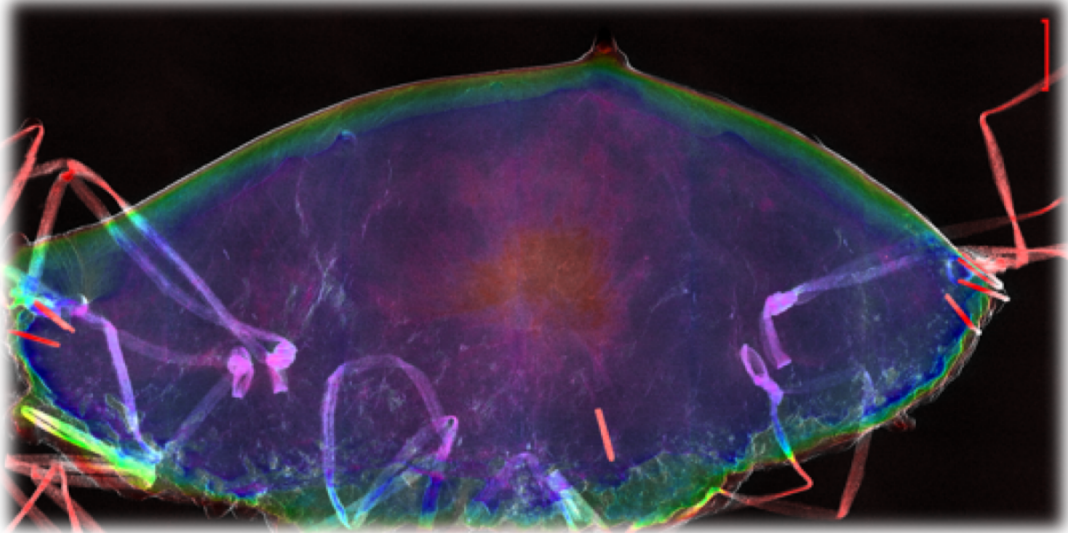
Material discrimination...



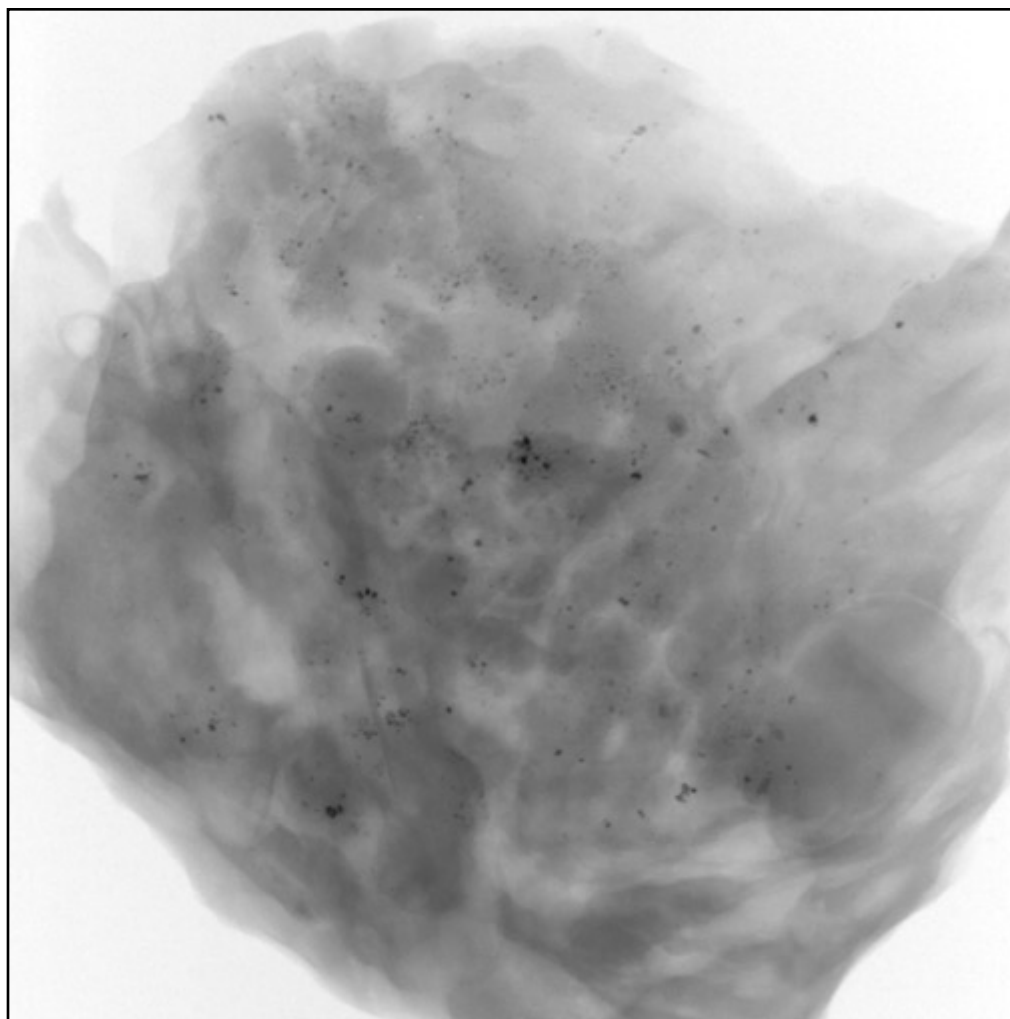
Absorption



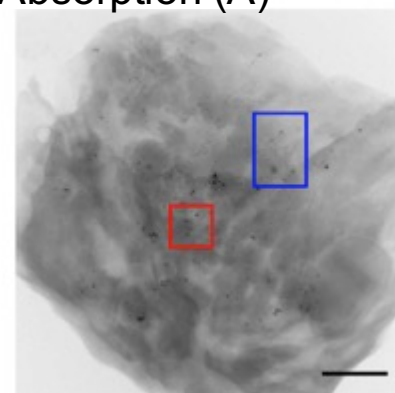
Scattering



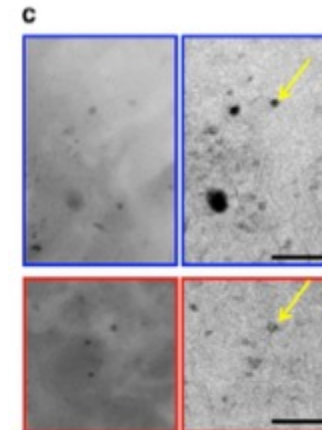
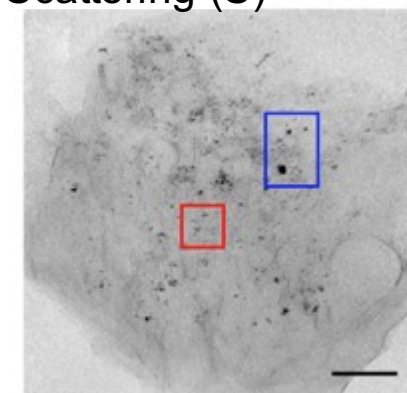
Our observation



Absorption (A)



Scattering (S)

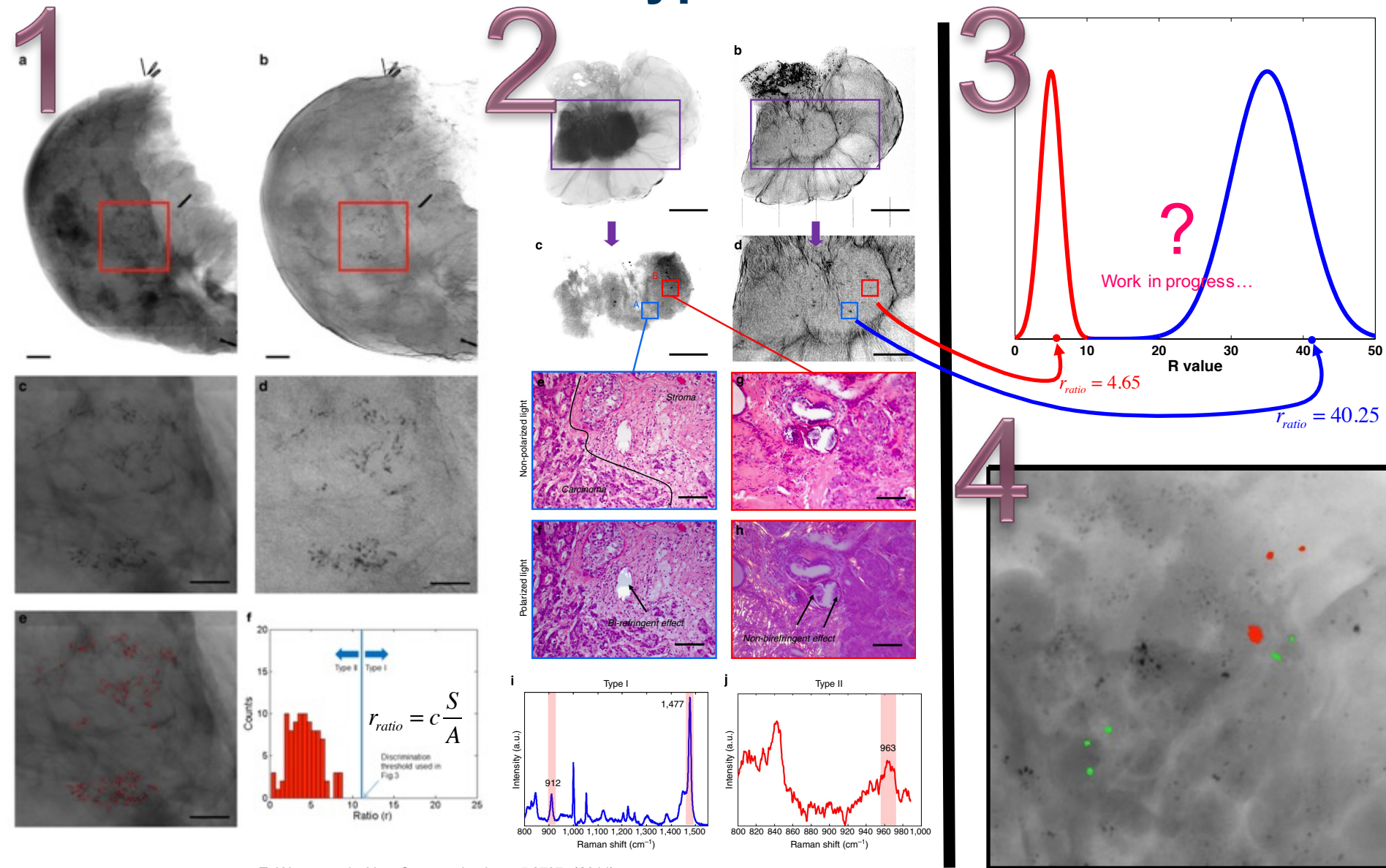


Opposite behaviors of A and S

Type I: calcium oxalate dehydrate, $\text{CaC}_2\text{O}_4(2\text{H}_2\text{O})$
Type II: calcium hydroxyapatite, $\text{Ca}_5(\text{PO}_4)_3(\text{OH})$

Can we discriminate between Type I (benign) and Type II (malignant) micro-calcifications *non-invasively*?

Our hypothesis



Z. Wang et al., Nat. Communications 5:3797 (2014)

Diagnosis and staging of pulmonary emphysema

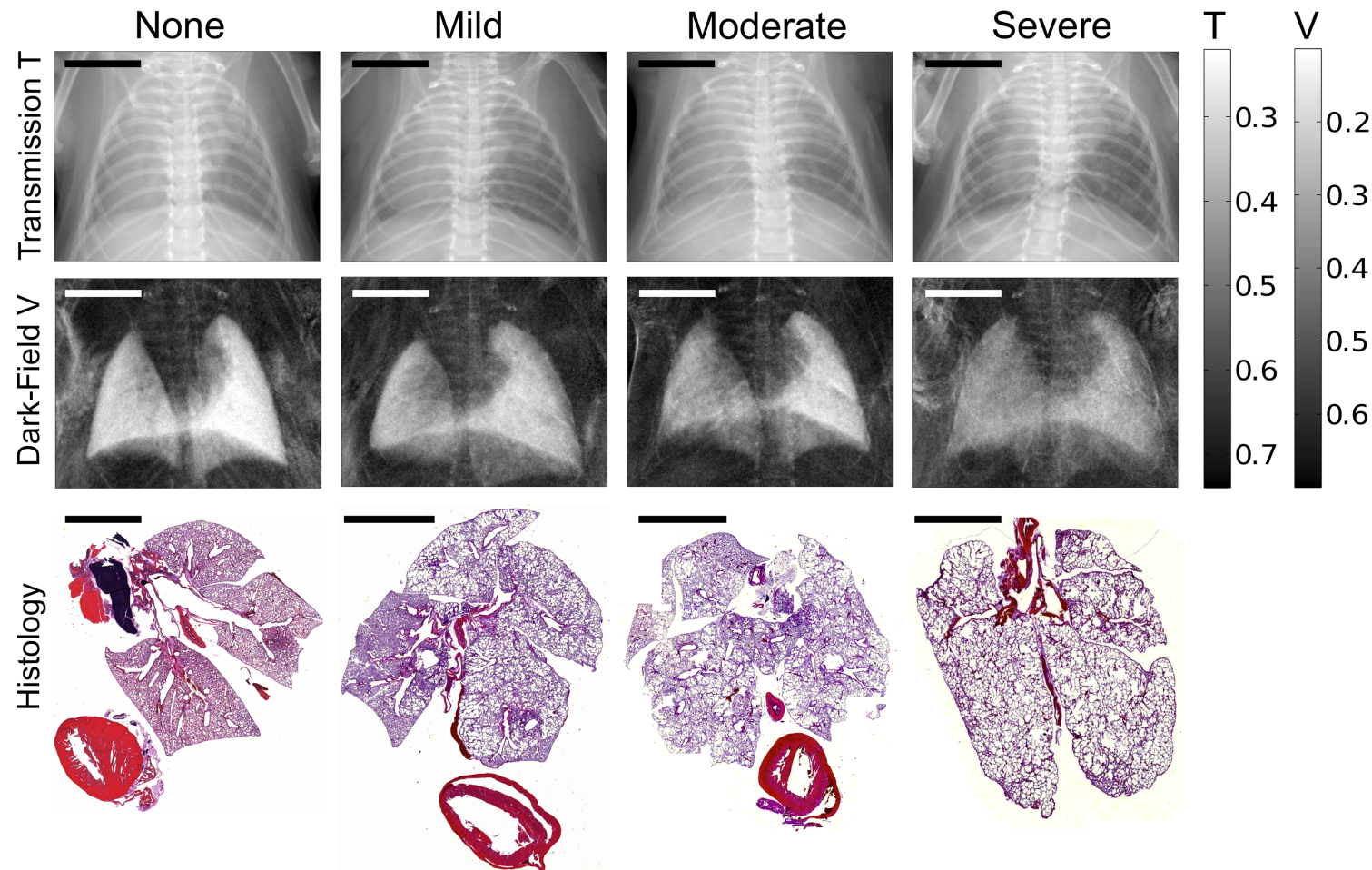


FIGURE 1. X-ray transmission and dark-field radiographs of mice in various stages of emphysema severity. Transmission (upper row), dark-field (middle row), and histology (lower row) are shown for healthy (left), mildly (middle left), moderately (middle right), and severely (right) emphysematous lungs. The scale bars in each image correspond to a length of 5000 μm . Figure 1 can be viewed online in color at www.investigativeradiology.com.

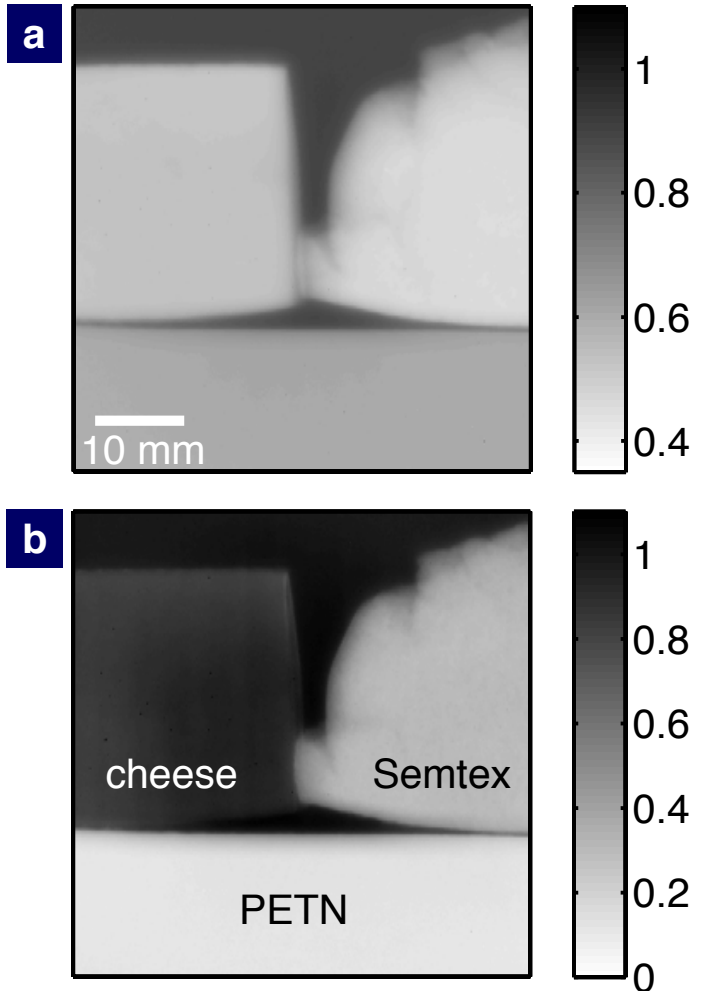
K. Hellbach, Investigative Radiology, in press: DOI: 10.1097/RLI.000000000000147

Cheese or not cheese? That's the (homeland) problem



250g of SEMTEX are sufficient to fully destroy an airliner

F. Pfeiffer et al., Nature Methods, 7, 134 - 137 (2008)



Different granular microstructures distinguish high-performance explosives from good cheese...